

PHOTOAUTOTROPHIC GROWTH OF EUKARYOTIC MICROALGAE
AND ELECTRON DETOURS UNDER
DEFICIENT SINK STRESS

by
Dylan C. Thomas

Copyright by Dylan C. Thomas 2018

All Rights Reserved

A thesis submitted to the Faculty and the Board of Trustees of the Colorado School of Mines in partial fulfillment of the requirements for the degree of Masters of Science (Chemistry).

Golden, Colorado

Date _____

Signed: _____
Dylan C. Thomas

Signed: _____
Dr. Matthew C. Posewitz

Golden, Colorado

Date _____

Signed: _____
Dr. Thomas Gennett
Professor and
Department Head of Chemistry

ABSTRACT

Eukaryotic microalgae have been an attractive target for use in the bioeconomy for over 70 years because of their ability to efficiently generate biomass from CO₂, sunlight, seawater, and fertilizer. In this thesis, I will demonstrate the isolation of a promising new industrial alga, *Picochlorum celeri*, which has one of the highest maximum growth rates ever reported. The organism's hallmark is a high chlorophyll concentration, a dynamic antenna regulated by light, and a high net oxygen evolution rate. In addition to this new biotechnology strain, a starchless mutant of the model organism, *Chlamydomonas reinhardtii*, was photosynthetically characterized which unmasked water-water cycles cause by uncoupled light reactions and carbon metabolism. In this analysis, the apparent maximal rate of Flavodiiron proteins was calculated as they activate under light transitions as well as the usage of the Plastid terminal oxidase under both inactive carbon metabolic stress and nitrogen deficiency.

TABLE OF CONTEXT

ABSTRACT	iii
LIST OF FIGURES	ix
LIST OF TABLES	xiv
ACKNOWLEDGEMENTS	xv
CHAPTER 1: INTRODUCTION TO ALGAE BIOTECHNOLOGY AND PHOTOSYNTHESIS.....	1
1.1 Photons to Fuels.....	1
1.2 Photoautotrophic Growth to Biomass to Energy	3
1.3 Improvements to Algae.....	5
1.3.1 Selection.....	6
1.3.2 Directed Evolution.....	6
1.3.3 Genetic Manipulation.....	7
1.4 Classical Algal Research.....	8
1.5 Industrial Algae.....	9
1.6 Photosynthesis.....	10
1.6.1 Light Harvesting	11
1.6.2 OEC to PQ pool to NADPH	12
1.6.3 Calvin-Benson-Bassham Cycle to Carbon Storage	14
1.7 Photosynthetic Phenotyping	14

1.7.1 Photosynthetic Kinetics	15
1.7.1.1 Photosynthetic Irradiance Response Curve	15
1.7.1.2 Light Induced Oxygen Uptake.....	17
1.7.2 Redox Properties Elucidate Electron Flow Availability.....	18
1.7.2.1 Pulse Amplitude Modulated Fluorescence Techniques.....	18
1.7.3 Measuring Optical Properties of Algae.....	21
1.7.3.1 Cell Size and Optical Cross Section	21
1.7.3.2 Functional Cross Section (Antenna Size) and Quantum Requirement.....	21
1.7.4 Growth Metrics of Algae	22
1.7.4.1 Maximum Specific Growth Rate	22
1.7.4.2 Biomass Primary Productivity	23
1.8 The Focus on Phenotyping Photosynthesis in Model and Non-Model Phototrophs	24
1.8.1 Starchless Mutation in <i>C.reinhardtii</i> Causes Photosynthetic and Metabolic Changes.....	24
1.8.2 Bioprospecting and Photosynthetic Characterization for Industrial Application	25
CHAPTER 2: ALTERNATIVE OUTLETS FOR SUSTAINING PHOTOSYNTHETIC ELECTRON TRANSPORT DURING DARK TO LIGHT TRANSITIONS.....	27
2.1 Abstract.....	27
2.2 Introduction.....	28
2.3 Results.....	32
2.3.1 At the onset of light electrons are redirected toward FLVs.....	34

2.3.2	Eliminating starch synthesis caused augmented O ₂ photoreduction.....	35
2.3.3	Interactions between starch synthesis and O ₂ photoreduction.....	37
2.3.4	Contribution of PTOX to O ₂ uptake in <i>sta6</i>	39
2.3.5	Overall contribution of FLV to photoreduction of O ₂	43
2.4	Discussion.....	46
2.5	Materials and Methods.....	50
2.5.1	Strains and cell growth.....	50
2.5.2	Chl concentration	51
2.5.3	Dark respiration	51
2.5.4	Chl fluorescence analysis.....	52
2.5.5	O ₂ production and light driven O ₂ photo-reduction.....	52
2.5.6	Data analyses	53
CHAPTER 3: HIGH-LIGHT SELECTION PRODUCES A FAST-GROWING		
	<i>PICOCHLORUM CELERI</i>	54
3.1	Introduction.....	54
3.2	Materials and Methods.....	56
3.2.1	Replication and Statistics.....	56
3.2.2	Growth conditions.....	56
3.2.3	Composition Analyses	57
3.2.4	Oxygen evolution.....	58

3.2.5 Growth rates.....	59
3.2.6 Optical absorption.....	60
3.2.7 Spectral Irradiance.....	60
3.2.8 Totalized absorption cross sections.....	61
3.2.9 Quantum Requirement.....	61
3.2.10 Photosystem II cross section (antenna size).....	62
3.3 Results and Discussion.....	62
3.3.1 High light diminishes specific growth rate of <i>Tetraselmis sp.</i>	62
3.3.2 <i>Picochlorum celeri</i> emerges from selection for fast reproductive rate in high light.....	66
3.3.3 Isolation of single cell lines from the <i>P. celeri</i> enrichments.....	68
3.3.4 Biomass Productivity of <i>Picochlorum</i> , <i>Tetraselmis</i> , and <i>Chlorella</i> in constant high light.....	70
3.3.5 Biomass Productivity of <i>Picochlorum</i> , <i>Tetraselmis</i> , and <i>Chlorella</i> in diel light.....	72
3.3.6 Oxygen evolution measurements.....	74
3.3.7 Comparative Specific Growth Rates and Optical Properties of <i>Picochlorum</i> , <i>Tetraselmis</i> , and <i>Chlorella</i>	81
3.3.7.1 Specific growth rate and culture stability.....	81
3.3.7.2 Chlorophyll content and absorption cross sections.....	85
3.3.7.3 Quantum requirement.....	88
3.3.8 Improving <i>P. celeri</i> Biomass Productivity.....	89

3.4 Summary	91
3.5 Acknowledgements	92
CHAPTER 4: CONCLUSION AND FUTURE WORKS	93
4.1 Algal Biotechnology Outlook and Future Considerations	93
4.2 Future Work of Photosynthetic Metabolism in Starchless Mutants	94
REFERENCE CITED	95
APPENDIX A: SUPPLEMENTAL DATA	105
APPENDIX B: PERMISSIONS	107

LIST OF FIGURES

Figure 1. 1 Amount of land area required to meet each country's fuel demands for 2010 estimates. Values compare the best biodiesel crop in the area and microalgal growth systems. (Correa et al. 2017).....	2
Figure 1. 2 Growth curve examples of batch and semi-continuous growth conditions. A: Batch growth is inoculated at a low density and then allowed to grow through an exponential and then stationary phase. B: Semi-continuous growth dilutes the culture daily and is allowed to regrow each day to maximize harvests daily for processing. Values are arbitrary	3
Figure 1. 3 The different biomass partitioning demonstrated by the circle chart affects the quality of energy produced by HTL. As shown, <i>Nannochloropsis salina</i> which has a high lipid quantity results in a larger portion of energy dense products than a lower oil content species, <i>Gladiaria sulphuraria</i> (Cheng et al. 2018).....	4
Figure 1. 4 Overview of photosynthetic electron flow. Electrons are liberated for water which are moved through photosystem II and photosystem I. That reductant is utilized in the Calvin-Benson-Bassham Cycle to fix Carbon dioxide. Carbon is then partitioned into proteins, lipids, and carbohydrates.....	10
Figure 1. 5 Linear electron flow in photosynthesis is depicted by the blue line which ends at NADPH to be utilized in the Calvin-Benson-Bassham Cycle. The red line depicts the proton motive force being pumped by ATP synthase for ATP production used by the Calvin-Benson-Bassham Cycle (Wikipedia).....	12
Figure 1. 6 Metabolism of the Calvin-Benson-Bassham Cycle fixation (A) of Carbon dioxide into generation of GA3P which is metabolized into glucose. (B) Glucose is then polymerized in starch. The STA6 gene is responsible for the rate limiting step in starch synthesis. Figure modified from Lumen and Shai Saroussi.....	14
Figure 1. 7 Photosynthetic Irradiance Response Curve relates net oxygen evolution rates to radiance levels.	15
Figure 1. 8 Pulse Amplitude Modulated Fluorescence experiments are performed in this way. Relevant parameters are labeled in the image.	19

Figure 2. 1 Integration of photosynthetic light reactions and carbon metabolism. The light reactions include the reaction center/electron transport components PSI and PSII (green), cytochrome *b₆f* (*b₆f*) (orange), ATP synthase (blue), with CBBC (cycle, upper right) and starch biosynthesis (pathway, upper left) using the products of these reactions. Metabolites are in blue [G3P- glyceraldehyde 3-phosphate; F6P- fructose 6-phosphate; G6P-glucose 6-phosphate; G1P- glucose 1-phosphate]. Carbon metabolism-related enzymes are highlighted in gold filled rectangles [Rubisco - ribulose phosphate carboxylase oxygenase; PGM - phosphoglucomutase; AGPase - ADP-glucose pyrophosphorylase; SS - starch synthase]. Other enzymes are: PTOX - plastid terminal oxidase; FLV - flavodiiron protein (blue-filled ovals; involved in reducing O₂); NDA2 – NADPH oxidoreductase (grey-filled rectangle; moves electrons into electron transport); FDX - ferredoxin; TRX - thioredoxin; FNR - flavin:NADPH reductase (grey-filled circles; moves electrons out of electron transport)..... 32

Figure 2. 2 Light-induced O₂ evolution and uptake. C6 (A) and *sta6* (B) were cultured photoautotrophically, bubbled with 2 % CO₂ in air and maintained in continuous light of 100 μmol photons m⁻² s⁻¹. Gross O₂ production (¹⁶O₂ evolution, green curve) and light-induced uptake of O₂ (¹⁸O₂ uptake, red curve) were monitored for 6 min using MIMS at 4 different light intensities (50, 150, 300 and 1000 μmol photons m⁻² s⁻¹, as indicated in the figure). Prior to turning on the light, the cells were maintained for 5 min in the dark (black bars on the left of each graph), and for an additional 3 min in the dark following the illumination (black bar, on the right of each graph). Gross O₂ uptake and both gross and net (blue curve) O₂ production were calculated according to the formula given in Materials and Methods. Each trace represents an average of at least 3 biological replicates. 33

Figure 2. 3 Maximal rates of light-induced O₂ production and uptake. Maximal values for gross and net O₂ production (green and blue, respectively) and net O₂ uptake (red) for C6 (A) and *sta6* (B), as indicated, are plotted as a function of light intensity. The left-hand Y axis gives gross and net O₂ evolution and gross O₂ uptake, as indicated on the top of the figure. The right-hand Y axis gives the fraction of maximal gross O₂ uptake relative to maximal gross O₂ production; this value is plotted as a function of light intensity (black line with black squares). For both A and B, the left panel presents the data for the first 3 min of the light phase while the right panel present the data for the final 3 min of the light phase (i.e. early and late periods during illumination, respectively; see main text for details). Each point is an average of at least 3 biological replicates ± SD. 37

Figure 2. 4 Kinetics of light induced O₂ production and uptake. A. MIMS traces of ¹⁶O₂ evolution (gross production, dotted-dashed lines) and ¹⁸O₂ uptake (gross uptake, solid lines) during dark to light transition (300 μmol photons m⁻² s⁻¹) for C6 (black) and *sta6* (red). Gross O₂ production (¹⁶O₂) along the first 20 s in the light period, were linearly fitted and the initial rates (ΔY/ΔX) was calculated (black

and red dash-dotted lines). The $^{18}\text{O}_2$ uptake plots were fitted to a first order exponential decay type curves to determine the rate (τ) at which a peak of $^{18}\text{O}_2$ uptake for C6 and *sta6* were attained (dashed black and red line for C6 and *sta6*, respectively). Inset: Presentation of the MIMS reaction for gross O_2 evolution and uptake during the entire light period. B. The ratio between gross $^{18}\text{O}_2$ uptake and $^{16}\text{O}_2$ production during the light period ($300 \mu\text{mol photons m}^{-2} \text{s}^{-1}$). Same conditions as in panel A. Gray box highlights the region in which the decline in the ratio for C6 and *sta6* cells is similar. Each data line represents an average of 3 biological replicates. 40

Figure 2. 5 Effect of a PTOX inhibitor on O_2 production and light-induced O_2 uptake. C6 (A) and *sta6* (B) were exposed to $300 \mu\text{mol photons m}^{-2} \text{s}^{-1}$ in the presence of 2 mM propyl gallate (PG) and gas exchange was analyzed using MIMS, as in Figure 3 (see Figure 3 legend). Comparisons of the first 2 min of $^{18}\text{O}_2$ uptake for C6 (C) and *sta6* (D) in the presence (dashed line with purple shading) and absence (solid line with red shading) of PG. The time (s) to achieve U_{max} for C6 and *sta6* are highlighted by dotted red lines that extend from the x axis to the U_{max} peak. Each trace represents an average of at least 3 biological replicates with the shaded area associated with each trace representing the SE. (E) 1-qL values of PG-treated/untreated cells. The cells were PG treated during the 5 min pre-incubation in the dark and then exposed to $300 \mu\text{mol photons m}^{-2} \text{s}^{-1}$ for 1 min. $N=3 \pm \text{SD}$ * t-test, $p\text{-value} = 0.01$. (F) 1-qL values of PG-treated/untreated cells exposed to increasing light intensities. Cells were exposed to each intensity for 30 s before raising the intensity. $N=3 \pm \text{SD}$. PAR = photosynthetic active radiation. 42

Figure 2. 6 O_2 Uptake attributed to FLV proteins: A. O_2 uptake rate of C6 cells exposed to different light intensities (shown in different colors) are plotted during the first 2 min of the light period (300 - 420 s). The rates of baseline O_2 uptake (uptake in the light after the CBBC becomes active), calculated from Figure A1.2, are shown as dashed lines in the color that corresponds to the measurements of total O_2 uptake. B. Total O_2 uptake at each intensity that cannot be attributed to the basal rate of uptake was calculated by integrating the area between the curve defining the uptake rate at the different intensities with the rate of basal uptake at that intensity. C. Maximal rate of O_2 uptake attributed to the FLV proteins. These values were calculated by subtracting the rate of O_2 uptake attributed to basal uptake from U_{max} depicted in the curve in A. For all panels $n=3 \pm \text{SD}$ 44

Figure 3. 1 Specific growth rates, based on changes in particulate organic carbon, for dilute (less than $0.5 \mu\text{g mL}^{-1}$ for 8 cm optical path length) suspensions of algae. Circles, light acclimation “steady” states of *Tetraselmis*, diluted semi-continuously; squares, *Tetraselmis* acclimated to $50 \mu\text{moles m}^{-2} \text{s}^{-1}$, moved to higher irradiances for 3-4 hours; triangles, light acclimation states of the high-light-selected alga, *Picochlorum celeri*, diluted semi-continuously. Each point represents the mean of level 1 biological replicates. The number of replicates for each point range from 2-33. 64

- Figure 3. 2 Specific growth rates of light-acclimated states of *P. celeri* enrichment E1 (black bars) and *P. celeri* TG1 (grey bars) at two irradiances ($\mu\text{moles m}^{-2} \text{s}^{-1}$ PAR). Number of level 1 biological replicates are listed left to right: 10, 3, 18, 5. 68
- Figure 3. 3 Biomass productivity (AFDW) of semicontinuously-diluted algal cultures grown under 24 hour continuous irradiance at $2000 \mu\text{moles m}^{-2} \text{s}^{-1}$. The number of level 1 biological replicates from left to right: 18, 3, 76, 25, 33. 71
- Figure 3. 4 Simulated solar day (PAR) used for diel illumination for algal growth..... 72
- Figure 3. 5 Biomass productivity (AFDW, black bars) and chlorophyll content (grey bars) of semi-continuously diluted algal cultures grown under diel illumination shown in Figure 3.4. The number of level 1 biological replicates for productivity data from left to right: 11, 14, 38, 49, 50. For Chl data (% POC): 11, 7, 15, 16, 14. 74
- Figure 3. 6 Photosynthesis-Irradiance curves for *P. celeri* TG1 and TG2. Circles are net oxygen evolution; squares are oxygen consumption in the dark. a. TG1 grown dilute under $2000 \mu\text{moles m}^{-2} \text{s}^{-1}$, in vessels 8 cm optical path length. Chlorophyll density of the suspension on the day the P-I response was measured was $0.6 \mu\text{g mL}^{-1}$. It was not diluted for the oxygen evolution assay. Total chlorophyll content of the biomass was 1.7% of the POC. b. TG2 grown dilute under $1000 \mu\text{moles m}^{-2} \text{s}^{-1}$. Suspension chlorophyll density was $0.6 \mu\text{g mL}^{-1}$. It was diluted 4-fold for the assay. Total chlorophyll content of the biomass was 2.7% of the POC. The number of level 1 biological replicates are: a: 4. b: 1..... 76
- Figure 3. 7 Photosynthesis-Irradiance response for algae grown under a diel cycle. *Chlorella*, *Tetraselmis*, and *P. celeri* TG1. Circles: *P. celeri* TG1. Squares: *Chlorella* 252. Triangles: *Tetraselmis* 2286. All data points are level 1 biological triplicates. 79
- Figure 3. 8 a. Photosynthetic oxygen production of *P. celeri* TG2 versus time at $2000 \mu\text{moles m}^{-2} \text{s}^{-1}$ for 20 minutes and consumption in the dark for 10 minutes. b. Rate of net oxygen evolution: Initial light, rate averaged during minutes 2-8; late light averaged during minutes 12-18; and rate of oxygen consumption in the dark averaged over minutes 22-27. Sample taken from a culture grown dilute at $1000 \mu\text{moles m}^{-2} \text{s}^{-1}$. All data are level 1 biological triplicates. In panel a, standard deviations are within the thickness of the line..... 80
- Figure 3. 9 Optical characteristics and pigmentation of algae. The X-axes in these graphs indicate the conditions of growth. 2000, 900, and 50 (or 60) refer to the constant irradiance at which dilute cultures were grown, in $\mu\text{moles m}^{-2} \text{s}^{-1}$. Diel and 24 h 2000 ($\mu\text{moles m}^{-2} \text{s}^{-1}$) indicate the incident irradiance illuminating dense cultures.

See text for explanation of data shown. The number of level 1 biological replicates for each panel are listed left to right as follows. A: 18, 14, 8, 23, 5, 3, 23, 19, 4, 2, 6, 2, 19, 6, 10. B: 24, 10, 11, 10, 8, 1, 23, 11, 7, 3, 8, 3, 27, 11, 15. C: 14, 8, 7, 4, 16, 1, 11, 26, 4, 2, 6, 3, 15, 6, 10. D: 10, 8, 11, 6, 4, 1, 23, 9, 6, 2, 6, 3, 15, 6, 10. E: 5, 6, 5, 3, 3, 1, 5, 1, 3, 1, 3, 2, 3, 3, 5. F: 6, 6, 5, 14, 4, 2, 23, 19, 4, 3, 4, 33, 15, 6, 10. 82

Figure A1. 1 Photosynthetic measurements of photoautotrophically grown *sta6* (red line) and C6 (black line) following dark to light transition. **A.** Apparent efficiency of PSII at different light intensities. The first data point reflects PSII maximal efficiency or Fv/Fm. (N=3 +/- S.D.). **B.** Dark respiration. O₂ uptake was calculated from the slope soon after the cells were transferred from light to dark light (N=3 +/- S.E.). For all measurements 2mM bicarbonate was added during the dark period. 105

Figure A1. 2 The ratio between gross ¹⁸O₂ uptake and ¹⁶O₂ production (presented as %). Each data line represents an average of 3 biological replicates. Cells were exposed to **A.** 50 **B.** 150 and **C.** 1000 μmol photons m⁻² s⁻¹. 105

Figure A1. 3 Steady state O₂ uptake in the light and overall consumption of O₂ by FLVs. **A.** ¹⁸O₂ uptake at steady state were fitted to linear curve and the uptake value at this point was calculated for each light intensity (labeled). The uptake value was estimated as mitochondrial respiration. **B.** A correlation between the mitochondrial respiration derived from A and the basal rates of O₂ uptake (dominated by mitochondrial respiration) calculated using an O₂ electrode. There is a strong correlation between the values measured by the electrode and by the MIMS and these values are not significantly different. **C.** Integration of ¹⁸O₂ uptake to calculate the overall amount of O₂ consumption during by FLVs during the initial O₂ uptake burst. Blue line represents O₂ uptake and dashed blue and red line represent the levels of mitochondrial respiration that act as a baseline for our estimation. 106

LIST OF TABLES

<p>Table 2. 1 Photosynthetic parameters of PG treated C6 and <i>sta6</i> cells at 300 $\mu\text{mol photons m}^{-2} \text{s}^{-1}$. O_2 gas exchange (P_{max}, U_{max} and Net O_2 evolution) presented as $\mu\text{mol O}_2 \text{ mg Chl}^{-1} \text{ h}^{-1}$</p>	45
<p>Table 3. 1 Reproductive rates of isolates of <i>P. celeris</i> E1 obtained by either FACS sorting to obtained single cells, growing in well plates, and selecting the first to green (isolate TG1), or by diluting six billion fold to isolate at most single cells (or no cells) in each growth vessel then exposed to 900 $\mu\text{moles m}^{-2} \text{s}^{-1}$ to measure specific growth rates (TG2 and other numbered isolates). <i>P. celeris</i> TG1 and TG2 were made axenic after isolation. $24 \cdot \tau^{-1}$ is doublings per day.....</p>	69
<p>Table 3. 2 Maximum rates of net oxygen evolution per chlorophyll and per POC (carbon per carbon per hour) for <i>Chlorella</i> and <i>P. celeris</i>. Growth conditions listed indicate whether the cultures were grown dense either under diel illumination or constant illumination at 2000 $\mu\text{moles m}^{-2} \text{s}^{-1}$, or grown dilute (chlorophyll density of the suspension kept generally below 0.5 $\mu\text{g mL}^{-1}$) under 1000 or 2000 $\mu\text{moles m}^{-2} \text{s}^{-1}$ constant illumination. Chl/POC were taken on the same sample as used for P_{max} measurement.</p>	78

ACKNOWLEDGEMENTS

I'd like to thank many of the people in my life that have helped me get this far. First, I'd like to thank Dr. Matthew Posewitz, whose guidance and expertise in algal biotechnology and photosynthesis kept me well fed of incredibly challenging and interesting research. I must thank Dr. Andrew Koppisch whose guidance throughout my undergraduate allowed me to truly develop into the scientist by allowed me to develop my own ideas, experiments, and passions. My lab mates Brian Vogler, Wei Fang, Devin Karns, Melissa Cano, Lyle Sisson, Amy Ashford, Fiona Davies, Katherine Remmerde, and Grace Gamba all provided advice and laughter that will always remind me of Colorado School of Mines. Ed Dempsey, for providing technical advice and training that will serve me well in many positions in the future. Alley York and Jill Murphy provided a great friendship as I first moved to Golden. And always a nod to my best friend back in Flagstaff, Kendall Williams. I'd also like to thank my committee Dr. Brian Trewyn and Dr. Dylan Domaille. There are many others who assisted me along the way who are not listed here but alas know I haven't forgotten your help.

This thesis is dedicated to my mother and father, Patricia and Chris Thomas. There isn't enough time in the world to explain how your love has made me the person I am today.

CHAPTER 1: INTRODUCTION TO ALGAE BIOTECHNOLOGY AND PHOTOSYNTHESIS

1.1 PHOTONS TO FUELS

As global transportation fuel sources deplete from increased fossil fuel harvesting and the harrowing impact of global climate change from dependence on carbon-positive fuels, there has been an increasing effort to utilize biological sources for vehicle propulsion. This effort is categorized as an approach for producing biofuels. Hallmarks of biofuels are carbon-based fuels with a short-term, balanced carbon cycle that doesn't increase the carbon concentration in the atmosphere—linked as the primary cause of global atmospheric heating(Rahman et al. 2017). This balanced carbon cycle is as result of plants fixing carbon dioxide from the atmosphere which is generated into biomass which is treated into usable transportation fuels. This contrasts with draining astronomical amounts of carbon (from ancient biological degradation) beneath of the Earth's surface for combustion into the atmosphere. Through balancing carbon usage and photosynthetically fixed carbon, the energy demand can be satiated by responsible energy generation.

Biofuels can be classified into three distinct generations. The first generation of biofuels is the utilization of common foods with high caloric content in forms of oils or sugars such as corn for corn syrup or canola for oil.(Correa et al. 2017) This intuitive solution takes the same energy humans metabolize for ATP generation for either direct combustion or as a feedstock for microbial fermentation into compounds capable for direct replacement of diesel fuel. The obvious concerns with this approach are first the direct competition between food and energy markets and second the imperfect carbon neutrality. When corn is grown in one place, shipped to a new location for treatment to corn sugar and then further shipped to microbial fermenters, the rate of carbon dioxide release out competes its fixation from the atmosphere. The second

generation of biofuels step away from oily or sugary crops and instead utilize the complex carbohydrate polymers found within the cell walls of woody plants after thorough processing using hydrothermal liquefaction or microbial fermentation to generate combustible fuels(Su et al. 2017)(Gollakota et al. 2018). The gains of the second generation are the move from plowable land to forests of high energy that aren't currently used feeding a growing global population. Although there are improvements from this step, the large amount of required land becomes less economical. This brings us to the third generation, and the focus of this thesis, algal biofuels. The utilization of photosynthetic microorganisms provides the most productive and efficient utilization of photosynthesis to transportation fuels. As shown in Figure 1.1, algae cultivation has a vastly smaller footprint as well as having the ability to utilize arid conditions such as deserts or floating ponds in the otherwise unfarmable oceans (Correa et al. 2017). These advances coupled with the ability to domesticate through breeding and genetically engineer photosynthetic microorganisms provides a capacity to generate a system of using photons to fuels (Lü et al. 2011).

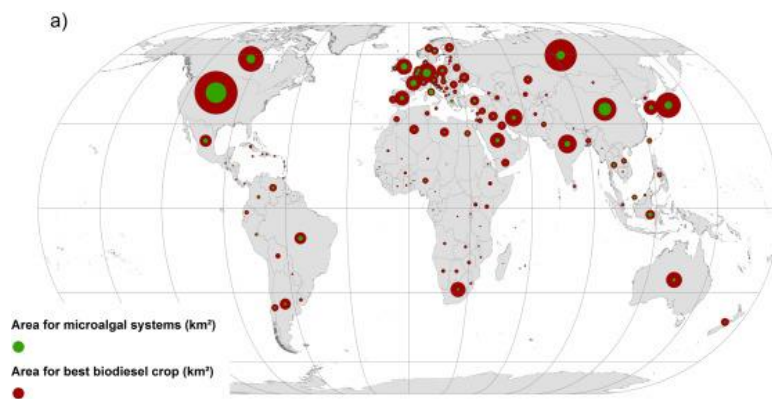


Figure 1. 1 Amount of land area required to meet each country's fuel demands for 2010 estimates. Values compare the best biodiesel crop in the area and microalgal growth systems. (Correa et al. 2017)

1.2 PHOTOAUTOTROPHIC GROWTH TO BIOMASS TO ENERGY

Algae can generate biomass from a carbon in several ways: heterotrophic growth from fixed carbon (sugar, lipids, acetate, etc.), photoautotrophic growth from sunlight and unfixed carbon (CO₂), and mixotrophic growth (CO₂, fixed carbon, and light). To realize the potential of algae, oppose to faster growing heterotrophic bacteria, photoautotrophic growth must be the ideal growth method. Therefore, for high biomass growth rates, algae must have a saturating amount of CO₂, light, and required mineral nutrient.

Beyond photoautotrophic growth, there are several methods of growing algae. For example, the most common—and easiest for laboratory infrastructure—is called batch growth. This requires inoculation of an algal culture at a low density which is then allowed to grow until the culture reaches a dense culture where it then either dies or arrests because of lack of available nutrient, efficient light penetration, or a metabolic signaling. This growth method is demonstrated by the growth curve in Figure 1.2A. This method of growth requires repeated

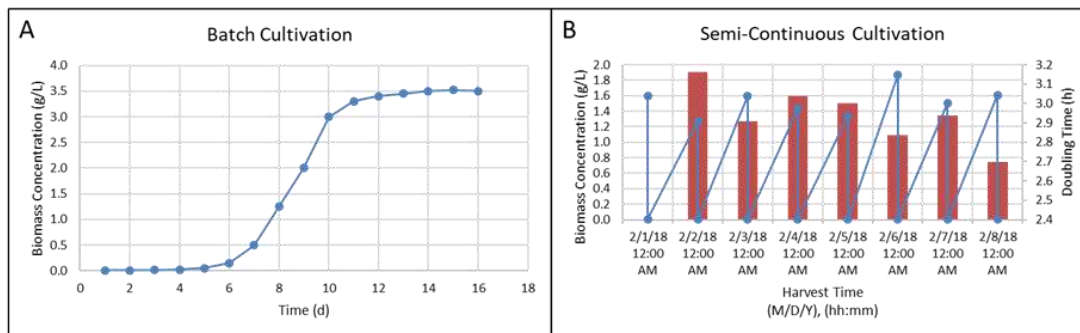


Figure 1. 2 Growth curve examples of batch and semi-continuous growth conditions. A: Batch growth is inoculated at a low density and then allowed to grow through an exponential and then stationary phase. B: Semi-continuous growth dilutes the culture daily and is allowed to regrow each day to maximize harvests daily for processing. Values are arbitrary

harvests and inoculation for biomass. Limitations of the method could come from lags in growth that can often occur from reacclimation to growth environment as well as factors from slow growth once culture reaches high density. Because of this, another method often used in industry, shown in Figure 1.2B, is continuous or semi-continuous growth, where partial harvesting and nutrient replenishment occurs either continuously or at standardized time or density. This method allows the culture to remain in a high biomass accumulating growth rate and avoidance of any reacclimation of the culture to the growth medium or environmental conditions such as light intensity.

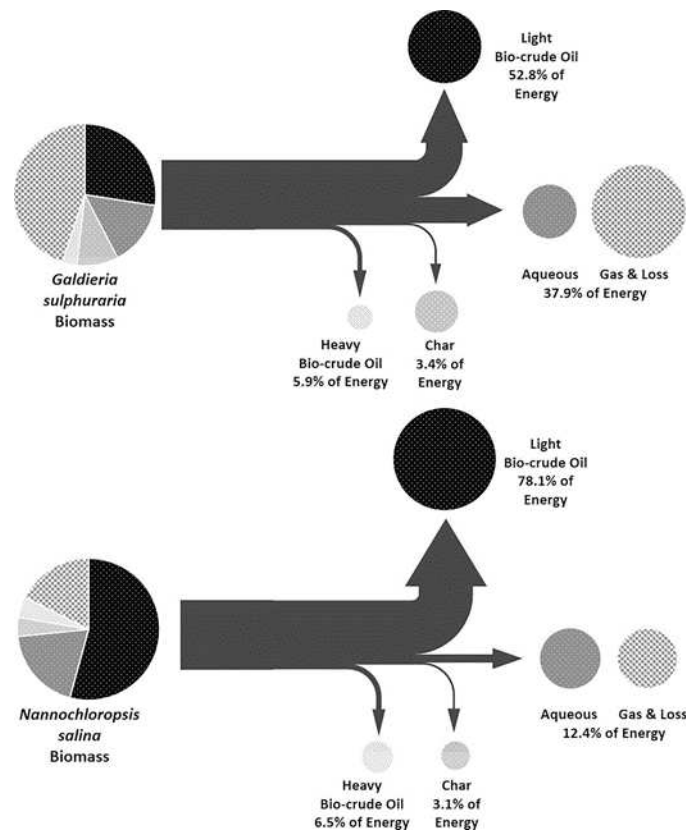


Figure 1. 3 The different biomass partitioning demonstrated by the circle chart affects the quality of energy produced by HTL. As shown, *Nannochloropsis salina* which has a high lipid quantity results in a larger portion of energy dense products than a lower oil content species, *Galdieria sulphuraria* (Cheng et al. 2018).

Also, important for biofuel consideration, is the type of biomass an organism accumulates. Much of the biomass algae accumulates is divided between carbohydrates, lipids, proteins, metabolites, and pigments. From a fuel standpoint, lipids are the idea biomass because of their similarity to diesel fuel. Biomass partitioned as the other heavy hitters also contribute to fuel through the advancement of technology known as hydrothermal liquefaction (HTL) with allows these other constituents to be converted into fuel types such as gas or liquid energy. In Figure 1.3, the flow diagram demonstrates the energy partitioning depending on the oil content of the algae through HTL processing.(Cheng et al. 2018)

1.3 IMPROVEMENTS TO ALGAE

Algae is the product of millions of years of evolution. Evolution generates organisms that are built to compete in an ever-changing environment. As light energy becomes scares, algae have evolved to harvest large amounts of light energy to compete with other organisms who also are absorbing light energy. This evolution has generated organisms capable of absorbing even more light than they can even use to grow, although this ultimately results in the ability for the genetic material to thrive and be passed to progeny(Melis 2009)(Cazzaniga et al. 2014). This is the same for organisms such as wheat built to store prolamins, a storage package of nitrogen, so in times of scarcity, there is a supply so the organisms do not die(Yu et al. 2017). Evolution has generated many of these mechanisms for algae to survive in the wild. But for the photons to fuels plan to work, millions of years of evolution must be untethered, so their biology can flourish in an environment where nutrient and light limitations do not exist. This is analogous to the domestication of wolves to dogs where they no longer have predators or direct competition for food. Algae must be domesticated to utilize the complexity of biology to generate biomass in industrially relevant growing conditions oppose to competitive ones.

To domesticate algae, there are three main methods: selection, directed evolution, and genetic manipulation(Radakovits et al. 2010). These will be further described below but in short, selection is a way of isolating wild algae strains predisposed to perform well in industrial environments, directed evolution is a means to evolving algae under conditions you intend to grow them in, and genetic manipulation is the direct change in genetics of organisms for specific beneficial phenotypes.

1.3.1 SELECTION

For algal organismal selection, the desire is for very fast growth rates under industrially relevant conditions such as high light, high temperature, and high salinity as well as the potential for high value storage products such as lipids or pigments.(Elliott et al. 2012) (Ratha and Prasanna 2012; Steinrücken et al. 2017) Therefore, estuary tidal waters with shallow waters provide these conditions are optimal bioprospecting locations where the water is has a short light pathlength as well as warm temperatures. Samples from these regions can then be utilized for an aggressive selection regiment where cultures are regularly diluted under dilute conditions where algae culture grow the fastest. Over time, slow growing algae are diluted out of existed and the most dominant population are the algae capable of fast growth in this environment. Through this selection, algae strains can be isolated that are predisposed for fast growth in industrially relevant conditions. This is a typical method for isolating strains for industrial value. These strains are then characterized to determine their suitability for biotechnology and can be further subjected to directed evolution or genetic manipulation.

1.3.2 DIRECTED EVOLUTION

After an organism has been selected that has advantageous attributes, directed evolution can be utilized to improve these alga in phenotypes it may not already have. For example, the

organism may be a fast grower, but it may not make enough lipids or even may be a fast grower, but under high oxygen concentration—often present in actively growing outdoor ponds—it may decrease its growth rate. For these phenotypes where a simple genetic switch may not be easily induced, directed evolution can play a role.

Evolution is a big numbers game where many organisms over long periods of time, slowly change their genomes through genetic drift, mutation, or random occurrence. To utilize this in the laboratory, there are several methods of speeding this up into an organism with desired phenotypes. For example, UV light is known to cause modifications in an organism's genome—sometimes lethal, sometimes beneficial. Also, CRISPR-Cas9 has been shown to generate edits in an organism's genome. These techniques can be utilized to cause mutations in the genome under selective conditions which allow strains to be evolved into certain directions on a faster time scale (Umeno et al. 2005; Jakočiūnas et al. 2017). This has been leveraged in many laboratories for mutating algae to make less pigmented or high lipid algae if there is a sufficient method of screening a library of mutants (Work et al. 2013; Davies et al. 2015).

1.3.3 GENETIC MANIPULATION

The prior two methods require an untargeted approach to achieve genomic changes that based on good selection parameters provides desired phenotypic improvements. Genetic manipulation requires an understanding of metabolism to make targeted changes that are believed to improve phenotypes. Genetic manipulation required an addition or removal of genetic material such as adding a gene that will increase starch production or removing a gene that degrades starch—both with the hopes of a high starch accumulation phenotype. These manipulations are done through random insertion of DNA into the genome or through the newer technology known as CRISPR-Cas9 (Gonzalez-Ballester et al. 2011; Larkum et al. 2012a; Poliner

et al. 2018). CRISPR has allowed for targeted genome editing where a protein, Cas9, locates a part of the genome to make a cut, and then inserts a new piece of DNA into that location. Therefore, through genetic modification a genome of a wild alga can be rewired into a domesticated alga capable of high biomass yields for biofuel purposes.

1.4 CLASSICAL ALGAL RESEARCH

Research of photosynthetic microorganisms has centered primarily on *Chlamydomonas reinhardtii*. *C. reinhardtii* is a freshwater organism isolated from a potato farm in Amherst, MA in 1945. The organism grows well at 20-25 °C, under low light conditions, both autotrophically and heterotrophically on acetate. These conditions are well suited for laboratory growth. Additionally, *C. reinhardtii* has been shown to reproduce asexually and sexually. Since the development of this strain, it has become the primary model organism for photosynthesis research and eukaryotic algae (Stern et al. 2008).

Since the development of this strain, genomic, transcriptomics, and proteomics data has become available (May et al. 2008). Additionally, molecular tools are now available for facile protein, nucleic acid, and storage compound characterization (Kindle 1990; Shimogawara et al. 1998; Posewitz et al. 2004; Work et al. 2010). This has led to efficient gene knockouts which are now available in full knockout libraries for biochemical study. With many laboratories focusing on this strain, elegant and thorough analysis has been done on this organism with the hopes of transferable knowledge to many other photosynthetic microorganisms.

One detriment of the study of this strain is this organism has been maintained through serial passage of the organism grown on agar plates. Although this allows easy maintenance and health of the culture, there has been documented concerns of genetic drift (Bell and Reboudt 1997). Labs have shown that as the organism is repeatedly streaked on agar plates, their genome

has changed over the decades to grow fantastic in laboratory conditions while evolving the strain to lose competitive phenotypes in exchange for weaker, laboratory phenotypes.

Because *C. reinhardtii* has been so well characterized, it is the strain utilized in my study of photosynthetic effects caused by of carbon storage stress in Chapter 2.

1.5 INDUSTRIAL ALGAE

To grow algae for biofuel purposes, there must be a minimization of nutrient input, and a maximization of biomass output. Algae requires light, carbon, minerals, and water to grow. To minimize the price of these input, light energy must be harvested from intense sunlight outside instead of expensive LEDs. Carbon should be sequestered from the ever-growing concentration of CO₂ in the Earth's atmosphere. Minerals should fertilize the media in optimal amounts. Lastly, another appeal of algae is their ability for growth in saltwater where our natural supply in the ocean is high and it has no direct competition with human usage of freshwater. The first realization from these desired phenotypes is that the ideal biotechnology alga is not *C. reinhardtii*. A new alga of industrially relevant phenotypes must be collected and then characterized chemically, physiologically, and then molecular toolkits developed for facile genetic manipulation.

Of the inputs listed, the seawater, CO₂, and fertilizer are of the easiest to build around as they come cheaply and abundantly. The most difficult it turns out, is finding a high light organism that grows quickly. Engineers have clever approaches to mixing seawater ponds, delivering adequate CO₂, and providing regular harvesting to supply nutrients. What remains the challenge, and what will be discussed in Chapter 3 is how to bioprospect for a high-light alga and then characterize that organism for industrial purposes.

1.6 PHOTOSYNTHESIS

Photosynthesis is the process within the chloroplast which utilizes light energy to move electrons from water to carbon dioxide to make organic molecules. This is assisted by the generation of ATP which is used for overcoming energy barriers by coupling its downhill process of ATP hydrolysis to an endothermic process such as building molecules. In more detail described below, light energy is absorbed by pigments within the alga that is then delivered to photosystems I & II where electrons are removed from water in the oxygen evolving complex.

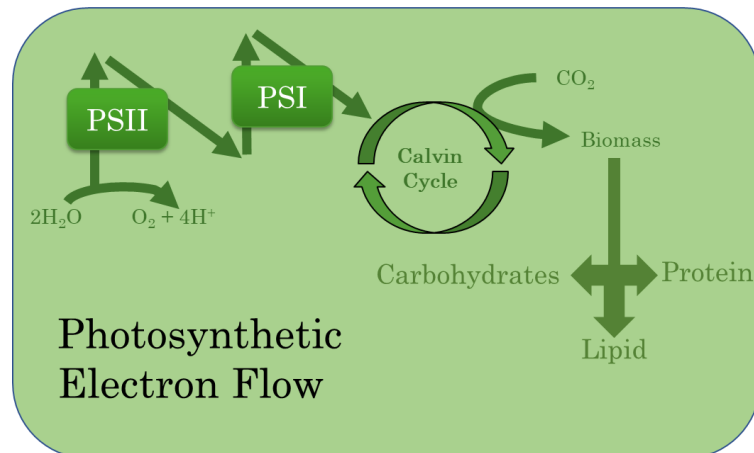


Figure 1. 4 Overview of photosynthetic electron flow. Electrons are liberated for water which are moved through photosystem II and photosystem I. That reductant is utilized in the Calvin-Benson-Bassham Cycle to fix Carbon dioxide. Carbon is then partitioned into proteins, lipids, and carbohydrates

Electrons are then moved through photosystems I & II until placed onto an electron donor molecule, NADPH. Additionally, in the oxygen evolving complex, protons are removed from water which establish a proton gradient within membranes of the chloroplast. This proton gradient creates a proton motive force (pmf) which is used to drive ATP synthesis. NADPH and ATP are then used in the Calvin-Benson-Bassham Cycle where they are used to fix CO_2 onto a

metabolite ribulose biphosphate. From here intermediates enter primary metabolism where energy is utilized or stored.

1.6.1 LIGHT HARVESTING

Pigment molecules are arranged within the chloroplasts of photosynthetic microorganisms. These molecules play the role of absorbing light in the visible region (390nm-700nm) of the light spectrum and through energy transfer, delivering it to the P680 enzyme in photosystem II. There are three main pigments in green algae arranged to absorb and deliver light energy: chlorophyll a (chl a), chlorophyll b (chl b), and carotenoids(Von Wettstein et al. 1995). Chl a is the primary pigment that absorbs light energy and directly delivers to the photosystems while Chl b while also delivering energy is associated with a photosynthetic antenna responsible optimizing photon capture. Carotenoids play a role throughout not only the chloroplasts but also in the cell wall absorbing light energy for various functions not limited to photosynthesis.

The photosynthetic antenna is a dynamic structure built with antenna proteins coated with chlorophyll molecules that allows the cell to absorb the greatest amount of light available. These structures on the membrane of the chloroplasts often strut out and absorb light energy to allow for adequate light absorbing competition under low light conditions. When algae are moved from low light to high light conditions, antenna structures are downregulated in several different ways depending on the alga. Some algae decrease expression of antenna proteins and chl a & b biosynthetic pathways as well as photosynthetic systems to avoid light saturation and light-induced damage(Melis et al. 1998; Fang et al. 2012; Choi et al. 2016). Another form of light absorption regulation is to only disassemble their antennas while leaving photosystems with chl a

attached: this is a desirable phenotype as it allows organism to maintain high levels of photosynthesis without absorbing too much light energy.

Organisms that absorb a high number of photons—more than their photosystems can utilize—result in several detrimental effects. Excess light energy in antenna structures that are unable to deliver their energy to reaction systems result in fluorescence or heat energy dissipation (Perrine et al. 2012). This is the safest option for the photosynthetic microorganisms as the light energy is safely returned to the ground state although in mass culture it results in a decrease in overall photosynthetic efficiency. Additionally, if very high light energy is absorbed, this can result in the production of reactive oxygen species within photosystems (Saroussi et al. 2016). The radical species produced can cause damage within the cell that results in an overall decrease in photosynthetic efficiency as the cell must now utilize resources to ameliorate these harmful products.

1.6.2 OEC TO PQ POOL TO NADPH

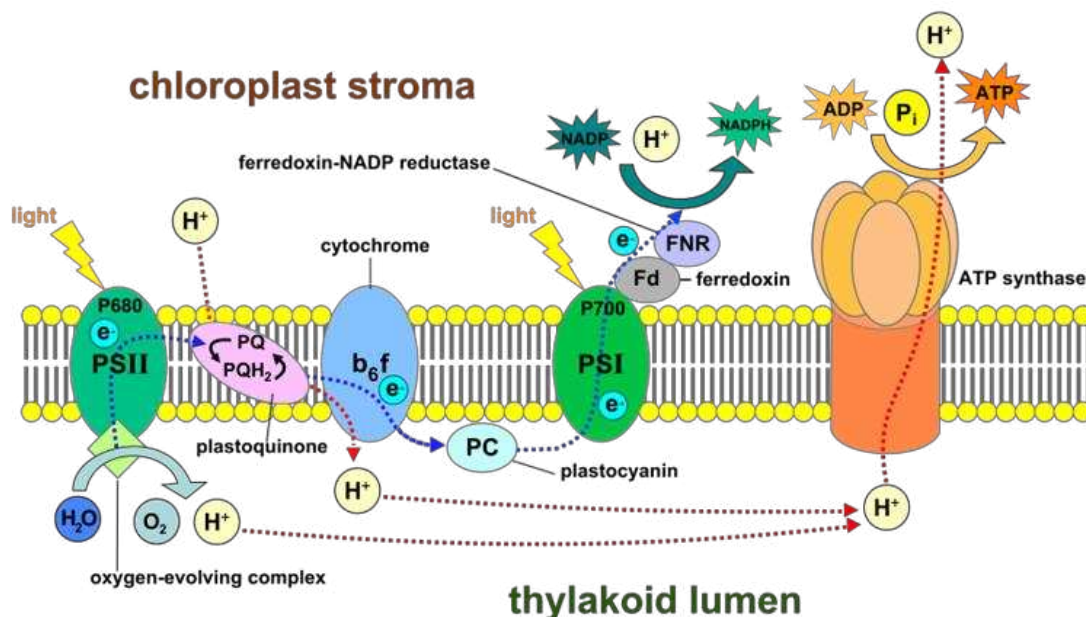


Figure 1. 5 Linear electron flow in photosynthesis is depicted by the blue line which ends at NADPH to be utilized in the Calvin-Benson-Bassham Cycle. The red line depicts the proton motive force being pumped by ATP synthase for ATP production used by the Calvin-Benson-Bassham Cycle (Wikipedia).

After light energy is absorbed by chlorophyll-like pigments, it is transferred to two reaction centers aligned in tandem. Through linear electron flow, shown in Figure 1.5, light energy is absorbed by P680 in Photosystem II which excites electrons liberated by the oxygen evolving complex. The high energy electron is then transferred down an energy gradient through several electron carriers: pheophytin, primary & secondary plastoquinone, cytochrome b6f complex, plastocyanin, and then P700. P700 is the start of Photosystem I (PSI). PSII is separated into two classifications the donor and the acceptor side. The donor side includes the oxygen evolving complex and P680 as these enzymes participate in the donating of electrons to PSII and the generation of their energy from light absorption. The acceptor side includes pheophytin, primary & secondary plastoquinone, and the cytochrome b6f complex. When electrons are transferred to plastocyanin and P700 the electrons are on the donor side of PSI. This reaction center absorbs light energy and excites the electron it received and again the electron moves downhill through several electron carriers: a chlorophyll-like molecule, phylloquinone, iron-sulfur protein, ferodoxin, and finally ferodoxin:NADP⁺ oxidoreductase. These enzymes make up the PSI acceptor side. The last enzyme catalyzes the reaction to generate NADPH. NADPH is an intermediate electron acceptor which is an electron wallet of sorts—capable of transferring its currency throughout the cell to generate new chemical bonds for energy storage or use.

Over the course of this process, ATP is also generated by utilizing the protons from oxidized water to generate a proton motive force (pmf). This pmf drives ATP production from an ATP synthase within the thylakoid membrane of the chloroplast. ATP provides the entropic power to catalyze thermodynamically unfavorable reactions through coupling to the downhill reaction of ATP hydrolysis.

1.6.3 CALVIN-BENSON-BASSHAM CYCLE TO CARBON STORAGE

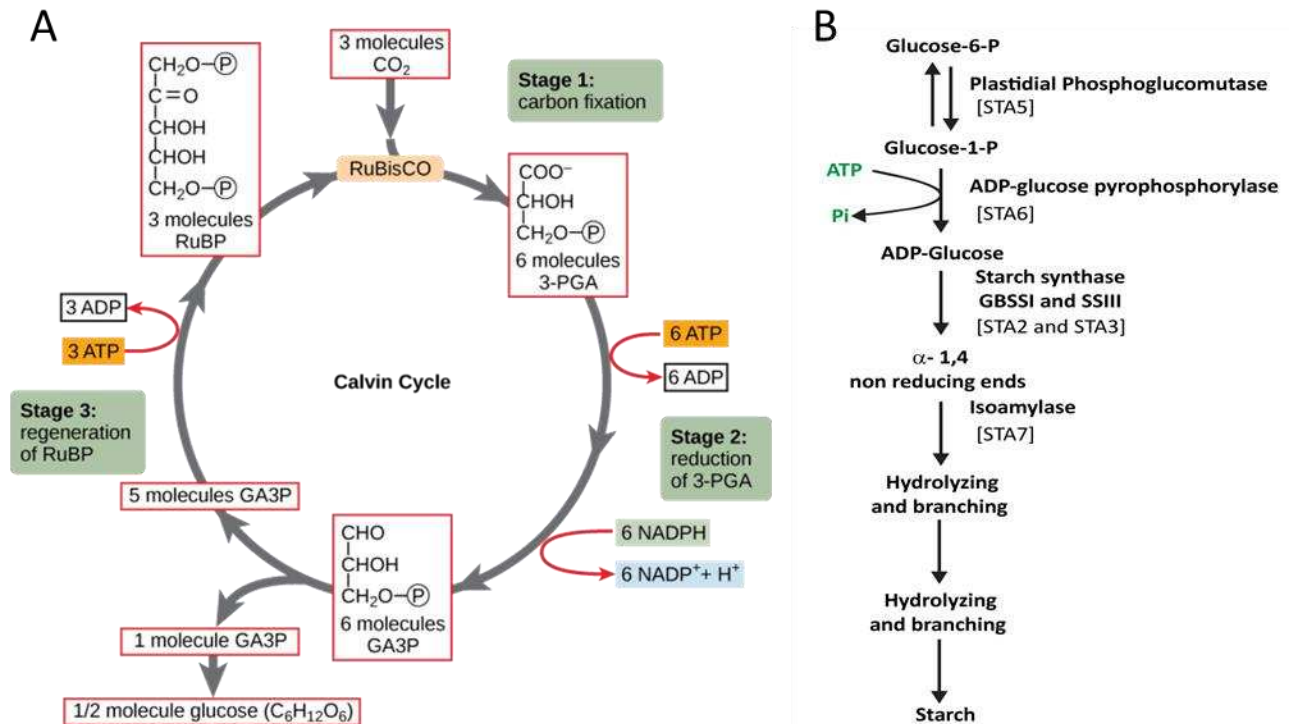


Figure 1.6 Metabolism of the Calvin-Benson-Bassham Cycle fixation (A) of Carbon dioxide into generation of GA3P which is metabolized into glucose. (B) Glucose is then polymerized in starch. The STA6 gene is responsible for the rate limiting step in starch synthesis. Figure modified from Lumen and Shai Saroussi.

With NADPH and ATP, to produce carbon-based biomass, carbon is needed. To do this oxygenic photosynthesis has the Calvin-Benson-Bassham Cycle to fix carbon dioxide from the atmosphere and incorporate it into metabolites. One of the important roles of carbon is its storage as retrievable energy in the forms of lipids or carbohydrates. Figure 1.6 outlines the pathway from CBB to storage as polymerized sugar: starch.

1.7 PHOTOSYNTHETIC PHENOTYPING

Although all algae may be photosynthetic, their photosynthetic characteristic vary by strain, environment, or genetic manipulation(Krishnan et al. 2015). Therefore, it is critical to phenotype these changes under constant conditions to understand the robustness of its

photosynthetic capacity. To understand light harvesting capability, measuring the antenna size, absorption cross section, or amount of fluorescence of pigments can provide valuable information. Also, measuring the net oxygen evolution rate provides an overall estimate of photosynthetic usage. Lastly, dissecting rates of individual enzymatic rates along the photosynthetic chain provides valuable information on how these organisms may regulate electron flow under different conditions. Measuring many of these parameters also are coupled with artificial electron acceptors or inhibitors which provide improved resolution on photosynthetic changes between organisms and environmental conditions. These measurements will be explored below.

1.7.1 PHOTOSYNTHETIC KINETICS

Kinetics is the study of the speed of reactions in chemistry. By measuring the rate at which photosynthetic reactions occur in algae, each alga can be compared to determine the differences between alga or the effects of some stimuli. Understanding the rate at which net photosynthesis occurs is an important variable to determine the overall ability for an organism to capture energy for usage in growth or chemical production.

1.7.1.1 PHOTOSYNTHETIC IRRADIANCE RESPONSE CURVE

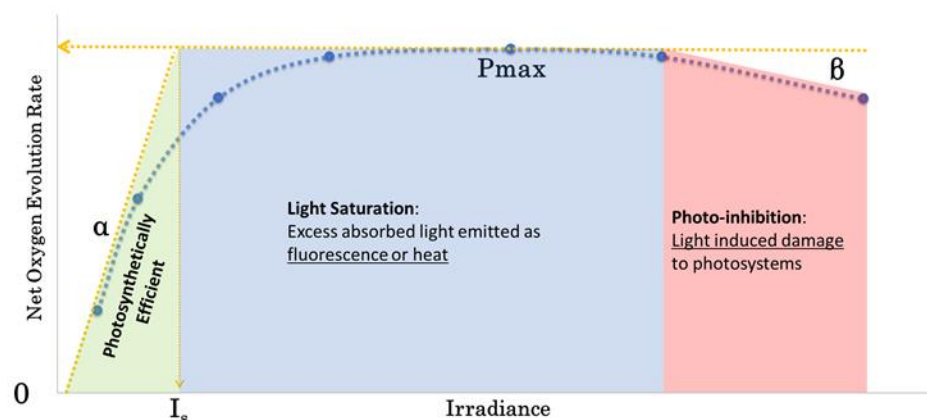


Figure 1. 7 Photosynthetic Irradiance Response Curve relates net oxygen evolution rates to radiance levels.

Oxygen evolution is an effective measurement of net photosynthesis for algae. For each mole of oxygen evolved from the cell, two moles of water were oxidized and electrons were liberated for electron flow. Although there are other reactions, that uptake oxygen in the light (ptox, aox, respiration, etc.), by measuring this net value, there can be an estimate of the overall productive use of electrons by photosynthesis.

A photosynthetic irradiance response curve (PI Curve) is the common way to measure the amount of net oxygen evolution by an algae culture. The PI Curve shown in Figure 1.7, is a titration of light on a culture of optically dilute algae to understand the relationship of net oxygen evolution to light energy. Several different values are calculated from this curve including the photosynthetic maximum (P_{max}) which dictates the highest rate of net oxygen evolution. Alpha (α) which is the slope of the initial line which dictates the photosynthetic efficiency of harvesting light energy and then using it for photosynthesis. The saturating irradiance (E_k) which is the intersection of alpha and P_{max} and dictates the light level in which photosynthesis is no longer linear with light intensity and is instead saturated. After this light intensity, light energy is instead managed instead of used for photochemistry. At high light intensities, there is resulting photodamage that results in a decrease in net oxygen evolution noted at beta (β). Also, in between each light intensity where light is irradiated on a culture for a set time, is a dark period. In the dark, oxygen is consumed through mitochondrial respiration. The oxygen consumption rate is often also included on a PI Curve to indicate the rate of respiration occurring at each light intensity. Although the rate cannot be measured directly, this rate is utilized as an estimation of this value. Through PI Curves, an alga's photosynthetic capacity, efficiency, and response to

different light intensity can be evaluated under different genetic stresses which will be evaluated in Chapter 2.

1.7.1.2 LIGHT INDUCED OXYGEN UPTAKE

PI Curves have their limitations to evaluating the photosynthetic ability of algae. For example, is a decrease in net oxygen evolution the result of decrease in water oxidation (gross production) or is there a concurrent oxygen uptake that is intercepting electrons in an oxygen uptake reaction before they reach the CO₂ fixation in the Calvin-Benson-Bassham Cycle? This can occur if electrons are liberated from the plastoquinone pool by pto_x or through a Mehler-type reaction at ferredoxin or if RuBisCO's cross-reactivity fixes oxygen instead of CO₂ (Asada; Heyno et al. 2009; Cousins et al. 2010; McDonald et al. 2011; Krieger-Liszkay and Feilke 2015; Curien et al. 2016). These inefficiencies are activated often when downstream pathways are clogged or not available for some reason which can occur for several reasons: commonly nutrient deprivation, genetic manipulation or oxygen saturation.

The technical issue with measuring this oxygen uptake in the light is because simultaneous oxygen uptake and evolution will not resolve on a standard Clark electrode used for oxygen measurements. Therefore, to measure this difference a mass spectrometer coupled through a gas-permeable membrane inlet is utilized. This allows for the use of an artificial ¹⁸O₂ background. Then by monitoring m/z 32 and 36, the kinetics of oxygen produced from water oxidation (m/z=32) and oxygen consumption (m/z=38) can be simultaneously measured. Then utilizing the following equations, rates can be calculated while considering the competition of decreasing O¹⁸ as ¹⁶O₂ is evolved: $\downarrow O_2 = \Delta^{18}O_2 \cdot (1 + [^{16}O_2]/[^{18}O_2])$ and $\uparrow O_2 = \Delta^{16}O_2 - \Delta^{18}O_2([^{16}O_2]/[^{18}O_2])$ (Beckmann et al. 2009b). The scoreable phenotype can then be monitored

with genetic knockouts or enzyme inhibitors to locate the source of inefficient electron usage. This will be further explored in Chapter 2 in a starchless mutant of *C. reinhardtii*.

1.7.2 REDOX PROPERTIES ELUCIDATE ELECTRON FLOW AVAILABILITY

Photosynthesis has a primary role is oxidizing water and moving those electrons up- and downhill energetically towards NADPH where it is later utilized in reducing CO₂. By measuring the redox properties of various aspects along linear photosynthetic electron flow, photosynthesis can be characterized. For example, regions of electron transport which are overly reduced may suggest a blockage at that point. That the electrons build up in this region before transferring electrons downstream. These characteristics are primarily characterized through fluorescence techniques. As stated earlier, if excited electrons are unable to be transferred for long periods of time, they instead are given off as heat and fluorescence. Therefore, it becomes important to measure this fluorescence. The technique utilizing Pulse Amplitude Modulated Fluorimetry, provides insights into the redox state and efficiency of linear electron flow in photosynthesis.

1.7.2.1 PULSE AMPLITUDE MODULATED FLUORESCENCE TECHNIQUES

As previously stated, it is important that the amount of light harvested by an algal cell is used for photochemistry in the form of oxidizing water and generating ATP and NADPH. It is generally understood that as a cell becomes nutrient limited, a cell regulates photosynthesis by absorbing less light energy or transferring less of it to its reaction centers.

Although light is absorbed by the cells, to measure the amount reaching reaction centers, it is important to consider the light energy absorbed can either be transferred to reaction centers or if it remains in the excited state too long, it will be lost to heat or fluorescence.

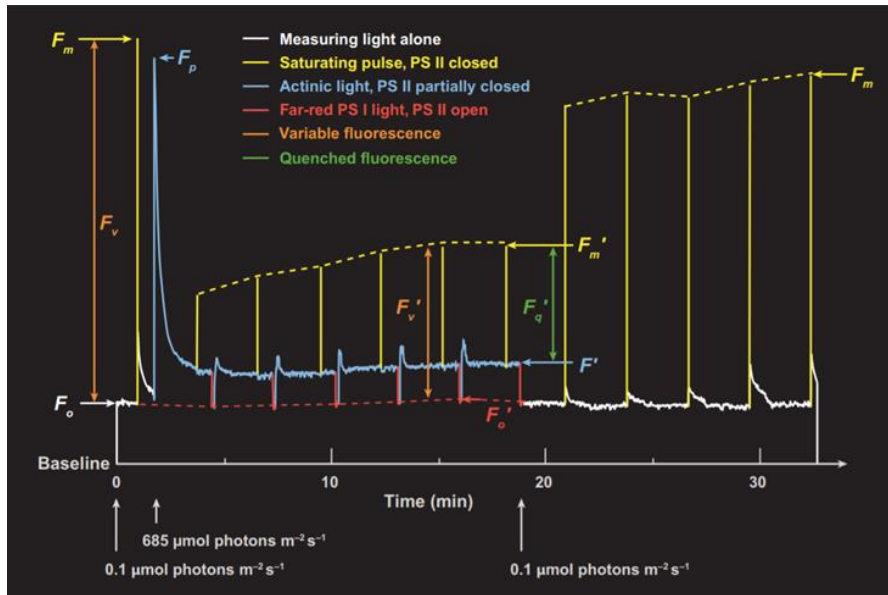


Figure 1.8 Pulse Amplitude Modulated Fluorescence experiments are performed in this way. Relevant parameters are labeled in the image.

By measuring fluorescence of an algal solution, several parameters can be measured to evaluate photosynthetic efficiency and redox properties of the quinone pool. To do so, there is a method called Pulse Amplitude Modulation Spectroscopy, in which the fluorescence of the cells is measured under different conditions including pulsed saturating light, dark periods, and at a constant irradiance. In Figure 1.8, the typical light scheme is demonstrated as well as several photosynthetic parameters (Baker 2008).

Using the equation: $\Phi_{PSII} = (F_m' - F') / F_m'$, the maximal photosynthetic efficiency of PSII is measured (Maxwell and Johnson 2000). This is a parameter that estimates the amount of light energy absorbed by chlorophyll that is utilized for photochemistry. This value is important

to realize if the light absorbed is being utilized for photosynthesis instead of simply fluoresced. This has an inverse relationship with light intensity because at higher light intensities, as reaction centers become saturated, more light is often fluoresced. It can also indicate if there is a backup on the donor side of PSII. This parameter is the difference in variable fluorescence under a certain light intensity and its maximal amount of fluorescence. The maximal amount of fluorescence is acquired by the fluorescence measured when a very fast saturating flash is utilized where the light isn't on long enough for the energy to be transferred to the reaction centers and is therefore fluoresced. This difference is then divided by the amount maximal amount of fluorescence from a saturating flash. Therefore, the maximal photosynthetic efficiency is the amount of light energy not used for fluorescence (used for photochemistry) divided by the amount of light it can possibly every utilize. Therefore, as light intensity increases more light is fluoresced instead of used for photochemistry and this parameter decreases.

Photochemical quenching, q_L , is calculated through the equation $(F_q'/F_v')*(F_o'/F')$ and is the measurement of the degree to which PSII is open—that is, whether the first electron acceptor Qa oxidized and ready to receive electrons. This measurement is done by a measurement of the fraction of F_q , which is the amount of photochemical activity (light energy not fluoresced, the numerator from Φ_{PSII}) and F_v which is the amount of photochemical activity possible (amount of total fluorescence possible in the dark following a saturating pulse). This parameter is actually known as qP and when divided by (F_o'/F') the value scales more true to the actual amount of photochemistry occurring which isn't actually linear with light energy which would be suggested if each reaction center had its own antenna (Kramer et al. 2004a; Lambrev et al. 2012). Reaction centers share antennas and compete for light energy.

1.7.3 MEASURING OPTICAL PROPERTIES OF ALGAE

The optical properties of an alga is a phenotype that relates to overall photochemical light absorption. Because photoautotrophic growth is a function of light absorption in a solution, it is important to realize the amount of light absorbed by a sized cell with an amount of pigment and amount of biomass.

1.7.3.1 CELL SIZE AND OPTICAL CROSS SECTION

The most obvious optical property of an algal cell is its size. Using a light microscope, the cell diameter can be measured. The cell size has important qualities related to its ability to harvest light and the kinetics of gas permeation. The next relevant parameter is the cross section of an alga which determines the amount of light it absorbs. By measuring the light absorbed by a solution of algae cells and then dividing by some factor that represents the cellular content such as particulate of organic carbon or chlorophyll, there is a metric of the amount of light absorbed by the cells. Then in a solution at some incident light, an estimate of the light absorbed by the cell can be determined. This is particularly useful in optically dilute cultures, in which the amount of incident light can be related to the amount of light absorbed.

1.7.3.2 FUNCTIONAL CROSS SECTION (ANTENNA SIZE) AND QUANTUM REQUIREMENT

To evaluate an alga's ability to harvest light energy to produce photochemical products, the quantum requirement and functional cross section allow for this quantification. The quantum requirement is a measurement of quanta required for every product formed. The higher the quantum requirement, the more light energy needed to be harvested to do photochemistry. Additionally, the functional cross section is a measurement of the alga's antenna system which indicates the amount of light energy harvested for the amount of incident irradiance.

The quantum requirement is measured in its easiest way through a relationship between the specific growth rate, the amount of carbon produced per amount of carbon per time, and the amount of light absorbed by the carbon in the organism per hour. Through some unit conversion, the amount of light energy per unit of carbon produced can be evaluated for this parameter.

The functional cross section is measurement of light absorption actually utilized compared with the optical cross section which is a measure of the light absorbed. The historic method is the measure the yield from different intensities of flashes in the form of oxygen evolved per flash intensity. The slope of this increase in yield is known as the functional cross section. Because this methodology is low-throughput, the modern method involves coupling this concept with fluorometry. By utilizing fluorescence, in section 1.7.2.1, a measurement of electron turnover can be modeled at different light intensities. By relating the change in electron turn over per intensity of light, an estimate of functional cross section, or antenna size, can be measured in a facile manner.

1.7.4 GROWTH METRICS OF ALGAE

Algal biotechnology is concerned primarily with the production of biomass from algae cultures. This is measured in several different manners in relation to maximal reproduction velocity and biomass production rates in a given volume or area. Because outdoor algal growth is contingent on light absorption on an area of land, biomass growth rates also are given in terms of area of land to best estimate land usage outside.

1.7.4.1 MAXIMUM SPECIFIC GROWTH RATE

Specific growth rate utilizes the following equation to determine to overall velocity of growth of an algal culture: $\mu = (\text{Ln} [\text{Initial Concentration} / \text{Final Concentration}]) / \text{elapsed time}$. For an algal culture, to measure the maximal growth rate, optically cultures are grown semi-

continuously under saturating lighting conditions. This maximizes growth rate by allowing all cells in the culture to be in a high light acclimated state which prevents antenna growth and excess fluorescence resulting from wasted light usage. Additionally, it is best to express biomass in terms of carbon concentration oppose to entire biomass to prevent organismal diversity in mineral accumulation.

To cross validate the maximum specific growth rate, instead of utilizing biomass growth, it can also be calculated from maximum photosynthetic rates. Using the PI-Curve from section 1.7.1.1, the P_{\max} evolution rate can be related to the photosynthetic quotient to determine carbon fixation over a period to estimate overall growth. The photosynthetic quotient is an estimate of the amount of moles of oxygen evolved for every mole of carbon fixed. This relationship is expressed by the equation: $\mu_{\max} = P_{\max} \cdot (1/PQ) \cdot \text{MW of Carbon} \cdot \text{Chl/C}$. Through cross validation, the specific growth rate can be validated as well as the photosynthetic measurement assays as representative of growth instead of an artificial assaying environment.

1.7.4.2 BIOMASS PRIMARY PRODUCTIVITY

Although algae may have a high maximum growth rate, this growth rate doesn't always transition into a large amount of biomass production. For example, if an alga divides very quickly while dilute but slowly when the population is denser, that the overall biomass production is low. The common equation for biomass productivity is as follows: $P = (C_f - C_i) / \text{elapsed time}$. Although this equation covers the production rate of a solution of algae, because algae's growth is contingent on light absorption, it's productivity rate is relative to an area like traditional agriculture. The primary measurement of algae productivity uses the equation: $P = [(C_f - C_i) / \text{elapsed time}] * \text{depth from light penetration assuming a rectangular vessel}$.

1.8 THE FOCUS ON PHENOTYPING PHOTOSYNTHESIS IN MODEL AND NON-MODEL PHOTOTROPHS

The focus of my thesis is in two parts: the study of photosynthetic electron valve usage of *Chlamydomonas reinhardtii* under anabolic sink stress from a starchless mutation. Additionally, this thesis focuses on the photosynthetic characterization of a new industrial alga, *Picochlorum celeri*.

1.8.1 STARCHLESS MUTATION IN *C.REINHARDTII* CAUSES PHOTOSYNTHETIC AND METABOLIC CHANGES

As photosynthetic organisms encounter different factors of abiotic and biotic stresses that limit growth, there must be mechanisms to regulate photosynthesis. As the light reactions of photosynthesis generate photosynthetically derived electrons, when growth is limited or cells are shifted from dark to light, electrons cannot always reach the terminal electron acceptor CO₂ and therefore must be rerouted to prevent the formation of reactive oxygen species (ROS) which is generated from the Mehler reaction. The Mehler reaction donates electrons from electron carriers to oxygen which generates harmful ROS. In order to safely transition excited electrons to the ground state, several enzymes are utilized which can reduce oxygen to water without ROS formation. These reactions are known as water-water cycles. Two of these cycles will be explored in this thesis which are catalyzed by the flavodiiron proteins and the plastid terminal oxidase.

In Chapter 2, energetic electron photochemical quenching will be investigated under absence of a sustainable sink caused by the inability to store polymerized carbon. Without the ability to quench electrons through carbon storage or growth, electrons must be quenched through unsustainable sinks that ultimately lose the chemical bond energy generated from photosynthesis.

In the biosynthesis of starch, ADP Glucose Pyrophosphorylase in the STA6 locus of *C.reinhardtii*, is the rate-determining step. Previously, a sta6 mutant has been generated that is unable to synthesize starch and has been characterized by no detectable starch. This mutant has generated interest because of its diminished photosynthetic capacity resulting from its metabolically downstream mutation. It has a decreased amount of net oxygen evolution and as well as linear electron flow. Previously, it was hypothesized that the diminished capacity was a result of low quantities of Pi and Mg²⁺ that act as activators of the Calvin-Benson-Bassham Cycle's RuBisCO (Krishnan et al. 2015). It was speculated that because of the generation of ATP from the pmf but not being consumed by starch synthesis, enzymes involved in Calvin-Benson-Bassham Cycle's carbon fixation would be downregulated and therefore feedback inhibit linear electron transfer. Also speculated was that a water-water cycle likely plays a role because of the saturation of net oxygen evolution occurs at a lower light level than the saturation of linear electron flow. This would indicate that even as net oxygen evolution reaches its maximal, electron flow continues to increase. This would be a prime situation where electrons instead of reaching CO₂, is being rerouted to oxygen uptake.

This thesis will go on to investigate the mechanisms by which the sta6 mutant diminishes energetic electrons as it copes with the inability to utilize starch synthesis as a sustainable sink which utilizing a variety of flavoproteins and plastid terminal oxidases to shift electrons onto oxygen as a terminal electron acceptor.

1.8.2 BIOPROSPECTING AND PHOTOSYNTHETIC CHARACTERIZATION FOR INDUSTRIAL APPLICATION

Many of the prospects of algae biotechnology have still been unrealized because of the loss in productivities when algal growth is scaled up. For example, algae cells are either

intolerant to seawater which dramatically increases the cost of production or their growth is inhibited by high light levels. These issues have long been sought to be changed by applying directed evolution or genetic manipulation strategies. The focus of Chapter 3, will be process sought to isolate a new saltwater alga with promising growth and growth condition phenotypes. The process led to the isolation of *Picochlorum celeri*.

This chapter will introduce the new organism that was harvested through high light selection for fast growth using a collection of estuarial saltwater. The consortium was directly evolved in the laboratory over months through rigorous dilution regime under dilute culture conditions in high light. This methodology led to an improvement of photosynthetic capacity and growth rates that led to the Texas Gulf 2 (TG2) which has of one of the highest growth rates ever reported by eukaryotic algae. After this isolation, it was characterized photosynthetically, optically, and growth metrics.

CHAPTER 2: ALTERNATIVE OUTLETS FOR SUSTAINING PHOTOSYNTHETIC ELECTRON TRANSPORT DURING DARK TO LIGHT TRANSITIONS

The following chapter contains text from (or adapted from) the submitted manuscript of the same title in *Proceedings of the National Academy of Sciences*.

Shai Saroussi¹, Devin A. J. Karns², Dylan C. Thomas², Matthew C. Posewitz², Arthur R. Grossman¹

¹The Carnegie Institution for Science, Department of Plant Biology, 260 Panama Street, Stanford, CA 94305, USA

²Department of Chemistry, Colorado School of Mines, Golden, CO 80401, USA

2.1 ABSTRACT

Light fluctuations and other environmental stresses dramatically impact the balance between the production of photosynthetically-derived electrons and the activity of the Calvin-Benson-Bassham Cycle (CBBC); an imbalance can promote reactive oxygen production and cell damage. Hence, photosynthetic organisms have developed several strategies to avoid photo-damage by routing electrons towards alternative outlets. In this work we explore the activities of three essential outlets associated with *Chlamydomonas reinhardtii* photosynthetic electron transport: (1) reduction of $O_2 + H^+$ to H_2O through Flavodiiron proteins (FLVs) and (2) the Plastid Terminal Oxidases (PTOX), and (3) the synthesis of starch. Real time measurements of O_2 exchange have demonstrated that FLVs likely immediately engage during dark to light transitions, allowing electron transport when the CBBC is not fully activated. Under these conditions we quantified, for the first time, the maximal FLV activity and its overall capacity to direct photosynthetic electrons towards the reduction of O_2 . However, when starch synthesis is absent, electron flow is diminished, a greater proportion of electrons is redirected toward O_2 and H^+ reduction through the FLVs, while PTOX, which is sensitive to the PQ pool redox state, is also activated. This may suggest, that the ability

to synthesize starch has an important role in priming/regulating CBBC and electron transport. Moreover, switching the circuitry of light-driven electrons between sustainable (starch; electrons that can be recaptured) and non-sustainable (O_2 and H^+ to generate H_2O ; electrons that cannot be recaptured) outlets is part of the energetic management that allows photosynthetic organisms to cope with frequent environmental fluctuations encountered in nature. Lastly, unmasking the repertoire of such energetic reactions reveals new directions for rational re-design and optimization of photosynthesis to satisfy global demands for food and other resources.

2.2 INTRODUCTION

Photosynthetic organisms evolved to transform solar energy to chemical bond energy stored in carbon (C) backbones that fuel most biosynthetic processes. The photosynthetic ‘light reactions’ drive the oxidation of water by photosystem II (PSII) and both linear and cyclic photosynthetic electron flow (LEF and CEF, respectively) that ultimately generate NADPH, ATP and other reduced electron carriers, including ferredoxins and thioredoxins (Figure 2.1); these compounds support the energetic demands of most cellular processes. While the light reactions can be described as an energy generator, a second component of photosynthesis utilizes the ATP and NADPH for the fixation of CO_2 into simple phosphorylated organic carbon compounds such as glyceraldehyde 3-phosphate (G3P) and fructose 6-phosphate (F6P) through a set of enzymatic reactions that comprise the Calvin-Benson-Bassham Cycle (CBBC). Some CBBC enzymes are indirectly activated by light through a redox switch controlled by reduced thioredoxin. Hence, prior to activation, photosynthetic electron transport and carbon (C) metabolism are not optimally coupled. Activation of the CBBC enzymes during a dark to light transition can increase their activities by up to 40-fold and the time required to complete this activation can last 2-3 min (Wirtz et al. 1982; Michelet et al. 2013a; Buchanan 2016).

The anabolic use of photosynthetically-derived electrons and ATP represents an extensive network of integrated reactions that ultimately couples the products of the light reactions with downstream C metabolism. An efficient coupling promotes cell growth and division as well as the storage of energy-rich, organic polymers. However, environmental fluctuations in light, nutrients and other abiotic factors may create an imbalance between the products of the photosynthetic light reactions and their utilization by the CBBC. Under such circumstances, the overflow of energetic electrons generated by photosystem I (PSI) and PSII can be photochemically quenched via a number of O₂ reducing pathways that occur within chloroplasts; these reactions have been designated H₂O-to-H₂O (water-to-water) cycles (Asada 1999; Curien et al. 2016). These ‘electron outlets’ include Mehler-type reactions (Mehler 1951; Mehler and Brown 1952), in which O₂ and H⁺ are directly reduced by electrons on the acceptor side of PSI, a process that can result in the generation of reactive oxygen species (ROS). Electrons can also be dissipated through a PSI-dependent enzymatic reaction catalyzed by specific heterodimeric flavodiiron proteins (FLVs, NADPH:flavin oxidoreductase) that directly reduce O₂ and H⁺ to H₂O without the release of ROS (Helman et al. 2003; Allahverdiyeva et al. 2013; Chaux et al. 2017) (Figure 2.1). Mutant organisms unable to synthesize FLVs exhibit compromised growth when exposed to fluctuating light as a result of oxidative damage caused by ROS accumulation and a decline in PSI activity (Helman et al. 2003; Allahverdiyeva et al. 2013; Gerotto et al. 2016; Chaux et al. 2017). Moreover, FLVs can prime PSII electron flow, O₂ evolution and lumen acidification under conditions in which the CBBC enzymes are not fully activated (Dang et al. 2014; Chaux et al. 2017). Chlororespiration represents an additional outlet in which electrons of quinols in the plastoquinone (PQ) pool can be used to reduce O₂ through the plastid terminal oxidase (PTOX, plastoquinol:oxygen oxidoreductase; Figure 2.1) (Peltier and Cournac 2002; Houille-Vernes et al. 2011; Nawrocki et

al. 2015). This reaction can be coupled with electron transfer from H₂O by PSII or by NADPH which can reduce PQ through the NAD(P)H-PQ reductase (Jans et al. 2008; Desplats et al. 2009; Peltier et al. 2016; Saroussi et al. 2016). It was previously demonstrated that PTOX controls the redox state of the PQ-pool in the dark and may act as a safety valve during periods of environmental stress (Krieger-Liszkay and Feilke 2015; Nawrocki et al. 2015). Finally, electrons can exit plastids in the form of organic compounds such as malate or triose-phosphate through the activity of the malate-oxaloacetate and triose phosphate redox shuttles (Johnson and Alric 2013; Alric and Johnson 2017) and be consumed by mitochondrial respiratory pathways (Yoshida et al. 2007; Bailleul et al. 2015).

Starch biosynthesis is another electron outlet; it involves a set of anabolic reactions that couple the use of NADPH and ATP generated by the photosynthetic light reactions with building and storing C polymers. Starch polymers (or granules) synthesized in the plastids of vascular plants and green algae are essential for the viability of photosynthetic organisms in their natural habitat. Aside from being a repository for fixed C, starch polymers form structural components and represent a sustainable outlet (i.e. the energy within the polymer can be re-used) for reductant and ATP. In plant leaves, starch transiently accumulates during the day and is used at night to fuel respiration, while in non-photosynthetic organs it provides the energy for growth, development, and more (Keeling and Myers 2010; Zeeman et al. 2010; Geigenberger 2011; Pfister and Zeeman 2016). In the green unicellular alga *Chlamydomonas reinhardtii* (hereafter *Chlamydomonas*), starch synthesis has been noted over the past two decades to be part of the cells' 'energetic management' strategy that becomes critical when light energy is not efficiently converted into growth (biomass), often in response to suboptimal environmental conditions such as low nutrient availability ((Siaut et al. 2011; Davey et al. 2014) and reviewed by (Saroussi et al. 2017)). The

pathway for starch synthesis requires several enzymes, as shown in Figure 2.1 (reviewed by (Ball and Deschamps 2009)(Harris 2009), and is fueled by ATP derived primarily from photosynthesis and carbon backbones synthesized by the CBBC. The rate limiting step in starch synthesis involves the enzyme ADP glucose pyrophosphorylase (AGPase, encoded by *STA6* locus) which uses ATP to convert glucose-1-phosphate (G1P) to ADP-glucose while releasing pyrophosphate (PPi) (Figure 2.1). In the last few decades, various *Chlamydomonas* “starchless” mutants have been isolated and characterized (Ball and Deschamps 2009). One mutant, disrupted for the gene encoding AGPase (designated *sta6*), accumulates no detectable starch (Zabawinski et al. 2001; Ball and Deschamps 2009). The *sta6* mutant also exhibited a marked reduction in photosynthetic capacity, although the mechanism underlying this phenomenon remains speculative (Sun et al. 1999; Krishnan et al. 2015)

We have begun to appreciate the critical nature of the light-driven reduction of O₂ (allowing a H₂O-to-H₂O cycle) in cell survival. However, we still know little about how these electron consuming pathways are coordinated with photosynthetic electron transport, CBBC activity and the activity of other C assimilatory/storage pathways like starch metabolism. In this work we explore the dynamics of alternative electron outlets during dark to light transitions, a situation in which photosynthetic electron transport is not optimally integrated with downstream C metabolism (the CBBC requires minutes to become activated upon exposure to light) (Michelet et al. 2013b). We demonstrate the importance of starch synthesis as a sustainable outlet for electrons generated by the light reactions. In the absence of this outlet, photosynthetic electron transport is impaired and PTOX activity increases, facilitating a H₂O-to-H₂O cycle that represents a non-sustainable outlet for electrons, but is essential to balance the redox state of the PQ pool. We also demonstrate that the reduction of O₂, catalyzed by FLVs, which immediately engages in the cells as they

transition from the dark to light, enabling electron transport when the CBBC is not fully activated. Finally, we unmasked the apparent maximum rate of FLV activity as well as the overall amount of O₂ being consumed by FLV at different light intensities when photosynthetic electron transport and C metabolism are not optimally integrated.

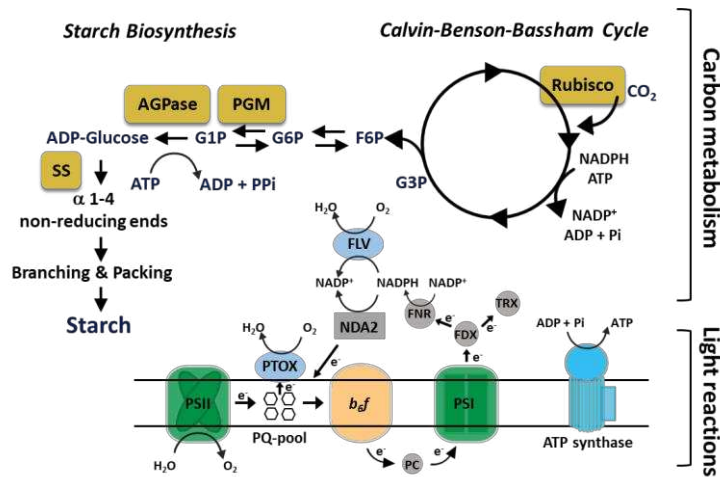


Figure 2. 1 Integration of photosynthetic light reactions and carbon metabolism. The light reactions include the reaction center/electron transport components PSII and PSI (green), cytochrome *b₆f* (*b₆f*) (orange), ATP synthase (blue), with CBBC (cycle, upper right) and starch biosynthesis (pathway, upper left) using the products of these reactions. Metabolites are in blue [G3P- glyceraldehyde 3-phosphate; F6P- fructose 6-phosphate; G6P-glucose 6-phosphate; G1P-glucose 1-phosphate]. Carbon metabolism-related enzymes are highlighted in gold filled rectangles [Rubisco - ribulose phosphate carboxylase oxygenase; PGM - phosphoglucomutase; AGPase - ADP-glucose pyrophosphorylase; SS - starch synthase]. Other enzymes are: PTOX - plastid terminal oxidase; FLV - flavodiiron protein (blue-filled ovals; involved in reducing O₂); NDA2 – NADPH oxidoreductase (grey-filled rectangle; moves electrons into electron transport); FDX - ferredoxin; TRX - thioredoxin; FNR - flavin:NADPH reductase (grey-filled circles; moves electrons out of electron transport).

2.3 RESULTS

Starch synthesis, a sink for reductant/fixed carbon and ATP, can potentially impact various cellular pathways that are used to consume photosynthetically-derived electrons. In the absence of starch synthesis, the excess electrons that cannot be coupled to downstream C metabolism could potentially be nonphotochemically quenched and/or photochemically quenched through activation

of alternative pathways that deliver photosynthetically-derived electrons to O_2 and H^+ to generate H_2O ; these pathways result in O_2 uptake. To explore the extent of photochemical processes associated with quenching of excess excitation, we monitored the dynamics of O_2 evolution and uptake during dark to light transitions in the *sta6* starchless mutant (Zabawinski et al. 2001). At the onset of a dark to light transition, the reactions involved in fixing CO_2 (CBBC) are not fully active and therefore are not optimally integrated with photosynthetic electron transport (Michelet et al. 2013b). As a control for the analyses of *sta6*, we used the genetically complemented (*sta6::STA6*) C6 strain (Li et al. 2010). These strains were previously used for evaluating *sta6* function (Siaut et al. 2011; Blaby et al. 2013; Schmollinger et al. 2014; Anderson et al. 2016).

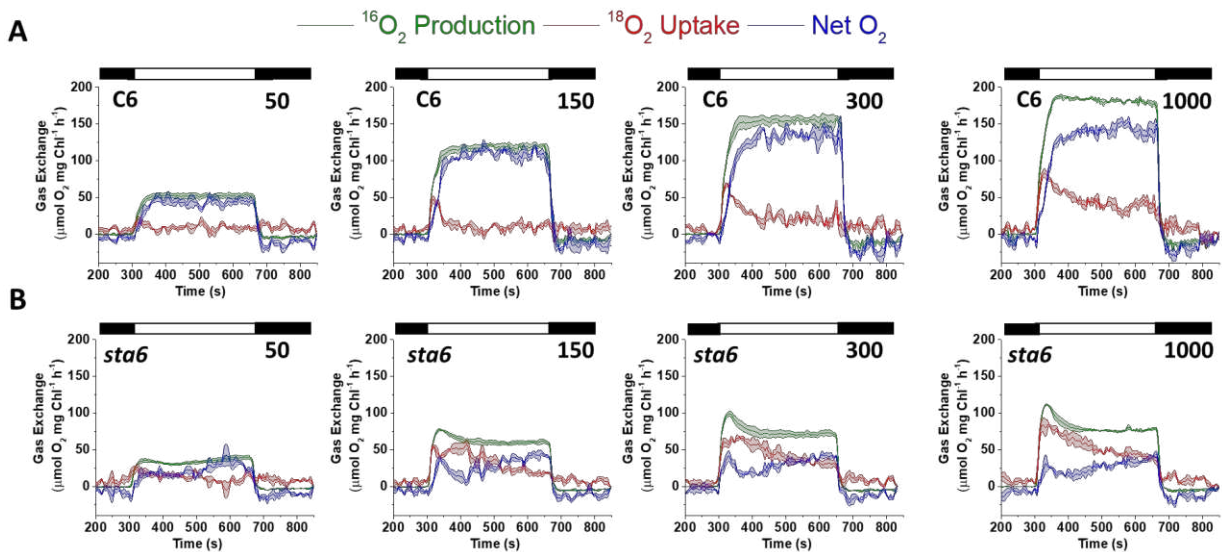


Figure 2. 2 Light-induced O_2 evolution and uptake. C6 (A) and *sta6* (B) were cultured photoautotrophically, bubbled with 2 % CO_2 in air and maintained in continuous light of $100 \mu\text{mol photons m}^{-2} \text{s}^{-1}$. Gross O_2 production ($^{16}O_2$ evolution, green curve) and light-induced uptake of O_2 ($^{18}O_2$ uptake, red curve) were monitored for 6 min using MIMS at 4 different light intensities (50, 150, 300 and $1000 \mu\text{mol photons m}^{-2} \text{s}^{-1}$, as indicated in the figure). Prior to turning on the light, the cells were maintained for 5 min in the dark (black bars on the left of each graph), and for an additional 3 min in the dark following the illumination (black bar, on the right of each graph). Gross O_2 uptake and both gross and net (blue curve) O_2 production were calculated according to the formula given in Materials and Methods. Each trace represents an average of at least 3 biological replicates.

Membrane Inlet Mass Spectrometry (MIMS) was used to quantify O₂ production (¹⁶O₂ evolution) and uptake (depletion of injected ¹⁸O₂ from the medium) upon exposure of *sta6* and C6 cells to increasing light intensities (50, 150, 300 and 1000 μmol photons m⁻² s⁻¹) during photoautotrophic growth in the presence of elevated CO₂ (Figure 2.2). The trends for O₂ production and uptake changed to some extent over the time of the light treatment (at any intensity used), we therefore divided the light period (6 min in total, represented by white bars above graph in Figure 2.2) into an early phase (first 3 min) and late phase (last 3 min).

2.3.1 AT THE ONSET OF LIGHT ELECTRONS ARE REDIRECTED TOWARD FLVS

When C6 cells were exposed to light after a 5 min dark preincubation, the rate of gross ¹⁶O₂ production rapidly increased to a maximal rate, or P_{max}, and remained steady for the remainder of the light treatment (green curve, Figure 2.2A). P_{max} was positively correlated with an increase in light intensity and attained a maximum value of ~190 μmol O₂ mg⁻¹ Chl h⁻¹ at 1000 μmol photon m⁻² s⁻¹ (Figure 2.2A and Figure 2.3A). We also measured the uptake of O₂ by C6 cells, which exhibited a pronounced peak at the onset of the light (red curve, Figure 2.2A). The U_{max}, or maximal O₂ uptake, like the P_{max} was positively correlated with light intensity, attaining a rate of ~80 μmol O₂ mg⁻¹ Chl h⁻¹ at 1000 μmol photon m⁻² s⁻¹ during the early phase of the light period (Figure 2.2A and Figure 2.3A). The ratio of U_{max} to P_{max} (U_{max}/P_{max}), which reflects the fraction of reductant generated by the photosynthetic light reactions that is not coupled to CO₂ fixation/ metabolism or nutrient assimilation (e.g. reduction of nitrite or sulfate), did not markedly vary at the different light intensities tested during the early phase of the light exposure (~0.4). It did, however, decline during the later stages of light exposure, and appeared to stabilize at ~0.25 (Figure 2.3A). Consequently, for C6, the rise in net O₂ production with increasing light intensity (blue graph Figure 2.2A) lagged behind the initial rise of gross O₂ production (green curve, Figure

2.2A). At all light intensities, immediately following the U_{max} peak, the net production of O_2 rose to its maximal value, or $P_{max_{net}}$ ($P_{max_{net}}$ values were correlated with light intensity as well, Figure 2.3A). These data agree with previous studies showing that a marked increase in O_2 uptake occurs immediately after cells are exposed to HL or during a dark to light transition (Allahverdiyeva et al. 2013; Chaux et al. 2017). Such a rise in O_2 uptake was demonstrated to reflect the activity of the FLV proteins, which use electrons on the donor side of PSI to reduce O_2 , and as a consequence drive water oxidation and O_2 evolution by PSII, and protect the photosynthetic apparatus from oxidative damage prior to full activation of the CBBC (Helman et al. 2003; Allahverdiyeva et al. 2013; Gerotto et al. 2016; Shimakawa et al. 2017; Chaux et al. 2017).

2.3.2 ELIMINATING STARCH SYNTHESIS CAUSED AUGMENTED O_2

PHOTOREDUCTION

Surprisingly, O_2 production and uptake by *sta6* cells showed trends that were notably different from those of C6 (Figure 2.2B). The mutant cells exhibited a burst of gross O_2 production (green curve, Figure 2.2B) soon after the cells were transferred from darkness to light, followed by a gradual decline to a steady state level of O_2 evolution. Similarly to C6 cells, P_{max} was positively correlated with light intensity, although levels of gross O_2 evolution were almost 2-fold lower than the levels observed for C6 (Figure 2.2 and 2.3B). Simultaneous with the burst in O_2 production, the rate of O_2 uptake began to increase, reaching U_{max} soon after the burst of O_2 production (red curve, Figure 2.2B). Although the U_{max} for *sta6* and C6 were similar during the early phase of the light period, the uptake of O_2 slowly declined in *sta6* over a longer period than the decay of O_2 uptake in C6 cells. Furthermore, the U_{max}/P_{max} value was ~ 0.8 during the early phase of the light period, resulting in a low rate of net O_2 production. These results suggest that a smaller proportion of the reductant generated by PSII in *sta6* was coupled to CO_2 fixation (or non-

oxygen related reduction reactions; Figures 2.2B and 2.3B) relative to C6. The U_{max}/P_{max} for *sta6* decreased (0.5-0.6; Figure 2.3B) during the late phase of the light period, suggesting reduced activity of pathways that use O_2 as a terminal acceptor of electrons relative to those in which the terminal acceptor is not O_2 .

To extend upon these findings, we compared the MIMS data to photosynthetic electron transport through PSII based on chlorophyll fluorescence (Figure A1.1A). The maximal PSII quantum efficiency (F_v/F_m) was similar for C6 and *sta6* (0.65 ± 0.00 and 0.66 ± 0.02 , respectively, Figure A1.1A), suggesting that *sta6* suffers no more damage to PSII than C6 under the standard conditions used to culture the strains. Furthermore, only a minor difference was observed in Φ_{PSII} for C6 and *sta6* (slightly lower for *sta6*) when the cells were exposed to up to $\sim 165 \mu\text{mol photons m}^{-2} \text{ s}^{-1}$. When the light intensity was raised above $165 \mu\text{mol photons m}^{-2} \text{ s}^{-1}$, the difference in Φ_{PSII} between *sta6* and C6 became slightly greater (15-25% difference), although it could not explain the pronounced difference in gross O_2 production between the strains based on MIMS measurements. This difference could be the consequence of cyclic electron flow around PSII (Lysenko et al. 2016) in *sta6*.

Taken together, these O_2 exchange analyses for C6 and *sta6* suggest that a defect in starch biosynthesis and the consequent loss of an outlet for electrons/fixing CO_2 and ATP resulted in a greater proportion of the light-generated electrons being directed toward outlets that involve O_2 reduction. Furthermore, a peak in light-dependent O_2 uptake in C6 occurred soon after the cells were exposed to light and prior to a rise in net light-dependent O_2 production. This O_2 uptake likely reflects FLV protein activity, which has been shown to engage immediately after the onset of light (Allahverdiyeva et al. 2013; Gerotto et al. 2016; Shimakawa et al. 2017; Chaux et al. 2017). Importantly, *sta6* cells exhibited a unique $^{18}O_2$ uptake pattern reflected by a broader peak (lasting

a few min) than in C6. This suggests that more than one component may contribute to photoreduction of O₂ and/or that the activity of the FLV proteins is more sustained in the mutant.

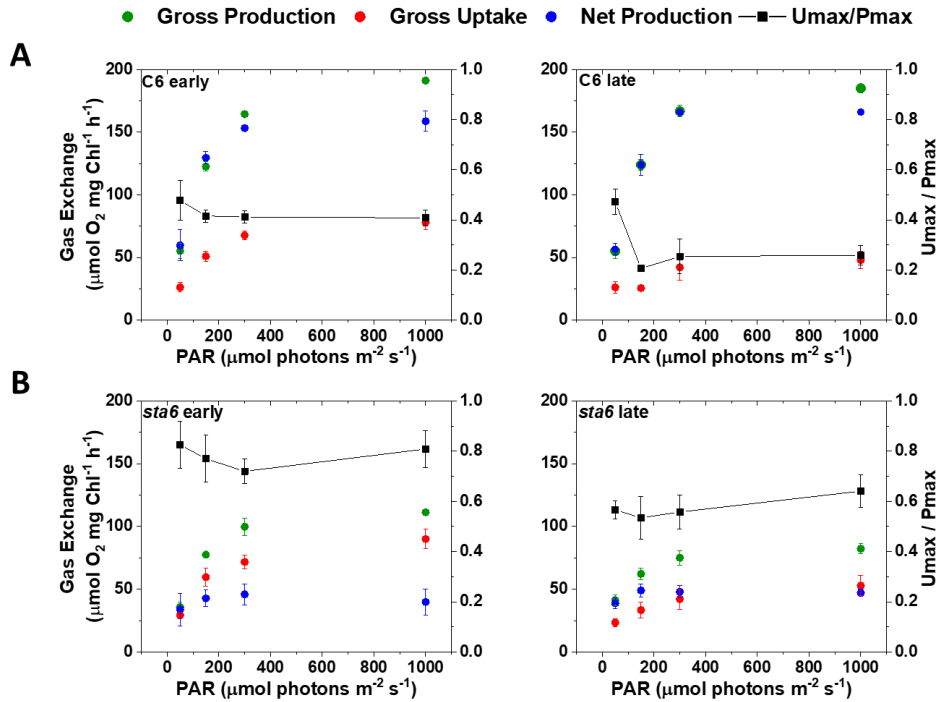


Figure 2. 3 Maximal rates of light-induced O₂ production and uptake. Maximal values for gross and net O₂ production (green and blue, respectively) and net O₂ uptake (red) for C6 (A) and *sta6* (B), as indicated, are plotted as a function of light intensity. The left-hand Y axis gives gross and net O₂ evolution and gross O₂ uptake, as indicated on the top of the figure. The right-hand Y axis gives the fraction of maximal gross O₂ uptake relative to maximal gross O₂ production; this value is plotted as a function of light intensity (black line with black squares). For both A and B, the left panel presents the data for the first 3 min of the light phase while the right panel present the data for the final 3 min of the light phase (i.e. early and late periods during illumination, respectively; see main text for details). Each point is an average of at least 3 biological replicates ± SD.

2.3.3 INTERACTIONS BETWEEN STARCH SYNTHESIS AND O₂

PHOTOREDUCTION

To further elucidate the nature of the light-dependent O₂ uptake and potential participation of alternative electron outlets during the transition from dark to light, we analyzed the kinetics of

O₂ production and uptake for C6 and *sta6* cells in more detail (Figure 2.4; cells were exposed to 300 μmol photons m⁻² s⁻¹). Although the rate of gross O₂ production was lower in *sta6* than in C6 (Figure 2.2 and 2.3), the kinetics of the initial rise of gross O₂ production over the first 20 s of the light period was similar between the strains (linear fitting of the initial rise of ¹⁶O₂ production initial; slopes are 4.5 and 4.1 for C6 and *sta6*, respectively; Figure 2.4A, dashed-dotted lines). Furthermore, during this period, the two strains exhibited similar kinetics for the rise in ¹⁸O₂ uptake (the rise in O₂ uptake was fitted to a first order exponential decay type curve. $\tau = 2.4 \text{ s}^{-1}$ and 2.0 s^{-1} for C6 and *sta6*, respectively; t-test, *p-value* =0.23; Figure 2.4A), suggesting that a similar mechanism may be involved in eliciting the initial light-driven production and uptake of O₂ for the two strains. However, while ¹⁸O₂ uptake for C6 cells decayed to a basal level soon after U_{max} was attained, the rate of O₂ uptake in *sta6* cells stayed constant for at least 100 s and decayed slowly following peak uptake. Overall, *sta6* cells showed 3-fold slower decay rate than C6 cells (decay slopes are -0.15 and -0.46, for C6 and *sta6*, respectively); longer term ¹⁸O₂ uptake curves are shown in inset of Figure 2.4). These observations demonstrate that the starchless mutant directed a greater proportion of electrons to photochemistry associated with the uptake of O₂ over the entire light period relative to the complemented strain.

We also observed this phenomenon when we compared the ratio of gross uptake and production of O₂ in C6 and *sta6* cells (Figure 2.4B). Immediately after the cells were exposed to light, the ratio of O₂ uptake to production was over 0.9 for both strains. After 20-30 s in the light, this ratio similarly declined to ~0.6 (highlighted in gray box), in both C6 and *sta6* cells. However, while this ratio keeps falling to ~0.1 in C6 cells, the proportion of O₂ uptake to production for *sta6* increased to ~0.8 after 100 s and remained much higher than that of C6 cells along the entire 6 min

light period (Figure 2.4B). Comparable trends were found if the cells were exposed to lower or higher light intensities (50, 150 and 1000 $\mu\text{mol photons m}^{-2} \text{s}^{-1}$; Figure A1.2).

In sum, immediately following exposure to light, the CBBC is not fully activated and the high energy electrons generated by photosynthetic electron transport cannot immediately be used for CO_2 fixation. Under such circumstances the cells, regardless of whether they have the capacity to store C as starch, share a common electron outlet, the FLV proteins (as mentioned in the above paragraph) that sustain PSII O_2 production with the concomitant reduction of O_2 and H^+ to H_2O . Moreover, the altered kinetics of O_2 uptake and decay in *sta6* (delay in attaining U_{max} , slower decay of $^{18}\text{O}_2$ uptake and a much higher $^{18}\text{O}_2/^{16}\text{O}_2$ ratio during much of the light period) suggest that reduction of O_2 is more dominant in the electron circuitry of *sta6* relative to C6 and raises the possibility that there is more than one component contributing to O_2 uptake during the light period. We therefore, hypothesized that a decrease in the pool of downstream electron acceptors resulting from the loss of starch synthesis in *sta6*, feeds back on electron transport and causes hyper-reduction of the PQ pool, which in turn may activate PTOX and result in increased O_2 consumption. Alternatively, if activation of the CBBC (or downstream reactions) was slower in the mutant, the contribution of FLV to the reduction of O_2 and H^+ would increase (the CBBC and FLV compete for the same pool of electrons). Lastly, we cannot rule out the possibility that mitochondrial respiration becomes a more dominant contributor to total $^{18}\text{O}_2$ uptake in *sta6*. This last possibility is less likely since the O_2 uptake rate measured in the dark (immediately following the light to dark transition) is slower in *sta6* than in C6 (Figure A1.1B).

2.3.4 CONTRIBUTION OF PTOX TO O_2 UPTAKE IN *STA6*

To further probe potential contributions of FLVs and assess the role of PTOX in routing electrons during a transition from darkness to light, we supplemented cultures with 2 mM propyl

gallate (PG), a reagent that inhibits alternative oxidases such as PTOX but does not inhibit FLV activity. This inhibitor was added to cultures at the beginning of the dark period (5 min prior to light exposure) and its impacts on O₂ production and uptake were monitored during the light (300 μmol photons m⁻² s⁻¹) period. PG did not affect the overall trends of O₂ production and uptake in C6 cells, however, the P_{max} (both net and gross) was ~60% of the value measured in the absence of PG (Figures 2.5A and Table 2.1). In contrast, in PG-treated *sta6* cells the initial burst of gross ¹⁶O₂ production was completely suppressed and P_{max} was 46% of that of untreated *sta6* cells (Figure 2.5B and Table 2.1), resulting in a similar rate of ¹⁸O₂ uptake and ¹⁶O₂ production and a net O₂ production of zero (blue graphs, Figure 2.5B). As the length of exposure to the light increased, ¹⁸O₂ uptake slightly declined while both net and gross ¹⁶O₂ evolution gradually rose (Figure 2.5B).

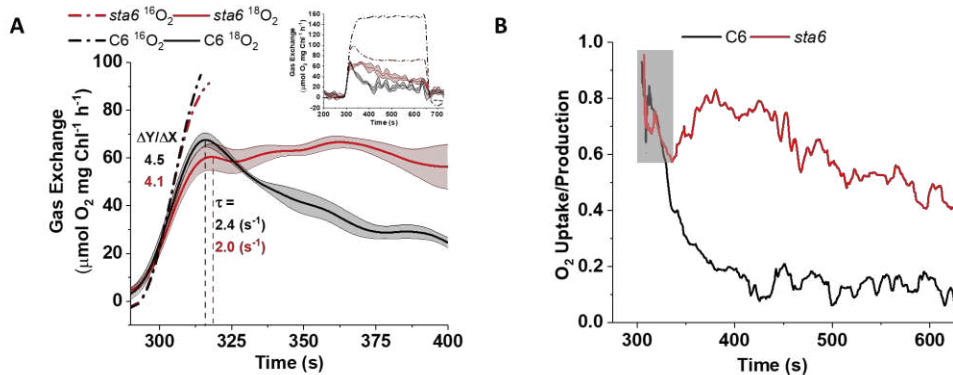


Figure 2. 4 Kinetics of light induced O₂ production and uptake. A. MIMS traces of ¹⁶O₂ evolution (gross production, dotted-dashed lines) and ¹⁸O₂ uptake (gross uptake, solid lines) during dark to light transition (300 μmol photons m⁻² s⁻¹) for C6 (black) and *sta6* (red). Gross O₂ production (¹⁶O₂) along the first 20 s in the light period, were linearly fitted and the initial rates (ΔY/ΔX) was calculated (black and red dash-dotted lines). The ¹⁸O₂ uptake plots were fitted to a first order exponential decay type curves to determine the rate (τ) at which a peak of ¹⁸O₂ uptake for C6 and *sta6* were attained (dashed black and red line for C6 and *sta6*, respectively). Inset: Presentation of the MIMS reaction for gross O₂ evolution and uptake during the entire light period. B. The ratio between gross ¹⁸O₂ uptake and ¹⁶O₂ production during the light period (300 μmol photons m⁻² s⁻¹). Same conditions as in panel A. Gray box highlights the region in which the decline in the ratio for C6 and *sta6* cells is similar. Each data line represents an average of 3 biological replicates.

U_{max} of both untreated and PG-treated C6 cells was attained at approximately the same time following exposure to light, but the U_{max} value of PG-treated C6 cells was ~68% of that of untreated cells (Table 2.1 and Figure 2.5C, U_{max} for untreated and treated cells are indicated with a solid and dashed lines extended from the x axis, respectively) and the rate at which U_{max} was attained was slower by more than 2-fold (initial slopes of 1.9 and 4.4 for PG-treated and untreated C6, respectively; Figure 2.5C). For *sta6*, untreated cells attained U_{max} 15 s faster than for PG-treated cells. The U_{max} value of PG-treated cells was ~60% of that of untreated cells (Figure 2.5D and Table 2.1, U_{max} for untreated and treated cells are indicated with a solid and dashed line, respectively, extended from the x axis) and the rate at which the U_{max} was attained was slower by ~3.5-fold (Table 2.1 and Figure 2.5D, initial slopes of 0.9 and 3.2 for PG-treated and untreated *sta6* cells, respectively). However, the overall trend of ¹⁸O₂ uptake in *sta6* cells following the initial rise was not markedly impacted; the rate of O₂ uptake stayed constant for an initial period of ~100 s in the light and then gradually slowed, but high values of U_{max}/P_{max} were maintained over the entire light period (Figure 2.5B, 2.5D and Table 2.1). Since PTOX modulates the redox state of the PQ pool (Trouillard et al. 2012; Krieger-Liszkay and Feilke 2015; Nawrocki et al. 2015), its inhibition by PG prior to the light period (5 min in dark before the light is turned on) could limit oxidation of the quinol pool, which would lead to a decline in the rates of both light driven O₂ production and uptake, a lower P_{max}, and a slower rise in the uptake of O₂, as shown in Figures 2.5C and D. To explore this possibility, we measured the redox state of the PQ pool, as 1-qL (Kramer et al. 2004a), after exposing PG-treated and untreated cells to 300 μmol photons m⁻² s⁻¹ for 1 min. The PQ-pool of both C6 and *sta6* was ~35% more reduced following PG treatment, but the actual redox state of the pool was higher (more reduced) in *sta6* than in C6 cells (0.83 ± 0.00

and 0.61 ± 0.06 , respectively; Figure 2.5E). These findings suggest that slower rates of O₂ production could be a consequence of elevated reduction of the PQ pool resulting from PTOX inhibition, however, the impact of this inhibition is much more pronounced in *sta6* cells. Furthermore, when we measured the redox state of the PQ pool as a function of increased light

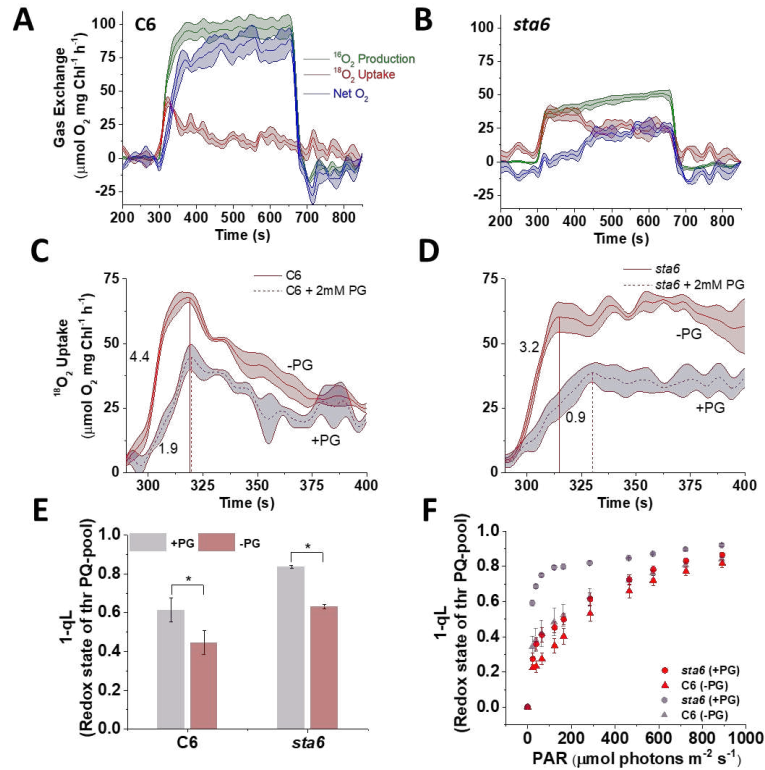


Figure 2.5 Effect of a PTOX inhibitor on O₂ production and light-induced O₂ uptake. C6 (A) and *sta6* (B) were exposed to 300 $\mu\text{mol photons m}^{-2} \text{s}^{-1}$ in the presence of 2 mM propyl gallate (PG) and gas exchange was analyzed using MIMS, as in Figure 3 (see Figure 3 legend). Comparisons of the first 2 min of ¹⁸O₂ uptake for C6 (C) and *sta6* (D) in the presence (dashed line with purple shading) and absence (solid line with red shading) of PG. The time (s) to achieve U_{max} for C6 and *sta6* are highlighted by dotted red lines that extend from the x axis to the U_{max} peak. Each trace represents an average of at least 3 biological replicates with the shaded area associated with each trace representing the SE. (E) 1-qL values of PG-treated/untreated cells. The cells were PG treated during the 5 min pre-incubation in the dark and then exposed to 300 $\mu\text{mol photons m}^{-2} \text{s}^{-1}$ for 1 min. N=3 \pm SD * t-test, *p*-value = 0.01. (F) 1-qL values of PG-treated/untreated cells exposed to increasing light intensities. Cells were exposed to each intensity for 30 s before raising the intensity. N=3 \pm SD. PAR = photosynthetic active radiation.

intensity, we found that C6 cells treated with PG maintained a redox state close to that of untreated cells (Figure 2.5F, triangles). Hence, PTOX appears to have a minor impact on total light-driven uptake of O₂ when starch metabolism is not impaired (i.e. in C6 cells) but is important when the cells are maintained in the dark. In contrast, the PQ pool of PG-treated *sta6* cells was more reduced than the non-treated cells at all light intensities (Figure 2.5F, circles), suggesting that the PG treated *sta6* cells are compromised in their ability to oxidize the PQ-pool, likely a consequence of an additive effect of PTOX inhibition and an inability to synthesize starch in the light. Together, these experiments suggest that PTOX is essential for balancing the redox state of the PQ pool when the cells are maintained in the dark. Eliminating PTOX activity slows the rate of O₂ production upon shifting the cells to the light regardless of whether the cells can synthesize starch. Moreover, the finding that PG-treated *sta6* cannot maintain the redox state of the PQ pool (unlike PG-treated C6; Figure 2.5F) suggests that the loss of starch synthesis eliminates an important electron outlet that may elicit feedback inhibition of CBBC and/or electron transport which leads to an increase in excitation pressure on the PQ-pool.

2.3.5 OVERALL CONTRIBUTION OF FLV TO PHOTOREDUCTION OF O₂

Based on prior work (Helman et al. 2003; Allahverdiyeva et al. 2013; Gerotto et al. 2016; Chaux et al. 2017), FLV proteins appear to be a prominent outlet for electrons when the light is first turned on and photosynthetic electron transport is not optimally integrated with downstream C metabolism. Moreover, in C6 cells (i.e. normal starch biosynthesis), we observed a burst of O₂ uptake during the dark to light transition, in which PTOX seems to have little impact on this uptake (Figure 2.5F), therefore, FLV is likely the dominant activity responsible for this uptake. We therefore sought to quantitatively evaluate the potential of FLV proteins to reduce O₂ during the dark to light transition. To quantify the contribution of FLV activity to O₂ uptake, we calculated

the basal rate of light-driven O₂ uptake using a linear fit of the ¹⁸O₂ uptake data at steady state (late phase of light period), shown in Figure 2.3 (Figure A1.3A). This uptake rate was correlated with uptake resulting from dark respiration based on O₂ electrode measurements (Pearson correlation, $r = 0.923$, $p\text{-value} < 0.05$, Figure A1.3B).

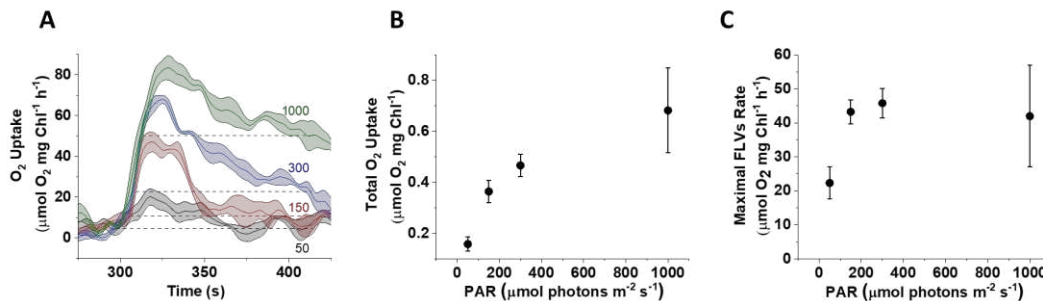


Figure 2. 6 O₂ Uptake attributed to FLV proteins: A. O₂ uptake rate of C6 cells exposed to different light intensities (shown in different colors) are plotted during the first 2 min of the light period (300 - 420 s). The rates of baseline O₂ uptake (uptake in the light after the CBBC becomes active), calculated from Figure A1.2, are shown as dashed lines in the color that corresponds to the measurements of total O₂ uptake. B. Total O₂ uptake at each intensity that cannot be attributed to the basal rate of uptake was calculated by integrating the area between the curve defining the uptake rate at the different intensities with the rate of basal uptake at that intensity. C. Maximal rate of O₂ uptake attributed to the FLV proteins. These values were calculated by subtracting the rate of O₂ uptake attributed to basal uptake from U_{max} depicted in the curve in A. For all panels $n=3 \pm \text{SD}$.

Figure 2.6a presents the overall O₂ uptake for C6 cells exposed to four different light intensities (solid lines, 50, 150, 300 and 1000 μmol photons m⁻² s⁻¹). Also shown are the calculated basal rates of O₂ uptake (which is probably dominated by mitochondrial respiration) at the different light intensities (horizontal dashed lines with the same colors as curves for ¹⁸O₂ uptake). By integrating the area under the O₂ uptake curve, using a baseline value established for the basal O₂ uptake at each of the four light intensities (e.g see Figure A1.3C), we calculated the total amount of consumed O₂ that is associated with shifting the cells from dark to light and potentially a consequence of FLV. The amount of O₂ consumed by putative FLV activity increased with

Table 2. 1 Photosynthetic parameters of PG treated C6 and *sta6* cells at 300 $\mu\text{mol photons m}^{-2} \text{s}^{-1}$. O_2 gas exchange (P_{max} , U_{max} and Net O_2 evolution) presented as $\mu\text{mol O}_2 \text{ mg Chl}^{-1} \text{ h}^{-1}$

C6

Photosynthetic parameter	Early					Late				
	PG+	SD	PG-	SD	PG+/PG- - x100	PG+	SD	PG-	SD	PG+/PG- x100
Pmax	100.5	10.8	164.4	1.0	61.2	103.0	13.6	166.7	4.6	61.7
Umax	46.5	7.0	67.6	3.6	68.8	25.4	0.8	42.0	0	60.3
Umax/pmax x 100	46.3	7	41.1	2.5	114.5	26.7	4.6	25.3	6.8	98.4
Net	91.4	9	153.3	0.4	59.7	98.3	15.9	165.9	1.9	59.2

sta6

Photosynthetic parameter	Early					Late				
	PG+	SD	PG-	SD	PG+/PG- - x 100	PG+	SD	PG-	SD	PG+/PG- x 100
Pmax	46.0	4.9	99.7	6.7	46.1	52.5	4.1	75.1	5.8	69.9
Umax	42.9	7.8	71.7	5.6	59.8	36.7	9.4	42.1	8.0	87.3
Umax/pmax x 100	93.2	0.3	72.0	4.8	129.0	77.3	9.3	55.7	6.8	124.4
Net	26.8	7.1	45.9	8.2	67.4	37.7	7.5	47.9	5.0	78.7

increasing light intensity. At 300 $\mu\text{mol photons m}^{-2} \text{s}^{-1}$, the FLV proteins consumed 0.46 ± 0.04 $\mu\text{mol O}_2 \text{ mg Chl}^{-1}$, with maximum consumption at 1000 $\mu\text{mol photons m}^{-2} \text{s}^{-1}$ (0.682 ± 0.016 $\mu\text{mol O}_2 \text{ mg Chl}^{-1}$; Figure 2.6B). Interestingly, the maximal rate of O_2 uptake (V_{max}) that we attributed to FLV activity was 45.7 ± 4.2 $\mu\text{mol O}_2 \text{ mg Chl}^{-1} \text{ h}^{-1}$ when the cells were exposed to 300 $\mu\text{mol photons m}^{-2} \text{s}^{-1}$. This rate is not significantly different from the rates measured for cells exposed to 150 or 1000 $\mu\text{mol photons m}^{-2} \text{s}^{-1}$ (Figure 2.6C). Therefore, while FLV proteins operate at V_{max} , even upon exposure to moderate light intensities, the amount of O_2 consumed following the

transfer of the cells to increasing intensities of light appears to be a consequence of prolonged activation of the FLV (more sustained uptake at higher light intensities).

2.4 DISCUSSION

In nature, photosynthetic organisms are frequently exposed to abiotic stresses, including marked variations in temperature and light intensities and suboptimal nutrient concentrations. Such environmental restrictions limit the growth/development of organisms and dramatically impact the use of photosynthetically-generated electrons for CO₂ fixation. To cope with environmental challenges, photosynthetic organisms have developed several strategies to manage excitation energy and reroute electrons to alternative pathways. To uncover the nature of various alternative pathways for electron flow and the flexibility of the energetic circuitry, we are analyzing the dynamics associated with FLV and PTOX activities during dark to light transitions, when photosynthetic electron transport and C metabolism are not in equilibrium, in cells that are either able or unable to synthesize starch. This analysis uses the *Chlamydomonas sta6* mutant, which is unable to synthesize starch, and the C6 strain, which is rescued for the *sta6* phenotype (Li et al. 2010).

Elimination of starch synthesis in *Chlamydomonas* resulted in a pronounced decrease in light-dependent O₂ evolution (Figure 2.2 and 2.3), suggesting interactions between photosynthetic electron transport and downstream processes that consume electrons. Real time analyses of gross O₂ exchange using isotopically labeled O₂ to distinguish between production (¹⁶O₂) and light-driven uptake (¹⁸O₂) demonstrated that *sta6* cells exhibited more sustained light-induced reduction of O₂ that was as high as 80% of the gross O₂ evolution (compared to 20-40% for C6 cells), and consequently the cells had low net O₂ evolution (Figures 2.2, 2.3 and 2.4B). The lower maximal ¹⁶O₂ production and the elevated ratio of O₂ uptake to production (reflecting the fraction of

reductant not used for CO₂ fixation and growth) highlights an essential role for starch synthesis as a transient outlet for storing reductant/energy generated by photosynthetic electron transport as the cells are activating downstream C metabolism. Furthermore, despite the lower rates of gross O₂ production exhibited by *sta6* relative to C6 cells, we did not observe a dramatic decrease in electron flow through PSII (measured as Φ_{PSII} , Figure A1.1A) when the cells were exposed to light intensities as high as 300 $\mu\text{mol photons m}^{-2} \text{ s}^{-1}$. This discrepancy may be explained by activation of cyclic electron flow around PSII (CEF-PSII). Although this type of alternative pathway has not been intensively investigated, several studies suggest that CEF-PSII is activated under conditions in which the PQ pool is highly reduced (Falkowski et al. 1986; Prasil et al. 1996; Onno Feikema et al. 2006; Lysenko et al. 2016). A potential role for CEF-PSII in *sta6* cells requires additional investigation.

Genes encoding FLV proteins are present in prokaryotes, green alga, moss, liverwort, lycophytes and gymnosperms but are not found in vascular plants (Yamamoto et al. 2016). These proteins function as an outlet for electrons when C metabolism is not optimally coupled to the rate of photosynthetic electron flow (Helman et al. 2003; Allahverdiyeva et al. 2013; Gerotto et al. 2016; Chaux et al. 2017). Our analyses revealed a rapid increase in light driven reduction of O₂ that takes place soon after *Chlamydomonas* cells are transitioned from the dark to the light. The kinetics of this ‘burst’ of O₂ uptake was similar for C6 and *sta6* ($\sim 2.4 \text{ s}^{-1}$ at 300 $\mu\text{mol photons m}^{-2} \text{ s}^{-1}$) (Figure 2.4A) and is consistent with the function of FLVs in priming photosynthetic electron transport (Chaux et al. 2017) and harmlessly dissipating electrons prior to the activation of the CBBC and downstream C metabolism. In this context, recent work has demonstrated that slowed electron transport in *Arabidopsis* resulting from a defect in CEF (*pgr5* mutant, associated with CEF control (DalCorso et al. 2008)) could be reversed by transforming the mutant plants with the

FLV genes (Yamamoto et al. 2016). Similarly, a *Chlamydomonas pgr5* mutant accumulates FLVs when the cells are exposed to HL (Dang et al. 2014). In these two examples, FLVs provide an alternative route for an ‘overflow’ of electrons (more electrons produced by the light reactions than can be used by downstream anabolic processes) by redirecting them toward the reduction of O_2 and H^+ to H_2O . Importantly, our analyses allowed us, for the first time, to estimate the energy loss through dissipation of electrons by FLV-mediated photoreduction during the dark to light transition and the maximum rate of electron flow from FLV to O_2 . C6 cells shifted from dark to light revealed a V_{max} for O_2 uptake by FLV of $\sim 45 \mu\text{mol } O_2 \text{ mg Chl}^{-1} \text{ h}^{-1}$ under the conditions of our study (Figure 2.6C), which is equivalent to $22.5 \text{ e}^- \text{ s}^{-1} \text{ PSI}^{-1}$ (conversion between units has been done according to (Johnson and Alric 2012)). A threshold for V_{max} could limit the capacity of electron dissipation under conditions of high photon flux. We therefore also measured the total O_2 uptake by the FLV proteins at different light intensities, (Figure 2.6A and A1.3C). Based on our calculations, the total amount of O_2 consumption associated with the dark to light burst increased as a function of light intensity (ranging from 0.15 to $0.7 \mu\text{mol } O_2 \text{ mg Chl}^{-1}$ for C6; Figure 2.6B). This increased photochemical dissipation is reflected by a broadening of the O_2 uptake peak resulting from a slower decay in the O_2 uptake (Figure 2.6A). This slowed decay may be part of a compensation mechanism that diverts electrons to FLV when the redox pressure on the CBBC and perhaps downstream C utilization processes increase because these pathways are not yet fully activated.

Other electron valves may also play a role in sustaining nondestructive electron transport during dark to light transitions. PTOX oxidizes quinol molecules downstream of PSII and is required for adjusting the redox balance of the PQ pool (Bailey et al. 2008; Houille-Vernes et al. 2011; Krieger-Liszkay and Feilke 2015; Nawrocki et al. 2015). The rate of quinol oxidation by

PTOX was found to be relatively slow, only $5 \text{ e}^- \text{ s}^{-1} \text{ PSI}^{-1}$ in *Chlamydomonas* (Houille-Vernes et al. 2011), ~4-fold slower than the rate of NADPH oxidation by FLVs (as calculated in this study). However, it was shown that stressed organisms that experience a highly reduced PQ pool accumulate high levels of PTOX proteins, which would facilitate PTOX-dependent reduction of O_2 and H^+ to H_2O (Quiles 2006; Bailey et al. 2008; Stepien and Johnson 2009; LAUREAU et al. 2013; Saroussi et al. 2016). Here we show that PTOX may have a minor contribution to overall O_2 uptake when C6 cells (i.e. normal starch biosynthesis) are shifted from darkness to $300 \mu\text{mol photons m}^{-2} \text{ s}^{-1}$ (Figure 2.5). Nevertheless, inactivation of PTOX using PG led to elevated reduction of the PQ pool for both C6 and *sta6* when the cells were maintained in the dark (Figure 2.5E), which highlights the importance of PTOX in regulating the redox state of the PQ pool in darkness. On the other hand, when starch synthesis was compromised (i.e. in *sta6* cells), the redox state of the PQ pool was highly elevated at all light intensities (Figure 2.5F). Hence, we suggest that PTOX can become an important alternative outlet for electrons when various aspects of C metabolism/utilization, such as the storage of electrons in starch, are compromised.

Re-routing of electrons through alternative outlets allows photosynthetic organisms to cope with fluctuating environmental conditions. Here we show that *Chlamydomonas* activates various ‘sustainable’ and ‘non-sustainable’ electron transport pathways. The transient storage of fixed C such as starch represents a sustainable sink for excitation energy; the energy is not lost but can be deployed for growth and maintenance when needed. However, under conditions in which CO_2 fixation and C storage are compromised and/or saturated, the cells can photochemically quench absorbed excitation energy through photoreduction of O_2 , a non-sustainable outlet (the energetic electron can no longer be used as a source of energy) in which photosynthetically-generated electrons are used for the catalytic reduction of O_2 and H^+ to water; FLV and PTOX can

both catalyze this reaction. While photosynthetic reaction centers and electron transport components provide reducing equivalents that fuel C metabolism, FLVs appear to function like a clutch, dissipating excess energy stored in the electron transport system when the CBBC has not been fully ‘switched on’, suggesting potential regulatory interactions between CBBC proteins/metabolites and FLV activity. On the other hand, PTOX proteins are sensitive to redox changes within the PQ-pool; they can be triggered by limitations in electron utilization by downstream reactions. As the redox state of the photosynthetic electron transport chain increases, and a greater proportion of the PQ pool becomes reduced, PTOX acts like a valve on a pressure cooker, facilitating routing of ‘overflow’ electrons to the reduction of O₂ and H⁺. PTOX enables continued functioning of PSII in generating a charge separation and driving H₂O oxidation, while at the same time limiting photodamage.

Future challenges in optimizing photosynthetic outputs will likely be facilitated by elucidating the regulation of enzymes involved in both sustainable and non-sustainable photochemical quenching. The information generated can be exploited to develop platforms for engineering the energetics of plants for better satisfying global food and resource needs.

2.5 MATERIALS AND METHODS

2.5.1 STRAINS AND CELL GROWTH

The *sta6* mutant (CC-4348; *sta6*⁻; *rbo1*⁻) and the genetically complemented *sta6::STA6* strain, designated C6 (CC-4567) (Li et al. 2010), were maintained at ~10 μmol photons m⁻² s⁻¹ on solid TRIS-Acetate-Phosphate (TAP) medium (Harris 2009). Cells were inoculated from solid TAP into liquid TAP medium and grown in flasks at ~40 μmol photons m⁻² s⁻¹ (aerated by shaking at ~150 rpm) to mid-logarithmic phase (~1 x 10⁶ cells mL⁻¹). The volume of cell culture containing 60 μg of Chl was pelleted by centrifugation [1000 x g, 4 min, room temperature (RT)], washed

twice with fresh photoautotrophic MOPS-TRIS medium (20 mM MOPS titrated with TRIS base powder to pH 7.5, 0.2 g L⁻¹ K₂HPO₄, 0.11g L⁻¹ KH₂PO₄, 50 mg L⁻¹ CaCl₂, 100 mg L⁻¹ MgSO₄, 37.5 mg L⁻¹ NH₄Cl, 1:1000 hutner trace elements) (modified from (Geraghty et al. 1990)) and re-suspended in the same medium to a final Chl concentration of 2-4 µg mL⁻¹ (~60 ml of medium). These cultures were bubbled with 2% CO₂ in glass tubes and grown at 100 µmol photons m⁻² s⁻¹ (white light) to a final concentration of 10-15 µg Chl mL⁻¹.

2.5.2 CHL CONCENTRATION

Chl concentrations were determined from methanol extracted pigments according to (Porra et al. 1989a). Briefly, cells were pelleted by centrifugation (13,000 x g, 2 min, RT) and resuspended in 100% methanol. Cell debris from methanol extracted samples was pelleted (13,000 x g, 5 min, RT) and the supernatant containing the pigments was transferred to plastic cuvettes. Total Chl was calculated according to the equation: Chl = 22.12 x A₆₅₂ + 2.71 x A₆₆₅, where A₆₅₂ and A₆₆₅ are absorbances at 652 and 665 nm, respectively.

2.5.3 DARK RESPIRATION

Dark respiration at different light intensities was measured using a Pt-Ag/AgCl polarographic electrode system (ALGI, Littleton, CO, USA) equipped with a temperature-controlled, 1 mL glass water-jacketed reaction chamber, two YSI 5331A electrodes (Yellow Springs Instruments, Yellow Springs, OH, USA) polarized at -0.8 V, and an atmospheric barometric pressure sensor (Infineon Technologies Americas Corp, El Segundo, CA, USA). Assays were performed using 1.5 mL of actively growing cells that were purged with 1% CO₂/99% He supplemented with 12 µL of 0.5 M potassium bicarbonate in 5 mM Tris (pH 8.5). After injection into the reaction chamber, the rate of change in O₂ levels was measured sequentially at light intensities of 40, 80, 160, 320, 640, 1280, 1600 µmol photons m⁻² s⁻¹ (PAR) (Luxeon III Star,

Lumileds, San Jose, CA, USA); each intensity was maintained for 3 min followed by a 3 min intervening dark period and then the light level was raised to the next higher intensity (stepped change) until the full range of intensities were tested. Prior to measurement of each experiment series, the electrodes were calibrated with air (~21% oxygen) and with 1% CO₂/99% He purged MOPS medium (0% oxygen). The intensity of light from the LEDs was calibrated using a Walz US-SQS/L spherical micro quantum sensor (Walz, Germany).

2.5.4 CHL FLUORESCENCE ANALYSIS

Chl fluorescence was measured using a DUAL-PAM-100 fluorometer (Walz, Germany). For monitoring Chl fluorescence at different light intensities (i.e. a light curve), the cells were supplemented with 2 mM NaHCO₃ and exposed to increasing light intensities for 1 min at each intensity. The quantum efficiency of PSII as well as photochemical quenching, qL (and accordingly 1-qL (Kramer et al. 2004a)) were directly calculated from the light curves.

2.5.5 O₂ PRODUCTION AND LIGHT DRIVEN O₂ PHOTO-REDUCTION

In vivo ¹⁶O₂ photoproduction rates and ¹⁸O₂ uptake rates were determined using a custom built membrane inlet mass spectrometer (MIMS) with a Pfeiffer quadrupole PrismaPlus QME-220 (Pfeiffer Vacuum, Germany) coupled with a Pt-Ag/AgCl polarographic electrode system (ALGI, Littleton, CO, USA) equipped with a temperature-controlled, water-jacketed 1 mL glass cell, a YSI 5331A electrode (Yellow Springs Instruments, Yellow Springs, OH, USA) polarized at -0.8 V, and an atmospheric barometric pressure sensor (Infineon Technologies Americas Corp, El Segundo, CA, USA). For performing MIMS assays, 1.5 mL of actively growing cells were purged with 1% CO₂/99% He that was spiked with 0.5 mL 99% ¹⁸O₂ and supplemented with 4 mM potassium bicarbonate that was suspended in fresh medium. After injection of the sample into the reaction chamber, a light regime (Luxeon III Star, Lumileds, San Jose, CA, USA) was applied as

follows: 5 min dark, 6 min light and then 3 min of dark. The light intensities used for these experiments were 50, 150, 300 and 1000 $\mu\text{mol photons m}^{-2} \text{ s}^{-1}$ (a single intensity of light was used for each experiment). The electrode and MIMS were calibrated before each measurement using atmospherically equilibrated medium, 1% CO_2/He balance purged medium, and purged medium spiked with 0.5 mL 99% $^{18}\text{O}_2$. The light intensity from the LED was calibrated using a Walz US-SQS/L spherical micro quantum sensor (Walz, Germany). Gross O_2 production and net uptake were calculated according the following equations (Beckmann et al. 2009b)

$$\text{Net O}_2 \text{ uptake} = {}^{18}\text{O}_2 \times [1 + ({}^{16}\text{O}_2)/({}^{18}\text{O}_2)]$$

$$\text{Gross O}_2 \text{ production} = {}^{16}\text{O}_2 - {}^{18}\text{O}_2 \times [({}^{16}\text{O}_2)/({}^{18}\text{O}_2)]$$

$$\text{Net O}_2 \text{ production} = \text{Gross O}_2 \text{ production} - \text{Net O}_2 \text{ uptake}$$

To inhibit alternative oxidases, samples were supplemented with 2 mM n-propyl gallate (Sigma) suspended in ethanol.

2.5.6 DATA ANALYSES

Data were analyzed (statistics, data filtering and curve fitting) using Origin 2017. Details regarding the calculation of the basal levels of light-driven O_2 uptake can be found in the supplementary materials.

CHAPTER 3: HIGH-LIGHT SELECTION PRODUCES A FAST-GROWING

PICOCHLORUM CELERI

The following chapter contains text from (or adapted from) the accepted manuscript of the same title in *Algal Research*.

Joseph C. Weissman¹, Maria Likhogrud¹, Dylan C. Thomas², Wei Fang², Devin A. J. Karns²,

Jeffrey Chung², Robert Nielsen¹, and Matthew C. Posewitz²

¹ Corporate Strategic Research, ExxonMobil Annandale, NJ

² Department of Chemistry, Colorado School of Mines, 1500 Illinois St., Golden, CO

3.1 INTRODUCTION

To use microalgae for the production of a commodity, low production costs are essential, which demands the highest levels of productivity and culture stability (Sheehan et al. 1998; Flynn et al. 2010; Larkum et al. 2012b). The algae must photosynthesize at a very high rate and dissipate the fewest photons possible under highly variable conditions where cells may be exposed to high light for prolonged periods of time, or alternatively low light for a long period, and may move from low light to high light, or the reverse very quickly (Blankenship et al. 2011). The cells should respond to these changes without lags, and without having their photosynthetic rates depressed by high irradiance. High photosynthetic rates may increase productivity by increasing the ratio of light utilization to light capture, which decreases the dissipation of photons due to light saturation. Additionally, when the commodity is a storage product or secondary metabolite, mass cultures will often be operated in batch, or semi-batch. Continuous cultivation is unlikely since these products are not related to reproductive fitness. A very fast doubling time is essential in the batch process for establishing a productive level of biomass and for recovering from process upsets.

Many algae are unstable when exposed to high light. It is not uncommon that when a dense algal culture (even one exposed to high incident irradiance) is inoculated into a high light situation, e.g., at low cell density, the newly inoculated culture “lags.” It may not grow at all or may grow very slowly. This lag may range from a few hours to weeks, or may be permanent, characterized by decreasing pigment concentration in the biomass and possibly the collapse of the culture. Many times such cultures, e.g., *Spirulina*, are covered with light-blocking screens to allow gradual adjustment to the higher light, as the culture becomes denser. In the laboratory, algal cultures are often moved from lower to intermediate to higher irradiance as they grow. Inoculating at higher density often shortens or eliminates this adjustment time. This is not adjustment to a fresh media, as inoculating from low light to low light, even at lower density, rarely causes such a perilous lag. A decrease in culture viability may occur when a semi-batch culture is continually re-started at too low a cell density, or if a continuous culture is operated at too low a cell density. We call these phenomena a sensitivity to light, to avoid confusion with any specific mechanism of photodamage. All the experiments we describe in this report were carried out indoors under visible light only, but similar, and often more drastic observations are commonly made outdoors with many types of algae.

For these reasons and others, we decided to enrich collections of natural waters for algal cells that reproduce the fastest under very high light in dilute culture, using a turbidostat, or alternative continuous-type culture. A new species of the genus *Picochlorum*, (*P. celeri*), emerged from these selections with the fastest reproduction rate in high light among the organisms collected. *Picochlorum celeri* is presented in this report and discussed in terms of the potential growth advantages it possesses. Characteristics of *P. celeri* are compared to two strains of commonly studied algal genera, *Chlorella* and *Tetraselmis*.

3.2 MATERIALS AND METHODS

3.2.1 REPLICATION AND STATISTICS

We assign two levels of biological replication. Level 1 entails successive sampling, often daily, from a single culture vessel where each daily sample is a replicate. Each data point represents the mean of these replicates with errors bars representing standard deviation. For level 2 replication, culture vessels were each independently inoculated. This is shown by multiple clustered data points. Two-tailed t-tests were calculated to determine statistical significance. These are discussed throughout the text.

3.2.2 GROWTH CONDITIONS

All algae were grown in 400 mL square Pyrex bottles (Corning Inc, Corning, New York, USA). Cool white LED light banks provided 2,000 $\mu\text{mol photons m}^{-2} \text{ s}^{-1}$ photosynthetically active radiation (PAR) and diel illumination. Six GE 54W T5 865 ECO HO 6500K high output daylight fluorescent lamps were used to provide irradiances of 900-1000 $\mu\text{mol photons m}^{-2} \text{ s}^{-1}$ PAR. Irradiances below 100 $\mu\text{mol photons m}^{-2} \text{ s}^{-1}$ PAR were provided by fluorescent T8 lamps. Cultures were continuously sparged with 0.75-1% CO_2 in air at about 1 v/v/minute, and stirred at ~280 rpm. Cultivation temperature was 29-33 °C. Cultures were diluted semi-continuously, unless otherwise specified in the text, by removing a specified fraction of the culture volume (after replacing evaporative losses with DI water) and replacing it with fresh medium.

Light intensity was measured using a Walz US-SQS/L spherical micro quantum sensor (Walz, Germany), or a Biospherical Instruments Amour –SL125PAR spherical probe (Biospherical Instruments, Inc., USA). Irradiance measurements were made either in the center of the 400 mL liquid culture volume, or for dilute culture quantum requirement measurements, in

80 locations within the 400 mL liquid volume, and averaged. Numerous light readings were taken. Standard deviations were about 10% of the mean.

For dilute cultivation, the target chlorophyll density prior to dilution was $< 0.5 \mu\text{g/mL}$. Medium used was 0.2 μm filter sterilized seawater, enriched with trace nutrients (40 g/L Instant Ocean, $1.0 \cdot 10^{-3}$ g/L $\text{FeSO}_4 \cdot 7\text{H}_2\text{O}$, $1.35 \cdot 10^{-3}$ g/L Na_2EDTA , $7.6 \cdot 10^{-2}$ g/L NH_4Cl , $2.23 \cdot 10^{-2}$ g/L KH_2PO_4 , $3.14 \cdot 10^{-4}$ g/L $\text{MnSO}_4 \cdot \text{H}_2\text{O}$, $2.42 \cdot 10^{-5}$ g/L $\text{CoCl}_2 \cdot 5\text{H}_2\text{O}$, $4.88 \cdot 10^{-5}$ g/L $\text{ZnSO}_4 \cdot 7\text{H}_2\text{O}$, $2.00 \cdot 10^{-6}$ g/L $\text{CuSO}_4 \cdot 5\text{H}_2\text{O}$, $6.81 \cdot 10^{-6}$ g/L $\text{Na}_2\text{MoO}_4 \cdot 2\text{H}_2\text{O}$, $1.82 \cdot 10^{-2}$ g/L thiamine HCl, $9.09 \cdot 10^{-5}$ g/L biotin, and $9.09 \cdot 10^{-5}$ g/L cyanobalamin). This composition was designed to support about 200 mg/L of algal biomass at 10% nitrogen content, but more importantly to minimize organic carbon content.

For dense cultures the following alterations of the dilute medium were used: urea was substituted for ammonium, and supplied in concentrations sufficient to support algal growth with nitrogen at 10% of the weight algal biomass expected; the iron concentration was increased by a factor of 3; EDTA concentration was increased by a factor of 5, phosphate was increased by a factor of 4, and the concentrations of vitamins was increased by a factor of 5.

For axenic cultivation, bacterial contamination was monitored every other day by plating liquid cultures on LB plates and checking for bacterial colonies the following day. Data from axenic cultures are labeled in the text, otherwise cultures were unialgal.

3.2.3 COMPOSITION ANALYSES

Ash free dry weights were performed by filtering samples from the culture suspensions through pre-ashed (in aluminum pans) Whatman GF/C filters. Enough suspension was used to obtain at least 5 mg of ash-free dry weight (AFDW) on the filter. The filters in the pans were dried at 105 °C for 24-72 hours, weighed on an analytical balance (0.00001 g) after cooling in a

desiccator, ashed at 550 °C for 30 min, weighed again after cooling, and the difference used as the AFDW. Samples were run in triplicate. Typical standard deviations of these replicates were 2% of the mean.

Chlorophyll was measured in duplicate by filtering 10 mL or more of culture through a 25 mm GF/C filter (Whatman, U.K.) and washing with 35 g/L NaCl. Pigments were then extracted from filters by vortexing with 100% methanol and 0.5 mm glass beads (BioSpec Products, Bartlesville, OK, USA). Filters were pelleted and the total chlorophyll concentration in the supernatant determined for *Picochlorum* using a dichromatic calculation at wavelengths 652nm and 665nm (Porra et al. 1989b). For *Chlorella* and *Tetraselmis* a trichromatic calculation was used (Ritchie 2008). The difference of the mean to each of the duplicates was <1.5% of the mean.

Total carbon in the algal biomass was quantified in duplicate by CHN analysis performed by the Marine Science Institute at the University of California at Santa Barbara. Briefly, 25 mL of the algal culture was filtered through pre-ashed 25 mm GF/C filters (Whatman, U.K.) followed by washing with 25 mL of 35 g/L NaCl. Filters were then dried for 24-72 h at 100 °C and samples were analyzed with a Rapid Analysis Element Analyzer CE440 (Exeter Analytical, Inc, Chelmsford, MA, USA). The difference of the mean to each of the duplicates was <1.0% of the mean.

3.2.4 OXYGEN EVOLUTION

In vivo O₂-photoproduction rates were determined using a custom-built Pt-Ag/AgCl polarographic electrode system (ALGI, Littleton, CO, USA) equipped with a temperature-controlled, water-jacketed 1 mL glass cell, two YSI 5331A electrodes (Yellow Springs Instruments, Yellow Springs, OH, USA) polarized at -0.8V, and an atmospheric barometric

pressure sensor (Infineon Technologies Americas Corp, El Segundo, CA, USA), as described previously (Meuser et al. 2011). The result of the two electrodes was within 5% of each other. For determining photosynthetic O₂-production and dark-consumption rates, 1.5 mL aliquots of actively growing cells were either purged with 1% CO₂/He followed by the addition of 12 μL 0.5 M potassium bicarbonate in 5 mM Tris, or in some instances the bicarbonate, without Tris, was first added and then the aliquots were sparged with 1% CO₂/He. Starting pH for these assays was 7.4. It was calculated that approximately 100 μM CO₂ was present at the end of the assay to avoid any CO₂ limitation during the assay. The sample was then injected into the glass sample cell through a septum sealed port. For standard assays, following an initial 5 min dark period, stepped light intensities (Luxeon III Star, Lumileds, San Jose, CA, USA) were applied as indicated to the sample for 3 min illumination increments, followed by 3 min darkness. Light intensities used were 50, 200, 500, 1000, 1500, 2000, 2500 μmol photons m⁻² s⁻¹ of photosynthetically active radiation (PAR), except for modifications described in the text. Net O₂-production and consumption rates were measured by the slope of the linear fit of the inner 50% of the illumination and dark periods. The temperature was maintained at 35 °C throughout the experiment. Electrodes were calibrated before each measurement using atmospherically equilibrated growth media and deoxygenated medium. The LED output was calibrated using a Walz US-SQS/L spherical micro quantum sensor (Walz, Germany).

3.2.5 GROWTH RATES

Specific growth rate was calculated as the natural log of the biomass density [AFDW, particulate organic carbon (POC), and/or chlorophyll] just prior to dilution at the end of a given growth period, divided by the biomass density just after dilution at the beginning of the same growth period, divided by the duration of the growth period (in hours).

Biomass productivity was calculated as the biomass density (AFDW and/or POC) just prior to dilution at the end of a given growth period, minus the biomass density just after dilution at the beginning of the same growth period, divided by the duration of the growth period (in days). This volumetric productivity was multiplied by the factor, $67 \text{ L} \cdot \text{m}^{-2}$, which is the volume of the culture suspension in the growth vessel (0.40 L) divided by the area of the illuminated surface (0.006 m^2).

3.2.6 OPTICAL ABSORPTION

Absorption cross section was measured from the visible absorption spectrum of the dilute (or diluted) suspension of algae in a Thermo Scientific Evolution 220 UV/Vis spectrophotometer with an integrating sphere attachment (Fisher, USA) and/or a Lambda 630 S UV/Vis spectrophotometer with integrating sphere attachment (Perkin Elmer, USA). Assays were done in triplicate. Standard deviations were $<1.0\%$ of the mean.

The spectral resolution was 1 nm, over the wavelength range 350-850 nm. Spectra were acquired as single traces with 500 ms integration time. Spectra were acquired and processed in triplicate. Post processing included a single-point baseline correction obtained from the average of OD in the 800-850 nm region. Spectra were digitally filtered by the application of a 1-2-1 filter three times

3.2.7 SPECTRAL IRRADIANCE

Spectral irradiances of all growth light sources were obtained with a spectral radiometer covering the wavelength range 199.5-992.6 nm with 0.8 nm resolution (Ocean Optics, QE65000). Spectra were acquired as 100 averaged traces with 100 ms integration time, using the factory nonlinearity correction, and with Ocean Optics cosine-corrected flat diffuser probe.

Absolute spectral radiance within the culture was determined as described above using a submersible PAR meter (Biospherical, AMOUR). The spectral irradiance from the Ocean Optics radiometer was normalized to the Biospherical PAR output using the Biospherical factory quantum efficiency correction over the PAR spectrum.

3.2.8 TOTALIZED ABSORPTION CROSS SECTIONS

For each 1 nm of wavelength of the absorption spectrum measured by the UV/Vis spectrophotometer the fraction of photons emitted within that wavelength range from the light source was obtained using the PAR intensity measured within the culture and spectral radiance measurement of the light source outside the culture. The total number of photons absorbed per unit of time for the suspension was calculated per wavelength over the PAR spectral range and then totaled over PAR photon absorption. This provided the overall extinction coefficient, K , of the suspension in m^{-1} , when normalized to PAR irradiance. One measurement per sample was typically performed. Analysis of multiple assays on a sample yielded standard deviations <1.0% of the mean. The POC based and chlorophyll a based absorption coefficients, were calculated by dividing K by the POC or chlorophyll density, respectively, of the suspension.

3.2.9 QUANTUM REQUIREMENT

For dilute cultures, quantum requirement was calculated by dividing the μ mol photons absorbed per unit carbon per unit time (POC based absorption cross section multiplied by the growth irradiance) by the specific growth rate of the culture (μ moles carbon per μ moles carbon per unit time), adjusting units of time and moles per gram carbon.

For dense cultures, quantum requirement was determined by dividing the total daily photon input (moles photons per m^2 per day determined by the incident irradiance integrated over the day) by the POC productivity (g POC per m^2 per day divided by 12 g per mole carbon).

3.2.10 PHOTOSYSTEM II CROSS SECTION (ANTENNA SIZE)

Fast Repetition Rate Fluorometry was used to obtain the functional photosystem absorption cross section of PSII (Satlantic Inc., FIRE fluorometer system). Green saturating flashes (540 nm, 65116 $\mu\text{E}/\text{m}^2\text{s}$) were applied for the maximum instrument duration setting of 400 μs with 1 μs resolution. A fluorescein standard was used for the reference excitation profile.

Samples were diluted to allow acquisition in the lower end of the detector gain range, 100-500 instrument-specified gain setting. Samples were dark adapted for several minutes prior to data acquisition.

Functional absorption cross section in nm^2 was obtained by fitting the fluorescence induction curve to a model of single turnover that includes exciton exchange between photosystems and fluorescence quenching following photosystem single turnover. Typically, only one measurement was taken per sample. Analysis of replicate assays yielded standard deviations <2.5% of the mean.

3.3 RESULTS AND DISCUSSION

3.3.1 HIGH LIGHT DIMINISHES SPECIFIC GROWTH RATE OF *TETRASELMIS SP.*

While studying the light-acclimation states (in dilute, semi-continuous cultivation) of a species of *Tetraselmis* (UTEX 2286), a genus that has performed well in outdoor cultivation (Fon Sing et al. 2014; Pereira et al. 2016), it became apparent that light (above saturation) acted to diminish specific growth rates as part of the acclimation response. In these acclimation experiments, algal cultures were manually diluted semi-continuously so that the biomass density, measured as chlorophyll, at the end of each growth period (approximately a day), was maintained below about 5 $\mu\text{g L}^{-1}$, that is, optically thin. Under these conditions, growth was exponential and balanced, so that cellular characteristics (e.g., biomass chlorophyll content and

light absorption per POC or chlorophyll) measured at the end of the growth day represented the conditions throughout the growth period. Exponential growth rates were calculated based on the daily POC or chlorophyll measurements and the amount of daily dilution. As shown in Figure 3.1, the curve of specific growth rates in these steady cultures versus irradiance had a slight decrease above $1000 \mu\text{mol m}^{-2} \text{s}^{-1}$, from a maximum of $0.127 \pm 0.005 \text{ h}^{-1}$ (which corresponds to a 5.5 ± 0.05 hour doubling time). Although this was a relatively fast rate of growth, several observations of the underlying acclimation response indicated the potential μ_{max} could have been greater. There was a large decrease in total chlorophyll (about 75% reduction) from acclimation at $50 \mu\text{mol m}^{-2} \text{s}^{-1}$ to acclimation at $1000 \mu\text{mol m}^{-2} \text{s}^{-1}$. However, the photosystem II functional cross section, measured by fast repetition rate fluorescence, did not diminish with acclimation to higher light. Thus, it can be presumed that the number of total photosystems (or photosynthetic units, PSUs, to encompass reaction centers and electron transport chains) in the cells must have been reduced to a great degree, even though likely not proportionate to the reduction in chlorophyll. In addition, some of these remaining photosystems were probably damaged in high light despite the lack of UV light. If the net effect of high light acclimation is to depress the number of photosystems to the extent that the remaining photosystems cannot produce enough electrons and energy to saturate carbon fixation, then both photosynthesis and reproductive rate would be reduced not only at the highest irradiance shown but at many irradiances above saturating.

To test this hypothesis, low-light acclimated cultures were grown at $50 \mu\text{mol m}^{-2} \text{s}^{-1}$. These cultures, which possessed high pigment levels and presumably many PSUs,

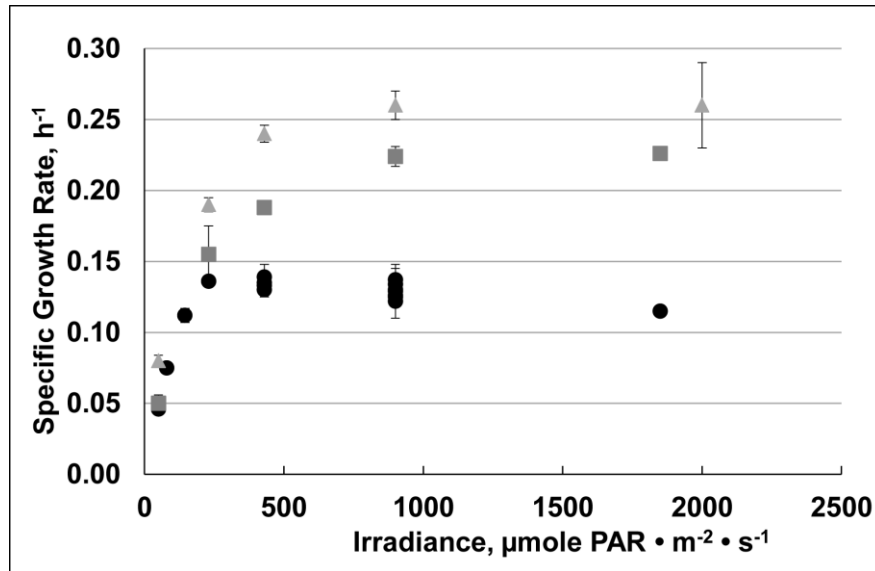


Figure 3. 1 Specific growth rates, based on changes in particulate organic carbon, for dilute (less than $0.5 \mu\text{g mL}^{-1}$ for 8 cm optical path length) suspensions of algae. Circles, light acclimation “steady” states of *Tetraselmis*, diluted semi-continuously; squares, *Tetraselmis* acclimated to $50 \mu\text{moles m}^{-2} \text{s}^{-1}$, moved to higher irradiances for 3-4 hours; triangles, light acclimation states of the high-light-selected alga, *Picochlorum celeri*, diluted semi-continuously. Each point represents the mean of level 1 biological replicates. The number of replicates for each point range from 2-33.

were then transferred to higher irradiances for 3-4 hours to measure the transient growth rates.

Higher specific rates of carbon accumulation were observed relative to the high-light acclimated cultures at all irradiances above $50 \mu\text{mol m}^{-2} \text{s}^{-1}$, including the higher irradiances where growth rate impacts had been observed with high-light acclimated states. Maximum specific growth rate for these transient states was $0.23 \pm 0.5 \text{ h}^{-1}$, which corresponds to a doubling time of $3.0 \pm 0.2 \text{ h}^{-1}$, if the rate of growth could be sustained, and cultures did not acclimate to the higher light intensities. The cellular growth rate was also measured from cell counts in addition to particulate organic carbon (POC). The maximum cellular growth rate was 0.18 h^{-1} , which was lower by about 25% than the specific growth rate measured by POC, but was much higher than for the

high-light acclimated states. The observed difference in cellular growth rate and specific growth rate indicates that the cell size increased in these transient states.

Regardless of cell proliferation rates, underlying these fast specific rates of POC growth, there must be fast rates of photosynthesis. The observed higher growth rates from the low-light acclimated transient growth experiments indicates that the low-light acclimation state retained the capacity for fast photosynthesis despite an interval of months of cultivation strictly in low light. However, since these were multi-hour light-shift experiments, it is possible that the cells underwent regulatory changes, or even increases in concentrations of some key proteins. In any case, low-light acclimated cells, when shifted to high light, demonstrated very high photosynthetic capacities not exhibited under other conditions.

Light shift experiments were repeated with other algae, but with responses different from *Tetraselmis* 2286. The specific growth rates of a *Chaetoceros* sp. (UTEX 1316) and *Chlorella* (CCMP 252, now NCMA 252), did not increase when low-light acclimated cultures were moved to higher light. The diatom differs from *Tetraselmis* 2286 in at least two characteristics: it has a lower high-light acclimated doubling time of 4.2 h versus 5-5.5 h and its carbon-specific optical absorption cross section is about 100% higher. *Chlorella* 252 also has a higher carbon-specific absorption cross section relative to *Tetraselmis* when high-light acclimated (see Section 3.7.2), but its specific growth rate is similar to that of *Tetraselmis*.

For stable growth in large ponds in which cells could be exposed to high light for sustained periods of time, it would be best to use an alga that retains very high photosynthetic and reproductive rates under such conditions, and retains these high rates no matter what its state of growth or light history. Searching for this led us to select algae under very high light in dilute

culture. The upper curve in Figure 3.1 is from the steady-state light acclimation states of the *P. celeri* alga that was selected, as described below.

3.3.2 PICOCHLORUM CELERI EMERGES FROM SELECTION FOR FAST REPRODUCTIVE RATE IN HIGH LIGHT

To obtain genetic variability to submit to a selection in high light for fast reproduction rate, water samples were collected in June and August, 2015 and then again in August and September, 2016. We chose the southeast coast of Texas to collect water samples because of the bright, warm weather, and waters that usually have relatively high plankton concentrations. Water samples were collected, gravity filtered through 30 μm mesh and immediately shipped overnight to the laboratory. To initiate selection of high light and high temperature tolerant strains, environmental samples were cultured under a 12:12 light-dark cycle illuminating at 1000 $\mu\text{moles PAR m}^{-2} \text{ s}^{-1}$ in a sea water medium and cycling the temperature to swing between 23 $^{\circ}\text{C}$ and 37 $^{\circ}\text{C}$ each day. Daily removal and replacement of 25% of the medium was done to select for fast growth, high-light, and high-temperature tolerant marine algae. After six weeks of selective pressure, subsamples of enrichments were put into cultivation vessels under constant illumination at 900 $\mu\text{mol m}^{-2} \text{ s}^{-1}$ at a temperature of $\sim 30^{\circ}\text{C}$. Within days, the culture had to be diluted almost 300-400 -fold to keep chlorophyll concentrations under 1 $\mu\text{g mL}^{-1}$. It attained a doubling time of 3.0 hours. Similarly, waters collected in 2016 were put under high-light selection in dilute, semi-continuous cultivation.

These initial enrichments were not unialgal. What eventually took over, *P. celeri* (as determined by 18S ribosomal gene sequence), is about 2-3 μm in longest size and was mostly in division-induced doublets. Species of *Picochlorum* (previously referred to as *Nannochloris* in some cases) are noted for their distinctive tolerance to a diversity of abiotic stresses (Henley et al.

2004; Foflonker et al. 2015; Wang et al. 2016; Dogaris et al. 2016; Foflonker et al. 2016). There were initially other algae of larger size, mostly in clumps. Once *P. celeri* isolates were introduced to the laboratory, any open, i.e., non-axenically operated dilute culture under high irradiance, inoculated or not, was overrun by self-inoculated *P. celeri*. Specific growth rates in the selection reactors hovered around 0.22 h^{-1} . The enrichment from the first 2015 collection (referred to as Enrichment 1 or E1) was split into three, semi-continuously diluted cultures. These were all cultured under continuous, high incident irradiance. One culture was kept very dilute, as above, to minimize light attenuation to continue the selection based on reproductive rate. The other two were diluted at about 60% per day to allow them to become dense. One was grown at seawater salinity, the other at twice that salinity (which performed as well as the seawater salinity culture). Since none of these were axenic or unialgal from the start, they were not operated as closed to other potential contamination. *P. celeri* continued to become more and more dominant in all cultures so that within a few months all of these enrichments became uniform under the microscope, without clumps. Despite subsequently isolating single cells from these enrichments, E1 has been ongoing because the attributes of the isolates and the enrichments they came from are not identical. These were not perfect enrichment cultures. In general, they were not diluted over the weekend, so densities were greater on Monday than during the week.

Light acclimation studies were then initiated with the *P. celeri* enrichment E1. The specific growth rate results are shown in Figure 3.1. *Picochlorum celeri* grew faster than our reference *Tetraselmis* at all irradiances. Importantly, when low-light-acclimated *P. celeri* cultures were moved to higher light the specific growth rates over the subsequent three hours were the same rate as *P. celeri* cultures already acclimated to the high light (data not shown).

Low-light and high-light acclimated cells had different characteristics (discussed below), but each maintained the potential to reproduce very fast at high irradiance with little or no lag noticed after inoculation.

3.3.3 ISOLATION OF SINGLE CELL LINES FROM THE *P. CELERI* ENRICHMENTS

Several attempts were made to isolate single cells from the *P. celeri* enrichment cultures. At first, cells were isolated by streaking on agar plates and incubating the plates under low-light conditions. The cultures obtained from this process did not have reproduction rates nearly as fast as the enrichment cultures (data not shown). To improve the outcome, single cells derived by FACS sorting were each put in a single well of a 96-well plate, and incubated in air under 1500

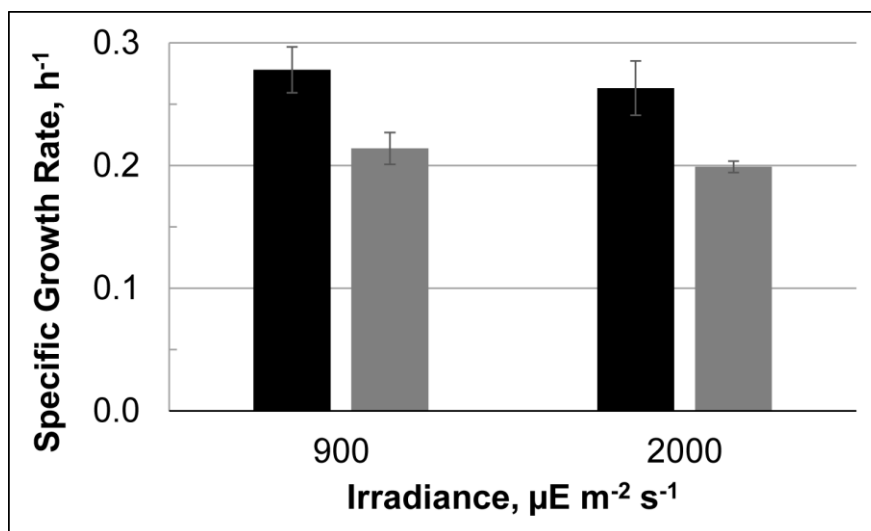


Figure 3. 2 Specific growth rates of light-acclimated states of *P. celeri* enrichment E1 (black bars) and *P. celeri* TG1 (grey bars) at two irradiances ($\mu\text{moles m}^{-2} \text{s}^{-1}$ PAR). Number of level 1 biological replicates are listed left to right: 10, 3, 18, 5.

$\mu\text{mol PAR m}^{-2} \text{s}^{-1}$. The first three wells that visibly greened were transferred and grown in flasks under moderate light. Samples of one of these clonal cell lines (named TG1) were then tested for specific growth rate in dilute cultures at high irradiance. Results of these specific growth rate experiments at 900 and 2000 $\mu\text{mol m}^{-2} \text{s}^{-1}$ are shown in Figure 3.2. Again, none of the

cultures derived from single cell isolates performed as well as the putatively more diverse population in the enrichment cultures.

Therefore, a different strategy was developed to obtain faster growing isolates. One issue with the previous methods is that isolates were first produced under conditions that were different from the highly selective growth conditions used for the ongoing high-light enrichment cultures. Afterwards the isolates obtained were tested in the highly selective conditions. The aim of the new method was to both obtain isolates and simultaneously use the selective conditions to grow the isolates and test their doubling times. To accomplish this, cell counts were performed on the ongoing dilute, high-light enrichment culture (E1). Then dilutions were performed (six billion fold) so that after inoculation of new growth units (to be incubated under the highly selective conditions), there would be a probability of just 0.25 cells per vessel (dilution towards extinction). Thus, a large dilution was used to obtain isolates, and the growth from single cells occurred under the conditions desired. Eight growth vessels were inoculated.

Table 3. 1 Reproductive rates of isolates of *P. celeris* E1 obtained by either FACS sorting to obtained single cells, growing in well plates, and selecting the first to green (isolate TG1), or by diluting six billion fold to isolate at most single cells (or no cells) in each growth vessel then exposed to 900 $\mu\text{moles m}^{-2} \text{s}^{-1}$ to measure specific growth rates (TG2 and other numbered isolates). *P. celeris* TG1 and TG2 were made axenic after isolation. $24 \cdot \tau^{-1}$ is doublings per day.

<i>P. celeris</i> Isolation Vessel, Name	μ, h^{-1}	SD (n)	τ, h	$24 \cdot (\tau^{-1})$
E1	0.28	0.012 (5)	2.5	9.7
FACS Sorted, TG1	0.22	0.014 (9)	3.2	7.5
FACS Sorted, TG1 axenic	0.21	0.005 (3)	3.4	7.1
#2	0.29	0.013 (6)	2.4	10.0
#3, TG2	0.33	0.009 (14)	2.1	11.5
#3 replicate, TG2	0.33	0.003 (6)	2.1	11.5
#3, TG2 axenic	0.34	0.026 (3)	2.0	12.0
#6	0.30	0.010 (8)	2.3	10.4

Three showed growth. Each of the three isolates obtained had different doubling times, one of which (TG2) was 2.1 hours compared to the enrichment culture doubling time of about 2.5 hours (significant with $p < 0.001$). Table 3.1 summarizes the results. It is evident that even a population enriched for a particular characteristic (reproductive rate in this case) contains substantial phenotype variability and thus the method used to isolate cells from the enriched population determines how the isolate performs relative to the enrichment. The doubling times of TG1 and TG2 as axenic, clonal cultures are also shown in the table. The axenic cultures grew as fast as the non-axenic ones.

3.3.4 BIOMASS PRODUCTIVITY OF *PICOCHLORUM*, *TETRASELMIS*, AND *CHLORELLA* IN CONSTANT HIGH LIGHT

As previously stated, enrichment cultures of high-light selected *P. celeri* were not only maintained at $2000 \mu\text{mol m}^{-2} \text{s}^{-1}$ constant light in dilute culture (the original enrichment situation) but also in dense culture diluted semi-continuously 80-90% per day during the week, and, what became routine, 800,000 fold for the weekend to keep the density on Mondays close to the steady-state values prevailing during the rest of the week. The biomass productivities of the dense cultures were measured. Figure 3.3 shows the productivities under constant high light of E1 (data combined from three biological replicates) along with isolates from E1 (TG1 and TG2). Using two-tailed t-tests, the isolate TG1 was less productive than the enrichment E1 or isolate TG2 ($p < 0.001$). The productivities of E1 and TG2 were not different to any high level of confidence. All of the *P. celeri* cultures could be semi-continuously diluted ten-fold per day. There was a shallow productivity optimum around seven-fold dilution. A four-fold dilution was about 20% less productive (data not shown). Growth was extremely stable. Some cultures were

grown for hundreds of days without mishap, despite the large dilutions for weekends. This extraordinary stability in culture is a hallmark of this *P. celeri*, and is repeatedly demonstrated in conditions where other strains failed to show robustness. It can be inoculated from a single cell (as in the isolation procedure) and always come up with little or no lag. It can be inoculated from a stock flask (grown on air, not enriched CO₂) with a one-million-fold or more dilution and virtually always come up with only a minor lag.

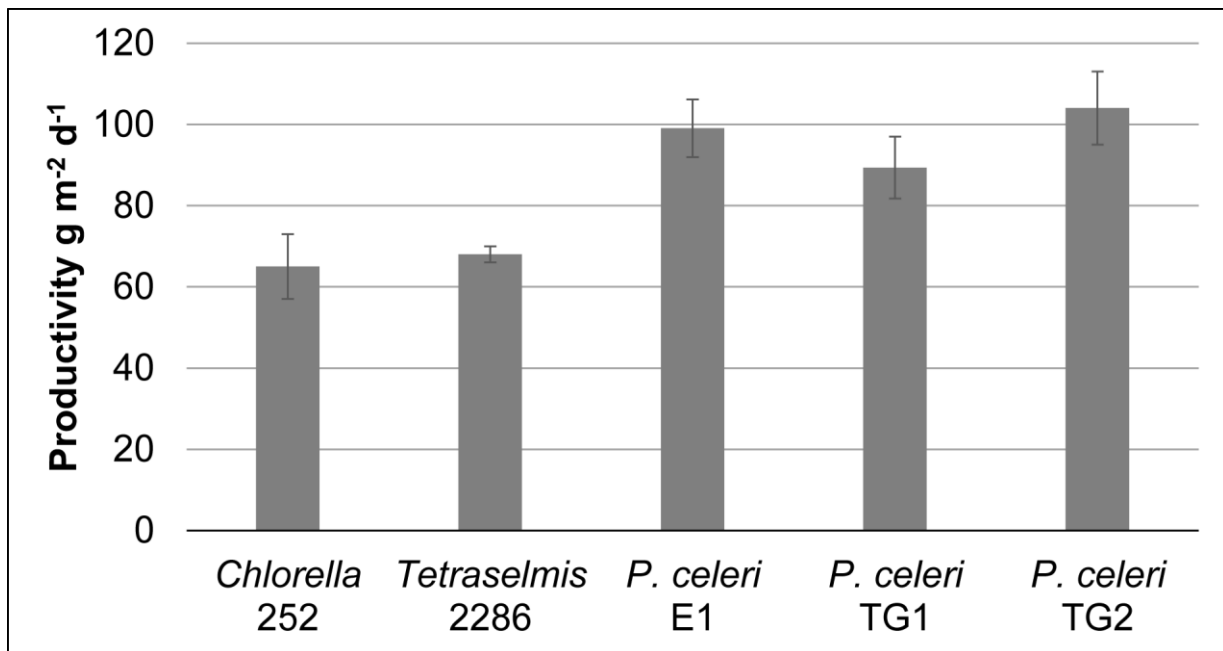


Figure 3.3 Biomass productivity (AFDW) of semicontinuously-diluted algal cultures grown under 24 hour continuous irradiance at 2000 $\mu\text{mol m}^{-2} \text{s}^{-1}$. The number of level 1 biological replicates from left to right: 18, 3, 76, 25, 33.

Also shown in Figure 3.3 are biomass productivities of *Chlorella* and *Tetraselmis*, two other marine genera of bio-commodity interest. Productivities of the two latter strains were essentially the same and well less than that of *P. celeri*. In addition, the semi-continuous dilution rate for these strains had to be kept much lower, about one-third per day, or the cultures grew progressively more poorly and eventually died. These strains grew well under constant light at

lower irradiance (circa $1000 \mu\text{mol m}^{-2} \text{s}^{-1}$). *Chlorella* and *Tetraselmis* also had to be brought up carefully through an inoculum train. If inoculated directly into $2000 \mu\text{mol m}^{-2} \text{s}^{-1}$, they died.

3.3.5 BIOMASS PRODUCTIVITY OF *PICOCHLORUM*, *TETRASELMIS*, AND *CHLORELLA* IN DIEL LIGHT

All three algae were also cultivated under diel conditions, again at favorable pH (7) and temperature ($30 \text{ }^\circ\text{C}$ twenty four hours a day). The diel irradiance profile that was used is shown in Figure 3.4. It is a simulation of a clear day in mid-May in Phoenix, AZ based on geometric models of incident solar light at this longitude, latitude and elevation. Mass algal cultivation for fuels or commodities will most likely be done within the tropics or other locations which have warm minimum daily temperature throughout the year. In these places, the declination of the sun will usually be great and thus most photons will hit a horizontal surface at high irradiance during times of illumination. For the diel curve shown in Figure 3.4, only 3% of the photons arrive at an irradiance $< 500 \mu\text{mol m}^{-2} \text{s}^{-1}$. Only about 9% arrive at an irradiance $< 900 \mu\text{mol m}^{-2} \text{s}^{-1}$. This emphasizes the importance of looking for algae that have high photosynthetic efficiency when the incident light is high and not worrying too much about how they perform when the incident light is low.

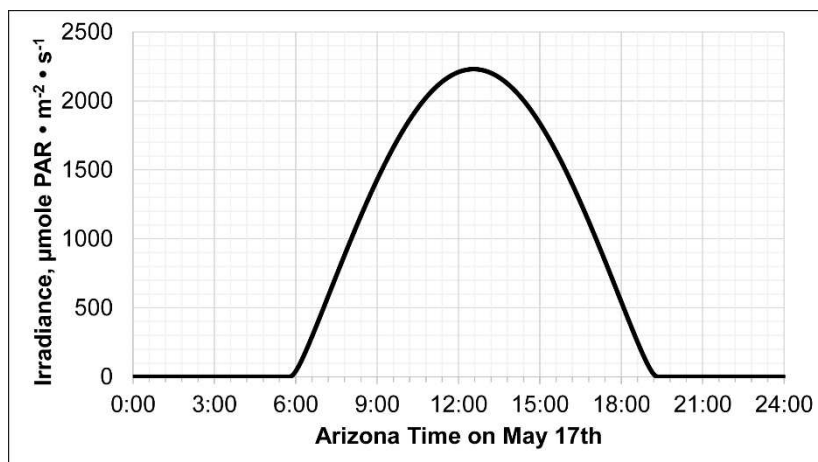


Figure 3. 4 Simulated solar day (PAR) used for diel illumination for algal growth.

The biomass productivities of *Chlorella*, *Tetraselmis* and three lines of *P. celeri* (the original enrichment culture and two isolates from it), along with chlorophyll content are shown in Figure 3.5. The productivities of the *P. celeri* cultures were all approximately the same. E1 was only different from TG1 or TG2 with $p < 0.1$. The two isolates were different at $p < 0.05$. The productivity of *Tetraselmis* was not statistically different from that of TG2 or *Chlorella*. Statistically significant differences would be more discernable on the figure if the uncertainties were expressed as standard errors, rather than standard deviations. The standard deviation was chosen because experience showed that this is more representative of the uncertainty between biological replicates, even though standard error reasonably represents the uncertainty for repeated days of productivity measurement of a given biological replicate. The *Chlorella* was less productive than the others, especially when one considers that the data shown is the best that *Chlorella* cultures provided in our laboratories to-date. Often *Chlorella* required days to even months of time to “adapt” to a high-light culture environment. It often grew in metastable states with about 30% less biomass productivity and chlorophyll content. The state was metastable in the sense that it could change to the state that gave the results shown.

For the diel culture data shown, cultures were diluted 60% per day. When *P. celeri* TG2 was diluted at 75% per day, productivity declined about 30%. *Picochlorum celeri* TG2 was also diluted three times during the daylight to see 1) if the productivity would become higher if density were kept lower throughout the day and 2) if the cells would transition into a state of higher-light acclimation. For the 60% dilution once per day, the culture AFDW varied between 400 and 1000 mg L⁻¹. In the three times per day dilution, 100% of the total culture volume was removed per day and the density remained close to 500 mg L⁻¹. The productivity was about 20% less when diluted three times per day compared to 60% dilution once per day, but the state of

acclimation changed very little. It is apparent that genetic engineering will be required to maintain *P. celerii* in a high-light acclimated state if it is to be used as a means to increase productivity in dense culture.

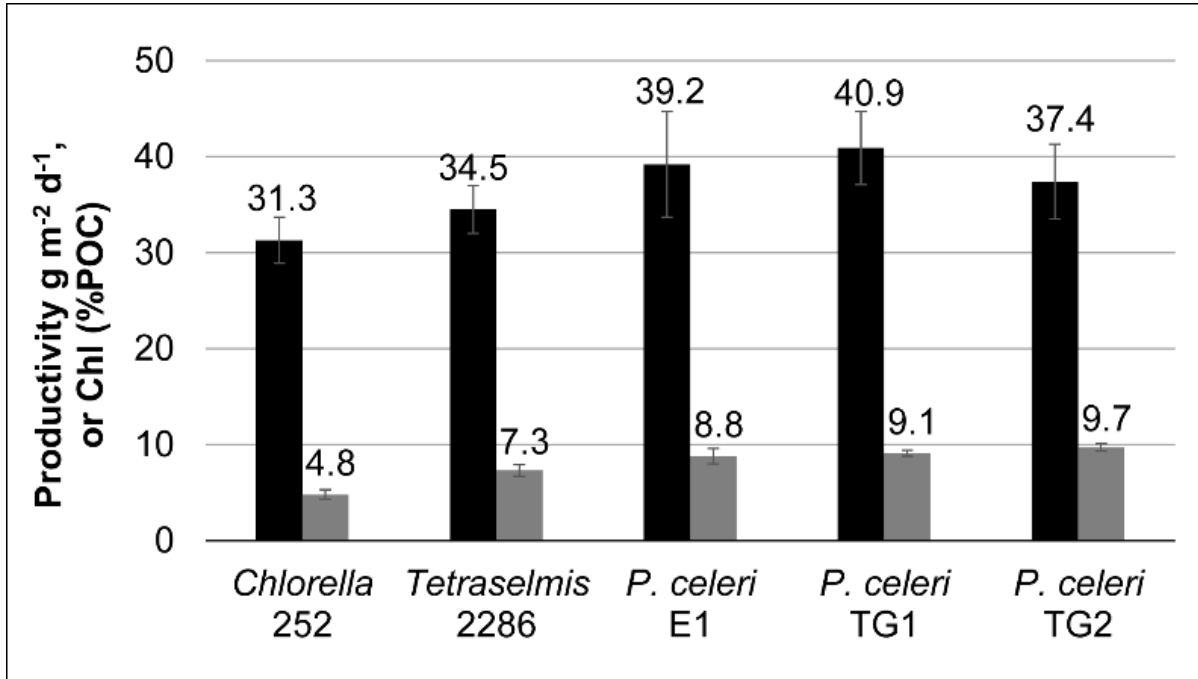


Figure 3. 5 Biomass productivity (AFDW, black bars) and chlorophyll content (grey bars) of semi-continuously diluted algal cultures grown under diel illumination shown in Figure 3.4. The number of level 1 biological replicates for productivity data from left to right: 11, 14, 38, 49, 50. For Chl data (% POC): 11, 7, 15, 16, 14.

3.3.6 OXYGEN EVOLUTION MEASUREMENTS

For any given reproductive rate of an algal cell, it must have an underlying photosynthetic rate that is fast enough to support its specific growth rate. Often photosynthetic rates are expressed as oxygen evolved or carbon assimilated per unit time per chlorophyll. To compare photosynthetic rates of different organisms and isolates to each other, and to measure specific growth rates, it is useful to express the photosynthetic rates on a POC basis. Expressed this way, the rates have units that are equivalent to specific growth rate. We measured

photosynthetic oxygen production. From net oxygen per unit time per unit chlorophyll, the following equation may be used to get the rate expressed as carbon per unit time per unit carbon:

$$\mu \sim P_{\max}(\text{O}_2) \cdot (1/\text{PQ}) \cdot \text{MW C} \cdot (\text{chlorophyll} \cdot \text{C}^{-1}), \quad (1)$$

where PQ is the photosynthetic quotient (moles O₂ evolved per CO₂ absorbed), estimated at about 1.15 for cells growing on urea or ammonia (Myers 1980), MW C = 12, and chlorophyll per C is the chlorophyll content of the algal biomass tested.

This is a hypothetical specific growth rate calculated from a short term photosynthetic rate where photosynthesis is assumed to occur at this rate continuously throughout the cell cycle. In any case, this hypothetical specific growth rate should be equal to or greater than, within error, a measured specific growth rate.

The photosynthesis irradiance (P-I) curves for dilute, axenic TG1 and TG2 are shown in Figure 3.6. TG1 was grown at 2000 μmol m⁻² s⁻¹, while TG2 was grown at 1000 μmol m⁻² s⁻¹.

Using the equation above, the conceptual specific growth rate calculated for TG1 from the P_{max} in Figure 3.6 is 0.17 ± 0.02 h⁻¹. The maximum specific growth rate (from growth studies) of TG1 was 0.20 ± 0.05 h⁻¹, which is the same within error. For TG2, using equation 1 and the average P_{max} measured converted to the POC basis was 0.30 ± 0.03 h⁻¹, while the maximum specific growth rate was about 0.34 ± 0.026 h⁻¹, again approximately the same. Table 3.2 summarizes the results comparing P_{max}, on a chlorophyll basis with the POC basis (expressed as a specific growth rate) calculated using equation 1 for *P. celeri* and *Chlorella*. Growth conditions are listed, as well as the type of oxygen evolution experiments that were used to determine P_{max}.

The POC-based P_{max} for high-light acclimated TG1 (grown dilute under high light) was similar to the specific growth rate measured from the culture. For a low-light acclimated culture

(grown under diel illumination), the POC-based P_{max} , was much higher than either one.

Apparently, low-light acclimated TG1 cultures have a much greater photosynthetic capacity than high-light acclimated cultures, at least in the oxygen evolution assay. A similar inference was made for the *Tetraselmis* strain studied in the short term 3-4 h light switching assay of section 2.1.

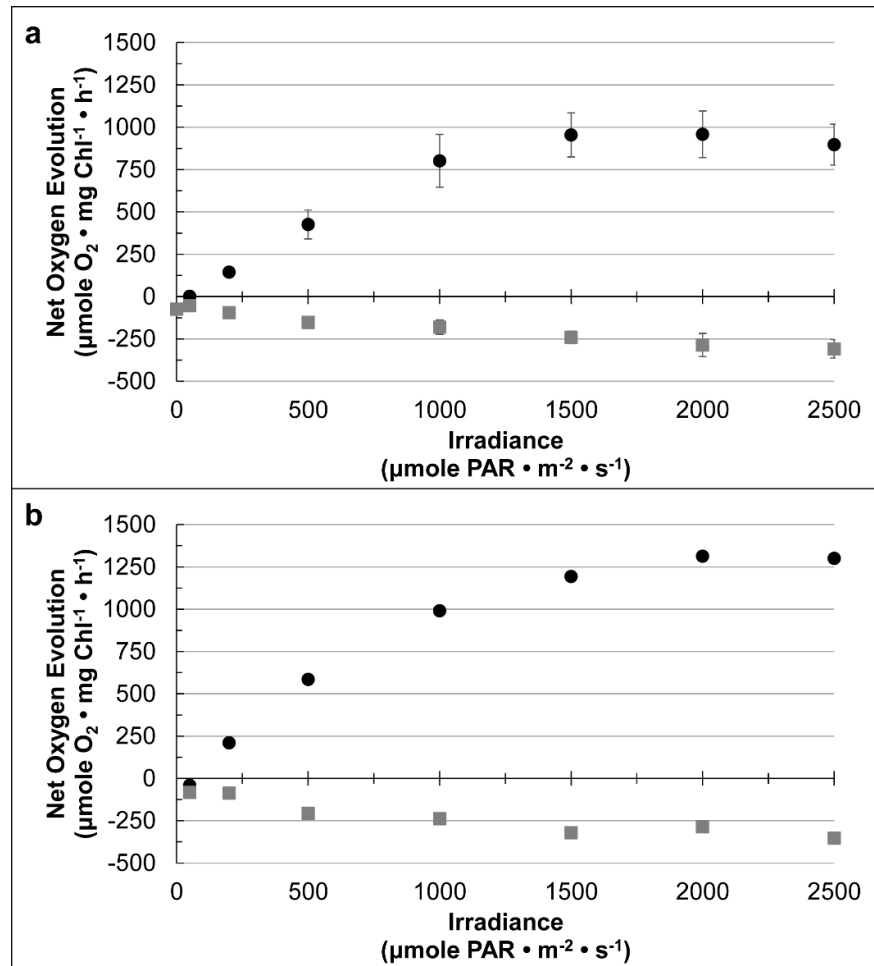


Figure 3. 6 Photosynthesis-Irradiance curves for *P. celeri* TG1 and TG2. Circles are net oxygen evolution; squares are oxygen consumption in the dark. a. TG1 grown dilute under 2000 $\mu\text{moles m}^{-2} \text{s}^{-1}$, in vessels 8 cm optical path length. Chlorophyll density of the suspension on the day the P-I response was measured was $0.6 \mu\text{g mL}^{-1}$. It was not diluted for the oxygen evolution assay. Total chlorophyll content of the biomass was 1.7% of the POC. b. TG2 grown dilute under $1000 \mu\text{moles m}^{-2} \text{s}^{-1}$. Suspension chlorophyll density was $0.6 \mu\text{g mL}^{-1}$. It was diluted 4-fold for the assay. Total chlorophyll content of the biomass was 2.7% of the POC. The number of level 1 biological replicates are: a: 4. b: 1.

On the other hand, as shown in Figure 3.6 and summarized in Table 3.2, the POC-based P_{\max} (measured by oxygen evolution) of high-light acclimated TG2 was very high, as high as the low-light acclimated TG1 results. This could be anticipated from the very short doubling time of TG2 and the longer doubling time of TG1. Although not tested, it seems probable that the POC-based P_{\max} from low-light TG2 (grown under the diel illumination) in the oxygen evolution assay would also be very high, as was the case for TG1. If so TG2 and TG1 would have very different response to high-light acclimation.

TG1 did have a lower chlorophyll to POC ratio than TG2, 1.7 versus 2.5, but about the same PS II antenna size (TG1 data not shown). Thus, TG1 may have fewer reaction centers than TG2 when both are high-light acclimated, which may be the reason for its lower P_{\max} and μ_{\max} in this state. Low-light acclimated *Chlorella* (Table 3.2, diel illumination) performed differently from low-light acclimated TG1. *Chlorella*'s P_{\max} , on a POC basis was lower than would have been required to support its fastest reproductive rate of 0.145 h^{-1} (see section 3.7.2, Figure 3.9).

Neither strain had to grow as fast as it was capable of growing to keep up with a 60% dilution under the diel condition. Still, TG1, even when low-light acclimated in diel culture could photosynthesize much faster as evidenced by its P_{\max} . Apparently for TG1, as well as for the *Chlorella*, P_{\max} on a POC basis is not independent of its light acclimation state as it is for many algae (MacIntyre et al. 2002).

The full P-I responses for samples taken from cultures of *P. celeri* TG1, *Chlorella*, and *Tetraselmis* grown under diel illumination are given in Figure 3.7. Although not shown in Figure 3.7, the sequence of irradiances was run from low to high light and then from high to low light. The results were statistically indistinguishable. On a chlorophyll basis, the P_{\max} for *P. celeri* was greater than that for *Chlorella* or *Tetraselmis*. Given that the chlorophyll content of *P.*

celeri was higher than that of the other algae under diel illumination (section 2.7.2), the computed μ_{\max} would be even greater. In a different experiment with *P. celeri* TG1, P-I curves were performed using samples taken from the diel culture, both three hours before sundown (irradiance of about $1300 \mu\text{mol m}^{-2} \text{s}^{-1}$), and 0.5 hours after (data not shown). The P-I curve results were the same.

Table 3. 2 Maximum rates of net oxygen evolution per chlorophyll and per POC (carbon per carbon per hour) for *Chlorella* and *P. celeri*. Growth conditions listed indicate whether the cultures were grown dense either under diel illumination or constant illumination at $2000 \mu\text{moles m}^{-2} \text{s}^{-1}$, or grown dilute (chlorophyll density of the suspension kept generally below $0.5 \mu\text{g mL}^{-1}$) under 1000 or $2000 \mu\text{moles m}^{-2} \text{s}^{-1}$ constant illumination. Chl/POC were taken on the same sample as used for P_{\max} measurement.

Strain	Growth Condition	P_{\max} ($\mu\text{mol O}_2 \cdot \text{mg Chl}^{-1} \cdot \text{h}^{-1}$) (n=)	Chlorophyll / POC	POC \cdot POC $^{-1} \cdot \text{h}^{-1}$, using eq. 1
<i>Chlorella</i> 252	Diel Conditions	130 ± 20 (6)	6.7 ± 0.7	0.09 ± 0.02
<i>Chlorella</i> 252	Dense, 2K	160 ± 20 (3)	5.5 ± 1.0	0.09 ± 0.01
<i>P. celeri</i> TG1	Diel Conditions	330 ± 20 (3)	9.0 ± 0.2	0.30 ± 0.01
<i>P. celeri</i> TG1 Axenic	Dilute, 2K	960 ± 140 (3)	1.7 ± 0.1	0.17 ± 0.02
<i>P. celeri</i> TG2 Axenic	Dilute, 1K	950 ± 40 (6)	3.0 ± 0.2	0.30 ± 0.03

Photon quantum efficiency for oxygen evolution (the ratio of oxygen evolved to photons absorbed) can be calculated from the slope of the P-I curve, which is equal to the absorption cross section times the quantum efficiency. For the P-I curves shown, at low irradiance only two or three data points could be used to determine the initial slope. Given this sparseness of points at low irradiance, the calculated initial slopes may underestimate the true initial slopes, and thus efficiencies. Aside from this, propagated error for the quantum efficiencies calculated from the initial slopes were about 10%. From the P-I curve for TG1 grown dilute at $2000 \mu\text{mol m}^{-2} \text{s}^{-1}$ (Figure 3.6), and a measured absorption cross section of $7.7 \text{ m}^2 (\text{g chlorophyll})^{-1}$, the quantum efficiency for this high-light-acclimated alga in subsaturating light was at least 0.03. Thus, the respective quantum requirement was at most 33. For TG2 acclimated to $1000 \mu\text{mol m}^{-2} \text{s}^{-1}$ the

absorption cross section was $6.2 \text{ m}^2 (\text{g chlorophyll})^{-1}$, the approximate quantum efficiency was 0.056 and the quantum requirement was about 18. This is at most 20% higher than the maximal quantum efficiency, 14.8 ± 2 , found from carbon quantum requirement growth experiments in dilute cultures grown at $60 \mu\text{mol m}^{-2} \text{ s}^{-1}$ (section 3.7.3). The difference in quantum efficiencies of high-light acclimated TG1 and TG2 could be due to the different growth conditions. TG1 was grown at higher light and therefore in a higher state of light acclimation. Or TG1 just may not have as high a maximum quantum efficiency, as TG2.

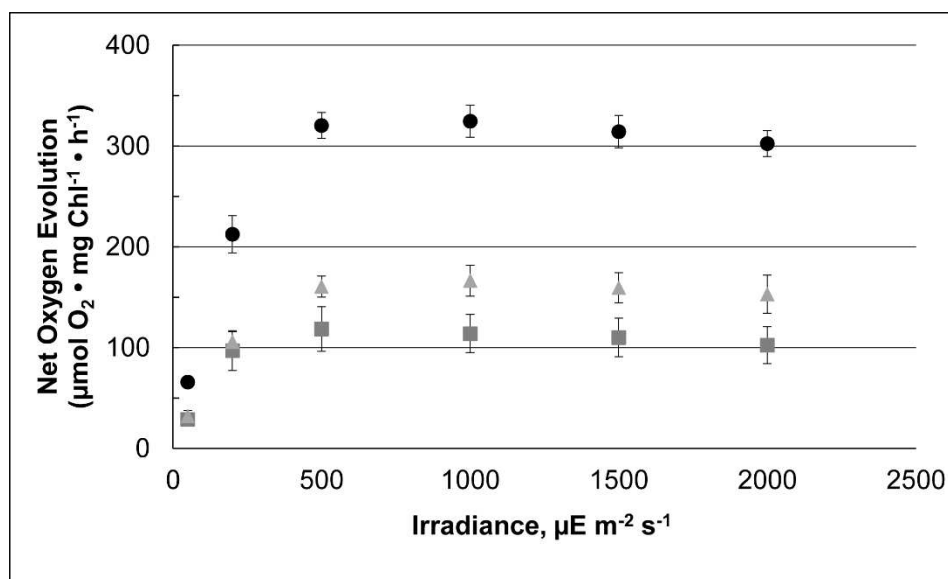


Figure 3. 7 Photosynthesis-Irradiance response for algae grown under a diel cycle. *Chlorella*, *Tetraselmis*, and *P. celeri* TG1. Circles: *P. celeri* TG1. Squares: *Chlorella* 252. Triangles: *Tetraselmis* 2286. All data points are level 1 biological triplicates.

Quantum efficiencies can also be calculated from the P-I responses of the algae grown under diel conditions, and hence low-light acclimated. For *P. celeri* TG1 these were 0.05 (QR = 20) and 0.06 (QR = 17). For *Chlorella* and *Tetraselmis* the quantum efficiencies were 0.023 and 0.035 respectively, with corresponding quantum retirements of 50 and 30. Both *Chlorella* and *Tetraselmis* either underperformed in these oxygen evolution experiments or the diel cultures

were such that the maximal efficiencies of these algae were not expressed. Carbon quantum requirement determined from growth experiments at $50 \mu\text{mol m}^{-2} \text{s}^{-1}$ in dilute culture was about 13 for *Chlorella* and 11.4 for *Tetraselmis* (data shown in Figure 3.9).

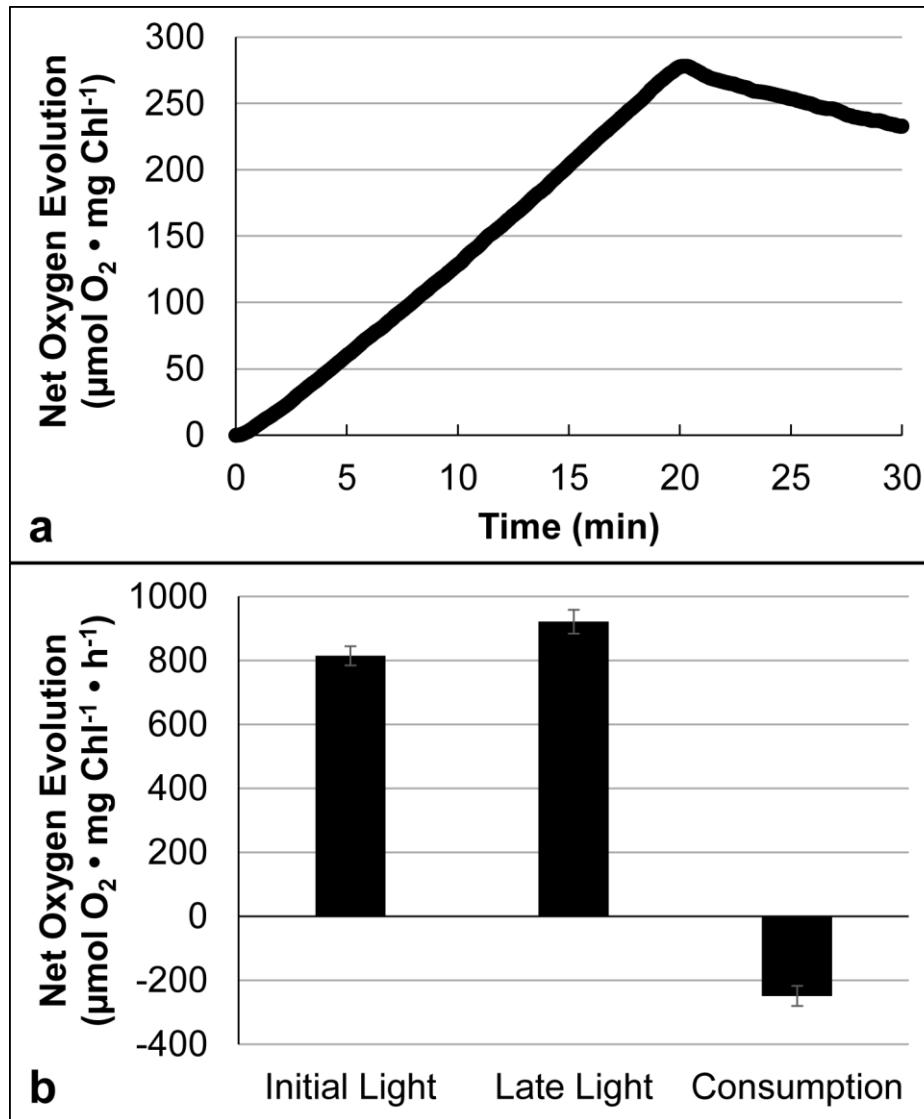


Figure 3. 8 a. Photosynthetic oxygen production of *P. celeri* TG2 versus time at $2000 \mu\text{moles m}^{-2} \text{s}^{-1}$ for 20 minutes and consumption in the dark for 10 minutes. b. Rate of net oxygen evolution: Initial light, rate averaged during minutes 2-8; late light averaged during minutes 12-18; and rate of oxygen consumption in the dark averaged over minutes 22-27. Sample taken from a culture grown dilute at $1000 \mu\text{moles m}^{-2} \text{s}^{-1}$. All data are level 1 biological triplicates. In panel a, standard deviations are within the thickness of the line.

One indication of photoinhibition is the decline of P_{\max} with time. Figure 3.8 shows the photosynthetic rate for 20 min at an irradiance of $2000 \mu\text{mol m}^{-2} \text{s}^{-1}$ for *P. celeri* TG2 (grown dilute at $1000 \mu\text{mol m}^{-2} \text{s}^{-1}$). The maximal rate is again very high. It does not drop off during the experiment. This is yet another indication that *P. celeri* is resistant to photoinhibition and stable when cultivated in high light. As described in the Methods, CO_2 was available at a saturating concentrations throughout the assay duration.

3.3.7 COMPARATIVE SPECIFIC GROWTH RATES AND OPTICAL PROPERTIES OF *PICOCHLORUM*, *TETRASELMIS*, AND *CHLORELLA*

3.3.7.1 SPECIFIC GROWTH RATE AND CULTURE STABILITY

Specific growth rates and optical characteristics of the fastest growing line of *P. celeri*, TG2, along with *Tetraselmis* 2286 and *Chlorella* 252 are shown in Figure 3.9. The X-axis corresponds to the growth condition. Irradiances, in $\mu\text{mol m}^{-2} \text{s}^{-1}$, of 2000, 900, and 60 or 50 refer to light-acclimated dilute cultures. The last two growth conditions refer to dense, semi-continuously diluted cultures grown under either diel illumination or constant $2000 \mu\text{mol m}^{-2} \text{s}^{-1}$. The light acclimation state of these dense cultures is a low-light state but the degree of low-light acclimation depends on dilution rate, i.e., average specific growth rate (which determines cell density) and is influenced by incident irradiance. The average specific growth rate was about the same for all three algal strains under the diel illumination in dense culture because all of these algal cultures shared a common dilution rate of 60% per day. Growth rates for the stains were also similar in dilute culture at low light. Under all other growth conditions, *P. celeri* grew faster than the other algae (Figure 3.9A). In dense culture, the specific growth rates shown are not constants, but rather averages over the day. For 60% semicontinuous dilution, the biomass

density increases 2.5 fold from the morning dilution to the next day just before dilution. Generally, the biomass productivity is fairly constant over dilution rates from 40-60%, and thus the specific growth rate over the day varies almost inversely with biomass density, just as in the linear portion of a batch growth curve. For the dilute cultures, specific growth rates were constant over the growth day because the chlorophyll concentrations of cultures were kept at about 0.5 $\mu\text{g}/\text{mL}$ or less, at the end of

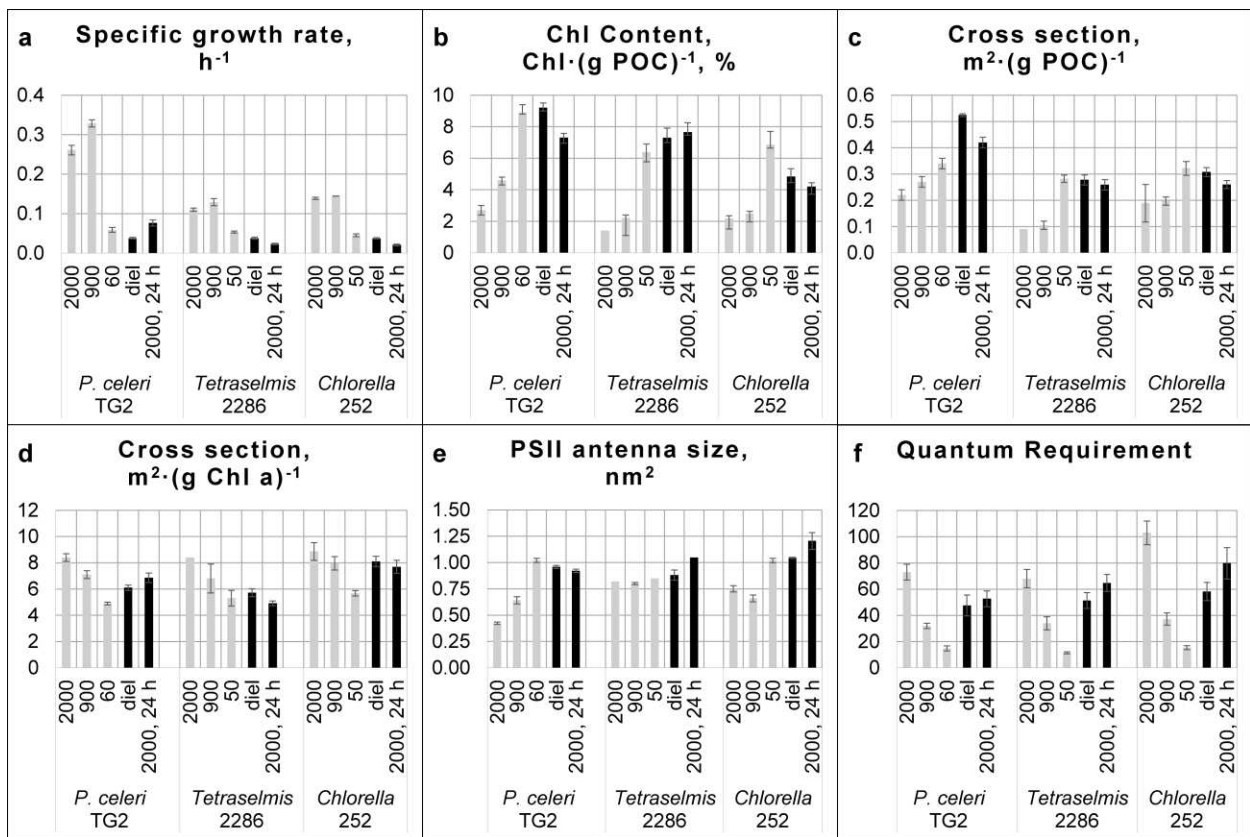


Figure 3.9 Optical characteristics and pigmentation of algae. The X-axes in these graphs indicate the conditions of growth. 2000, 900, and 50 (or 60) refer to the constant irradiance at which dilute cultures were grown, in $\mu\text{moles m}^{-2} \text{s}^{-1}$. Diel and 24 h 2000 ($\mu\text{moles m}^{-2} \text{s}^{-1}$) indicate the incident irradiance illuminating dense cultures. See text for explanation of data shown. The number of level 1 biological replicates for each panel are listed left to right as follows. A: 18, 14, 8, 23, 5, 3, 23, 19, 4, 2, 6, 2, 19, 6, 10. B: 24, 10, 11, 10, 8, 1, 23, 11, 7, 3, 8, 3, 27, 11, 15. C: 14, 8, 7, 4, 16, 1, 11, 26, 4, 2, 6, 3, 15, 6, 10. D: 10, 8, 11, 6, 4, 1, 23, 9, 6, 2, 6, 3, 15, 6, 10. E: 5, 6, 5, 3, 3, 1, 5, 1, 3, 1, 3, 2, 3, 3, 5. F: 6, 6, 5, 14, 4, 2, 23, 19, 4, 3, 4, 33, 15, 6, 10.

the growth day, through manual semi-continuous dilution. When they got denser, cultures were diluted more, until a steady state was reached. Thus, throughout the growth period, the cell concentration was very low and growth was balanced. Growth could be monitored by any cellular parameter. Chlorophyll was used on a daily basis, but all data is based on POC which was measured when culture growth became consistent. Specific growth rate results based chlorophyll and POC were essentially identical (data not shown).

For semicontinuously-diluted dense cultures illuminated twenty four hours a day at 2000 $\mu\text{mol m}^{-2} \text{s}^{-1}$, the amount of dilution could be greater for *P. celeri*, due to its stability in high light, than for both *Tetraselmis* and *Chlorella*. As stated above, *Tetraselmis* and *Chlorella* were difficult to establish in dense culture under these conditions. Dilution rate was kept under 33% per day for these algae as opposed to 80-90% per day for *P. celeri*. Even so the cultures were difficult to maintain for more than a week or two. These algae could also be difficult to establish at lower 24 hour irradiance, e.g., 900 $\mu\text{mol m}^{-2} \text{s}^{-1}$, but once established they usually could be maintained indefinitely. *Picochlorum celeri* was easy to establish (as is clear from the isolation protocols) under all conditions, and was maintained virtually indefinitely under all growth conditions.

Culture stability was investigated further using *P. celeri* TG1 and *Chlorella* by diluting cultures grown at 900 and 2000 $\mu\text{mol m}^{-2} \text{s}^{-1}$ (24 hours) tenfold or more and sampling every 2.5 hours for 7.5 hours and/or over subsequent days of batch growth. At 900 $\mu\text{mol m}^{-2} \text{s}^{-1}$ and 10 fold dilution, *P. celeri* began to high-light acclimate somewhat over the first day (data not shown) but mostly recovered pigmentation by the end of the first day and fully by the end of the second day. Chlorophyll to POC was 9.3% of POC before dilution, then reducing to 8.3% the next day and 9.0% the second day of batch. The culture maintained full biomass productivity

compared to a semicontinuous culture diluted 50% per day. Under $900 \mu\text{mol m}^{-2} \text{s}^{-1}$ and 100 fold dilution of a *P. celeris* culture, chlorophyll to POC went from 9.3% before the dilution to 5.5, 7.9, and 8.4 percent of POC for the three subsequent days of batch. Productivity during the first day after dilution was reduced (due to the very low culture density) to $7.8 \text{ g POC m}^{-2} \text{ d}^{-1}$, but returned to the normal $19 \text{ g POC m}^{-2} \text{ d}^{-1}$ (50% dilution per day culture) during the subsequent two days of batch growth. Under $2000 \mu\text{mol m}^{-2} \text{s}^{-1}$ (24 hours), 10 fold dilution led to chlorophyll changes of 6.7% of POC before dilution to 4.4 to 3.3 to 3.5 at 2.5, 5, and 7.5 hours after dilution to 5.5 the next morning with no change in productivity compared to 80% per day diluted culture.

Chlorella, on the other hand, under $900 \mu\text{mol m}^{-2} \text{s}^{-1}$ lost pigment content during the day after tenfold dilution, going from 5.5% of POC before dilution to 4.4, 3.8, 3.2 percent at 2.5, 5, 7.5 hours after the 10 fold dilution and getting even lower, to 2.2, the next morning. Growth did not recover over the next two days. Usually the culture productivity never returned to normal even when the amount of dilution did. *Chlorella* demonstrated an inability to re-pigment under high light in dense culture. This is in contrast to dilute cultures of all three algae, in which pigmentation was always lower under high light than under lower light, but was stable.

Due to this ability to high-light acclimate quickly and remain stable as culture density increases, *P. celeris* can be inoculated (e.g., into large-scale batch or semi-batch culture) at very high dilution from an inoculation system. *P. celeris* TG2, grown under the diel illumination regime was diluted by 50, 100, and 200 fold to start batch cultures also under diel illumination. With 50-fold dilution batch cultures were 40% as productive as controls (cultures diluted 60% per day) during day 1 (the day right after dilution), and produced normally over the next two days in batch. 100-fold diluted cultures were hardly productive over the first day, but grew at a specific growth rate of 0.10 h^{-1} . By the second day they were up to normal productivity. 200-

fold dilution resulted in very high first day specific growth rates (0.19 h^{-1}) but almost no productivity (they were so dilute), 50% productivity the next day and normal productivity was established by the third day following “inoculation.” All of these high dilution inoculum lost 40-50% of their chlorophyll at the end of the first day of batch but regained normal chlorophyll content when they regained normal productivity.

In summary, the reproductive rate of dense cultures under 24 hour constant high light ($2000 \mu\text{mol m}^{-2} \text{ s}^{-1}$) was much higher for *P. celeris* than for *Tetraselmis* or *Chlorella* because the dilution rate could be set much higher, 85-90% per day versus, 33% per day. At greater dilution, both *Tetraselmis* and *Chlorella* decreased in biomass density and were washed out or died within several days to one week. Cells of these species could not be exposed to very high light, in dense culture. In dilute culture, *Tetraselmis* and *Chlorella* could acclimate and thus reproduce much faster and grow stably. *P. celeris*, on the other hand, could reproduce stably under all conditions. In dilute culture, *P. celeris* specific growth rates were higher than the other algae, and at supersaturating irradiance, much higher. Thus, the most striking differences in growth between the other two algae and *P. celeris* is not only that the latter is able to reproduce much faster but is also able to maintain stable growth in dense culture after dilutions when cells are exposed to greater irradiance. Pigment content of *P. celeris* decreases much more rapidly when density is decreased (possibly because cells grow faster) and returns back to its higher level as density increases. *P. celeris* does not get stuck in a state in which it appears pigment levels are inhibited by high light.

3.3.7.2 CHLOROPHYLL CONTENT AND ABSORPTION CROSS SECTIONS

Picochlorum celeris had the highest chlorophyll content per POC of the strains studied under all of the growth conditions with the exception of *Tetraselmis* in dense cultures under 2000

$\mu\text{mol m}^{-2} \text{s}^{-1}$ (Figure 3.9B). Another distinguishing characteristic of *P. celeri* is its optical absorption cross section when normalized to POC. The POC-normalized cross section was higher under all growth conditions than the other algae, and usually much higher (Figure 3.9C). The normalized cross section is the most useful optical parameter in comparing the rate of light absorption relative to the rate of carbon fixation.

In contrast, the optical absorption cross section, when normalized to chlorophyll content (Figure 3.9D), exhibited different patterns among the three algae studied due to effects from several different factors. In part, variation of the chlorophyll-normalized cross section was due to cellular pigment packaging effects for which both the absolute pigment concentration within a cell and the relative cell size both influence the optical cross section. In particular, the cellular diameter of *Tetraselmis* is over 5x larger than *P. celeri*, leading to an important influence of cell size. For a fixed cell size, a suspension optical absorption cannot increase indefinitely with increasing pigment per cell, but is ultimately limited by the interception of light by the geometric cross section of the cells. Consequently, for highly pigmented cells, the measured absorption cross section enters a regime where it depends non-linearly on the pigment content. With increasing pigment content per cell the spectral features also increasingly become compressed, the classic tell-tale indication of pigment packaging being a decrease in the relative high difference between the Soret (blue) and Q (red) bands with increasing pigment loading per cell.

Relative cell size is one reason why the dilute, low-light acclimated states of all three of the algal types had similar $\text{m}^2 \cdot (\text{g chlorophyll } a)^{-1}$ despite variation in pigment content per cell. While *P. celeri* exhibited higher chlorophyll content per cell, the smaller cell size resulted in higher cellular optical transparency relative to the much larger *Tetraselmis* cells, despite the

lower relative pigment concentration prevailing in the latter. Similar considerations help explain the cross sections of the three algae at $900 \mu\text{mol m}^{-2} \text{s}^{-1}$ dilute cultures.

Other considerations affecting the chlorophyll-normalized cross section are also important. In dense culture at $2000 \mu\text{mol m}^{-2} \text{s}^{-1}$ *P. celeris* cultures were diluted much more each day than the other algae cultures. Thus, its state of light acclimation was higher than that of *Tetraselmis*. This was reflected in a higher chlorophyll-based optical cross section for *P. celeris*. Although *Chlorella* was also diluted much less than *P. celeris*, its pigment content was diminished proportionally more in dense culture in its particular response to higher light (see both the diel and high light cultures with consequently higher chlorophyll-based optical cross section).

Another factor that influences absorption cross sections when normalized to chlorophyll is content of carotenoid pigments. Solvent-extracted pigment spectra taken from dilute cultures of *P. celeris* clearly showed enhanced absorption in the 400-500nm wavelength range in high-light acclimated cells (900 and $2000 \mu\text{mol m}^{-2} \text{s}^{-1}$, in comparison to cells acclimated to $50 \mu\text{mol m}^{-2} \text{s}^{-1}$ (data not shown)). This additional absorption corresponds to about 20-30% of the total absorption over the visible spectrum. Direct estimation of auxiliary pigment contribution to the whole-cell optical absorption spectrum is confounded by the effects of pigment packaging.

The amount of carotenoid in high-light acclimated *P. celeris* is under investigation, along with the role these carotenoids play in the dissipation of photons observed in growth-determined quantum requirement. As discussed above, low-light-acclimated *P. celeris* cells are also very stable in high light. The speed at which this alga acclimates to changing light may be part of its stability in high light.

Photosystem II functional cross sections, estimated using induction fast repetition rate fluorometer (referred to as functional cross section since these are not measured directly by an optical absorption) are shown in Figure 3.9E. These functional photosystem cross sections are closely related to photosystem II antenna size based on the number of chlorophyll molecules, but are influenced by carotenoid content, pigment packaging, and photosystem quantum efficiency in a complicated manner. *Picochlorum celeri* had functional antenna sizes similar to *Chlorella* and *Tetraselmis* in low-light-acclimated states, but much lower antenna size in high-light acclimated states. The combination of high chlorophyll content, high absorption cross section, and lower antenna size, is consistent with the assumption that the excess pigmentation is partitioned as greater photosynthetic reaction center content, as asserted in Section 2.1 above. Comparing the pigment content and antenna size of high-light versus low-light *P. celeri*, it seems that the reduced number of reactions centers were still able to turn over fast enough to maintain the very high photosynthetic rates implying an excess capacity of Rubisco activity/content. Biochemical analysis is another area for further study. Thus, there may be opportunity to tune reaction center content, i.e., light absorption, while maintaining enough photosynthetic electron transport to support very high rates of carbon fixation. *P. celeri* could be a good model strain for this engineering endeavor.

3.3.7.3 QUANTUM REQUIREMENT

Carbon quantum requirements (QR) assessed during growth (as opposed to the QR assessed at low light from the initial slope of oxygen evolution assays) were similar under subsaturating light for all of the algal types (Figure 3.9F). *Tetraselmis* had the lowest quantum requirement in dilute culture under subsaturating light at 11.4 ± 0.8 photons per POC, *Chlorella* was next at 15.4 ± 1.5 and *P. celeri* was highest at 14.8 ± 2 . The quantum requirement of

Tetraselmis was significantly different from both *P. celeri* TG2 and *Chlorella* ($p < 0.001$), but the latter two were not significantly different from each other. *P. celeri* grew as fast as the others at low light, but it absorbed more photons. In dilute culture at $900 \mu\text{mol m}^{-2} \text{s}^{-1}$, all of the algae had similar quantum requirements for growth, around 35. *Chlorella* and *Tetraselmis* absorbed about the same number of photons per POC and had similar specific growth rates. *P. celeri* had both substantially higher absorption cross section and specific growth rate. In dilute culture at $2000 \mu\text{mol m}^{-2} \text{s}^{-1}$, *Tetraselmis* had a lower QR, 68 ± 7 , than *P. celeri* at 73 ± 6 . These were statistically different only to $p < 0.1$. The much lower POC-based absorption cross section of *Tetraselmis* more than made up for its lower specific growth rate. *Chlorella* had the highest quantum requirement, 103 ± 9 . It grew as fast as *Tetraselmis*, but absorbed many more photons per POC under this high light, dilute condition. In dense culture under diel conditions all the algae had a QR of about 50, but at high constant light, *P. celeri* had the lowest QR, at 53 ± 6 (it was the most productive), compared to *Tetraselmis* at 65 ± 6.5 and *Chlorella* at 80 ± 12 . All pairwise differences were statistically significant.

3.3.8 IMPROVING *P. CELERI* BIOMASS PRODUCTIVITY

Although *P. celeri* exhibited much higher photosynthetic rates (as oxygen evolution) than the other algae tested, this did not result in much greater biomass productivity, i.e., photosynthetic efficiency, under diel conditions. Photosynthetic efficiency is dependent on many factors including photoinhibition (through culture instability or depressed photosynthesis), light saturation losses due to dissipation of photons as well loss of electrons during photosynthetic electron flow, and respiration/maintenance (Weissman and Nielsen 2016). The amount of light energy that must be dissipated due to light saturation is related to the irradiance at which saturation occurs, E_k . E_k is a conceptualization used to describe the balance between

the rate at which photosynthetically produced electrons and ATP are used by carbon fixation (and other essential functions) and the rate of absorption of photons. Typically, the rate of absorption is 5 to 20 times higher than utilization, depending on the time of day, requiring that most photons be dissipated. E_k can be described on a P-I curve as the intersection of the line extended from the initial rise of photosynthetic rate with increasing irradiance, and the line representing the asymptote of saturated photosynthetic rate. As such it should increase about linearly with increases in P_{max} , with everything else unchanged. Although productivity is not expected to increase linearly with E_k , biomass productivity did not increase much at all for *P. celeris* relative to the other algae under diel conditions. Of course E_k is also affected by the cellular rate of photon absorption, i.e., the optical absorption cross section of the cells in the suspension. As shown above, *P. celeris* had nearly 100% higher optical absorption cross section per unit POC than *Chlorella* and *Tetraselmis*, respectively. Thus, the increase in E_k that might have translated to productivity gain due to a very high P_{max} may have been entirely mitigated by the greater rate of light absorption. *P. celeris* seems adapted to reproduce very quickly, especially in light-saturated environments. Like most algae it has not evolved to be efficient in its use of light. Yet, in large-scale systems this fast reproductive rate and stability at high irradiance may turn out to be valuable for bringing cultures to scale, recovery from upsets, and preventing loss of culture productivity due to culture instability in high light. Also, the ability to maintain a high photosynthetic rate even at lower rates of absorption per unit carbon, 0.22 to $0.27 \text{ m}^2 \cdot (\text{POC})^{-1}$, under high-light acclimation versus $0.52 \text{ m}^2 \cdot (\text{POC})^{-1}$ in the low-light acclimation state in diel cultures, may make this alga a good host for genetically engineering less absorption so that each cell absorbs less light in diel light (Beckmann et al. 2009a; Radakovits et al. 2010; Oey et al. 2013). In addition, the PS II antenna size of the cells in the state of highest light acclimation

investigated was 40% of that of cells in in the lowest state of light acclimation. One question is if the high stability of *P. celeri* in its natural high-light acclimated state can be maintained if the absorption cross section is engineered to be lower.

3.4 SUMMARY

This report shows that very fast reproductive rates can be selected in algae by imposing high irradiance in dilute continuous or semi-continuous cultures. Definitive experiments to pinpoint the cause for the short doubling times will be the subject of future investigation. However, certain characteristics of the new strains are consistent with the fast growth. *P. celeri* has a high pigment content, very high carbon-specific absorption cross section, higher than other strains under virtually all growth conditions. The selection protocol imposed also selected for reduced antenna size and one that is very sensitive to irradiance. Extrapolating from the small antenna size, it has a high content of photosynthetic reaction centers. Thus, it seems that this alga puts much of its cell activity towards growth. Still, further biochemical investigation is needed to demonstrate whether high rates of light absorption and high carbon fixation rates are solely due to high concentrations of the cell constituents related to light absorption and photosynthesis. The role of regulation is unknown. It was shown that *P. celeri* seems poised to reproduce fast no matter what its conditions of grown, whereas a species of *Tetraselmis* and a species of *Chlorella* were not, even if they had the capacity. It was demonstrated that the phenotypes of isolates depended upon the isolation procedures, with fastest reproductive rates obtained by isolating under conditions similar to the original enrichment conditions. Future work is planned to discover the genomic differences of isolates with different phenotypes.

3.5 ACKNOWLEDGEMENTS

This work was financially supported by Corporate Strategic Research, ExxonMobil Research & Engineering. We would like to thank Amy Ashford (Colorado School of Mines) for her extensive culturing efforts and sample preparations in support of this research. Conception and design: JCW, MCP; Collection and assembly of data: JCW, ML, WF, DCT, DAJK, JC; Analysis and interpretation of the data: JCW, MCP, RN, DCT, WF; Drafting of the article: JCW; Critical revision: MCP, RN, DCT; Final approval of the article: JCW, MCP.

CHAPTER 4: CONCLUSION AND FUTURE WORKS

4.1 ALGAL BIOTECHNOLOGY OUTLOOK AND FUTURE CONSIDERATIONS

Algae remain as a promising organism to design the future's bioeconomy upon. As shown in this thesis, they have the capability for fast reproductive growth utilizing CO₂, light, water, and fertilizer. Additionally, they remain capable for genetic manipulation and commodity chemical production which can drop in to existing food, fuel, or material economies.

Picochlorum celeri has demonstrated itself as a capable chassis strain for biomass growth in the outdoor ponds required for cheap cultivation because of its high light acclimation and high temperature and salt tolerance. Much work remains to generate an organism that can further the bioeconomy such as genetic tools, multi-omic analysis, and thorough biomass characterization.

Remaining is to high-throughput the process of genetic manipulation and characterization so that goals such as antenna reduction or lipid production can be realized in a cost-effective manner. Algae still lags behind heterotrophic bacteria in this way because of the large amounts of time required to grow and engineer these promising organisms. Comparing common algae to *Escherichia coli*, algae may double every few hours while the bacteria double every half hour, or a transformation may take 2-4 weeks while bacteria take 24 hours. The wide difference clarifies this lag in technology. Therefore, it is important as algae are developed to learn the lessons from bacteria and engineer the learned lesson into the ideal cell factory—one that utilizes CO₂ instead of farmed sugar.

Additionally, as *P.celeri* is further studied, there must be a strong effort to understand the genetic expression and regulation it goes through in high light. To understand how the organism grows so fast and how it regulates its changes to high density growth. Through transcriptomics,

metabolomics and proteomics, many of the appealing characteristics can be elucidated and further improved or mined.

Lastly, because of the appeal of *P.celeris* its biomass composition must be thoroughly characterized for natural products. Because with the ability to grow quickly comes the possibility to generate new and interesting chemicals that can replace non-renewable sources. At this moment, its high maximum specific growth rate may make it desirable from a biomass perspective but if it can also accumulate pigments, nutraceuticals, or other desirable products, it will have an entirely new market interest oppose to food or fuel.

4.2 FUTURE WORK OF PHOTOSYNTHETIC METABOLISM IN STARCHLESS MUTANTS

The regulation of photosynthesis which is caused through metabolic changes occurring under biotic and abiotic stresses must be further understood to better genetically manipulate photosynthetic microorganisms for industrial purposes. Downstream manipulations with the desire the partition biomass to value products have often generated undesirable effects on photosynthetic capacity. As well, nutrient starvation has been utilized to shift partitioning to storage compounds although ultimately the desire remains to sustain high levels of photosynthesis. Understanding valves such as water-water cycles will illuminate the regulatory mechanisms within photosynthesis that effectively waste reducing power generated from the light reactions of photosynthesis. With a clearer image of the front end of metabolism, engineering strategies can be utilized to recapture this reductant into biomass.

REFERENCE CITED

- Allahverdiyeva Y, Mustila H, Ermakova M, et al (2013) Flavodiiron proteins Flv1 and Flv3 enable cyanobacterial growth and photosynthesis under fluctuating light. *Proceedings of the National Academy of Sciences* 110:4111–4116. doi: 10.1073/pnas.1221194110
- Alric J, Johnson X (2017) Alternative electron transport pathways in photosynthesis: a confluence of regulation. *Current Opinion in Plant Biology* 37:78–86. doi: 10.1016/J.PBI.2017.03.014
- Anderson A, Laohavisit A, Blaby IK, et al (2016) Exploiting algal NADPH oxidase for biophotovoltaic energy. 22–28. doi: 10.1111/pbi.12332
- Asada K The water–water cycle as alternative photon and electron sinks. doi: 10.1098/rstb.2000.0703
- Asada K (1999) THE WATER-WATER CYCLE IN CHLOROPLASTS: Scavenging of Active Oxygens and Dissipation of Excess Photons. *Annual Review of Plant Physiology and Plant Molecular Biology* 50:601–639. doi: 10.1146/annurev.arplant.50.1.601
- Bailey S, Melis A, Mackey KRM, et al (2008) Alternative photosynthetic electron flow to oxygen in marine *Synechococcus*. *Biochimica et Biophysica Acta (BBA) - Bioenergetics* 1777:269–276. doi: 10.1016/J.BBABIO.2008.01.002
- Bailleul B, Berne N, Murik O, et al (2015) Energetic coupling between plastids and mitochondria drives CO₂ assimilation in diatoms. *Nature* 524:366–369. doi: 10.1038/nature14599
- Baker NR (2008) Chlorophyll Fluorescence: A Probe of Photosynthesis In Vivo. *Annual Review of Plant Biology* 59:89–113. doi: 10.1146/annurev.arplant.59.032607.092759
- Ball SG, Deschamps P (2009) Starch Metabolism. *The Chlamydomonas Sourcebook* 1–40. doi: 10.1016/B978-0-12-370873-1.00009-5
- Beckmann J, Lehr F, Finazzi G, et al (2009a) Improvement of light to biomass conversion by de-regulation of light-harvesting protein translation in *Chlamydomonas reinhardtii*. *Journal of Biotechnology* 142:70–77. doi: 10.1016/J.JBIOTECH.2009.02.015
- Beckmann K, Messinger J, Badger MR, et al (2009b) On-line mass spectrometry: Membrane inlet sampling. *Photosynthesis Research* 102:511–522. doi: 10.1007/s11120-009-9474-7
- Bell G, Reboudt X (1997) Experimental evolution in *Chlamydomonas* II. Genetic variation in strongly contrasted environments

- Blaby IK, Glaesener AG, Mettler T, et al (2013) Systems-level analysis of nitrogen starvation-induced modifications of carbon metabolism in a *Chlamydomonas reinhardtii* starchless mutant. *The Plant cell* 25:4305–23. doi: 10.1105/tpc.113.117580
- Blankenship RE, Tiede DM, Barber J, et al (2011) Comparing Photosynthetic and Photovoltaic Efficiencies and Recognizing the Potential for Improvement Downloaded from
- Buchanan BB (2016) The Path to Thioredoxin and Redox Regulation in Chloroplasts. *Annual Review of Plant Biology* 67:1–24. doi: 10.1146/annurev-arplant-043015-111949
- Cazzaniga S, Dall’Osto L, Szaub J, et al (2014) Domestication of the green alga *Chlorella sorokiniana*: reduction of antenna size improves light-use efficiency in a photobioreactor. *Biotechnology for Biofuels* 7:157. doi: 10.1186/s13068-014-0157-z
- Chaux F, Burlacot A, Mekhalfi M, et al (2017) Flavodiiron Proteins Promote Fast and Transient O₂ Photoreduction in *Chlamydomonas*. *Plant physiology* 174:1825–1836. doi: 10.1104/pp.17.00421
- Cheng F, Cui Z, Mallick K, et al (2018) Hydrothermal liquefaction of high- and low-lipid algae: Mass and energy balances. *Bioresource technology* 258:158–167. doi: 10.1016/j.biortech.2018.02.100
- Choi SY, Park B, Choi I-G, et al (2016) Transcriptome landscape of *Synechococcus elongatus* PCC 7942 for nitrogen starvation responses using RNA-seq. *Scientific Reports* 6:30584. doi: 10.1038/srep30584
- Correa DF, Beyer HL, Possingham HP, et al (2017) Biodiversity impacts of bioenergy production: Microalgae vs. first generation biofuels. *Renewable and Sustainable Energy Reviews* 74:1131–1146. doi: 10.1016/J.RSER.2017.02.068
- Cousins AB, Ghannoum O, Von Caemmerer S, Badger MR (2010) Simultaneous determination of Rubisco carboxylase and oxygenase kinetic parameters in *Triticum aestivum* and *Zea mays* using membrane inlet mass spectrometry. *Plant, Cell and Environment* 33:444–452. doi: 10.1111/j.1365-3040.2009.02095.x
- Curien G, Flori S, Villanova V, et al (2016) The Water to Water Cycles in Microalgae. *Plant and Cell Physiology* 57:pcw048. doi: 10.1093/pcp/pcw048
- DalCorso G, Pesaresi P, Masiero S, et al (2008) A Complex Containing PGRL1 and PGR5 Is Involved in the Switch between Linear and Cyclic Electron Flow in *Arabidopsis*. *Cell* 132:273–285. doi: 10.1016/J.CELL.2007.12.028
- Dang K-V, Plet J, Tolleter D, et al (2014) Combined increases in mitochondrial cooperation and oxygen photoreduction compensate for deficiency in cyclic electron flow in *Chlamydomonas reinhardtii*. *The Plant cell* 26:3036–50. doi: 10.1105/tpc.114.126375

- Davey MP, Horst I, Duong G-H, et al (2014) Triacylglyceride Production and Autophagous Responses in *Chlamydomonas reinhardtii* Depend on Resource Allocation and Carbon Source. *Eukaryotic Cell* 13:392–400. doi: 10.1128/EC.00178-13
- Davies FK, Jinkerson RE, Posewitz MC (2015) Toward a photosynthetic microbial platform for terpenoid engineering. *Photosynthesis Research* 123:265–284. doi: 10.1007/s11120-014-9979-6
- Desplats C, Mus F, Cuiné S, et al (2009) Characterization of Nda2, a plastoquinone-reducing type II NAD(P)H dehydrogenase in *chlamydomonas* chloroplasts. *The Journal of biological chemistry* 284:4148–57. doi: 10.1074/jbc.M804546200
- Dogaris I, Brown TR, Loya B, Philippidis G (2016) Cultivation study of the marine microalga *Picochlorum oculatum* and outdoor deployment in a novel bioreactor for high-density production of algal cell mass. *Biomass and Bioenergy* 89:11–23. doi: 10.1016/J.BIOMBIOE.2016.02.018
- Elliott LG, Feehan C, Laurens LML, et al (2012) Establishment of a bioenergy-focused microalgal culture collection. *Algal Research* 1:102–113. doi: 10.1016/j.algal.2012.05.002
- Falkowski PG, Fujita Y, Ley A, Mauzerall D (1986) Evidence for Cyclic Electron Flow around Photosystem II in *Chlorella pyrenoidosa*. *Plant Physiology* 81:310–312. doi: 10.1104/pp.81.1.310
- Fang W, Si Y, Douglass S, et al (2012) Transcriptome-wide changes in *Chlamydomonas reinhardtii* gene expression regulated by carbon dioxide and the CO₂-concentrating mechanism regulator CIA5/CCM1. *The Plant cell* 24:1876–93. doi: 10.1105/tpc.112.097949
- Flynn KJ, Greenwell HC, Lovitt RW, Shields RJ (2010) Selection for fitness at the individual or population levels: Modelling effects of genetic modifications in microalgae on productivity and environmental safety. *Journal of Theoretical Biology* 263:269–280. doi: 10.1016/J.JTBI.2009.12.021
- Foflonker F, Ananyev G, Qiu H, et al (2016) The unexpected extremophile: Tolerance to fluctuating salinity in the green alga *Picochlorum*. *Algal Research* 16:465–472. doi: 10.1016/J.ALGAL.2016.04.003
- Foflonker F, Price DC, Qiu H, et al (2015) Genome of the halotolerant green alga *Picochlorum* sp. reveals strategies for thriving under fluctuating environmental conditions. *Environmental Microbiology* 17:412–426. doi: 10.1111/1462-2920.12541
- Fon Sing S, Isdepsky A, Borowitzka MA, Lewis DM (2014) Pilot-scale continuous recycling of growth medium for the mass culture of a halotolerant *Tetraselmis* sp. in raceway ponds under increasing salinity: A novel protocol for commercial microalgal biomass production. *Bioresource Technology* 161:47–54. doi: 10.1016/J.BIORTECH.2014.03.010

- Geigenberger P (2011) Regulation of starch biosynthesis in response to a fluctuating environment. *Plant physiology* 155:1566–77. doi: 10.1104/pp.110.170399
- Geraghty AM, Anderson JC, Spalding MH (1990) A 36 Kilodalton Limiting-CO₂ Induced Polypeptide of *Chlamydomonas* Is Distinct from the 37 Kilodalton Periplasmic Carbonic Anhydrase 1. *Plant Physiology* 93:116–121
- Gerotto C, Alboresi A, Meneghesso A, et al (2016) Flavodiiron proteins act as safety valve for electrons in *Physcomitrella patens*. *Proceedings of the National Academy of Sciences of the United States of America* 113:12322–12327. doi: 10.1073/pnas.1606685113
- Gollakota ARK, Kishore N, Gu S (2018) A review on hydrothermal liquefaction of biomass. *Renewable and Sustainable Energy Reviews* 81:1378–1392. doi: 10.1016/J.RSER.2017.05.178
- Gonzalez-Ballester D, Pootakham W, Mus F, et al (2011) Reverse genetics in *Chlamydomonas*: a platform for isolating insertional mutants. *Plant Methods* 2011 7:1 7:24. doi: 10.1186/1746-4811-7-24
- Harris EH (2009) No Title. In: Witman EHHBSB (ed) *The Chlamydomonas Sourcebook* (Second Edition). Academic Press, London, p ix
- Helman Y, Tchernov D, Reinhold L, et al (2003) Genes encoding A-type flavoproteins are essential for photoreduction of O₂ in cyanobacteria. *Current biology : CB* 13:230–235. doi: 10.1016/S0960-9822(03)00046-0
- Henley WJ, Hironaka JL, Guillou L, et al (2004) Phylogenetic analysis of the ‘Nannochloris-like’ algae and diagnoses of *Picochlorum oklahomensis* gen. et sp. nov. (Trebouxiophyceae, Chlorophyta). *Phycologia* 43:641–652. doi: 10.2216/i0031-8884-43-6-641.1
- Heyno E, Gross CM, Laureau C, et al (2009) Plastid alternative oxidase (PTOX) promotes oxidative stress when overexpressed in tobacco. *The Journal of biological chemistry* 284:31174–80. doi: 10.1074/jbc.M109.021667
- Houille-Vernes L, Rappaport F, Wollman F-A, et al (2011) Plastid terminal oxidase 2 (PTOX2) is the major oxidase involved in chlororespiration in *Chlamydomonas*. *Proceedings of the National Academy of Sciences of the United States of America* 108:20820–5. doi: 10.1073/pnas.1110518109
- Jakočiūnas T, Jensen MK, Keasling JD (2017) System-level perturbations of cell metabolism using CRISPR/Cas9. *Current Opinion in Biotechnology* 46:134–140. doi: 10.1016/j.copbio.2017.03.014
- Jans F, Mignolet E, Houyoux P-A, et al (2008) A type II NAD(P)H dehydrogenase mediates light-independent plastoquinone reduction in the chloroplast of *Chlamydomonas*. *Proceedings of the National Academy of Sciences* 105:20546–20551. doi: 10.1073/pnas.0806896105

- Johnson X, Alric J (2013) Central carbon metabolism and electron transport in *Chlamydomonas reinhardtii*: metabolic constraints for carbon partitioning between oil and starch. *Eukaryotic cell* 12:776–93. doi: 10.1128/EC.00318-12
- Johnson X, Alric J (2012) Interaction between starch breakdown, acetate assimilation, and photosynthetic cyclic electron flow in *Chlamydomonas reinhardtii*. *The Journal of biological chemistry* 287:26445–52. doi: 10.1074/jbc.M112.370205
- Keeling PL, Myers AM (2010) Biochemistry and Genetics of Starch Synthesis. *Annual Review of Food Science and Technology* 1:271–303. doi: 10.1146/annurev.food.102308.124214
- Kindle KL (1990) High-frequency nuclear transformation of *Chlamydomonas reinhardtii*. *Proceedings of the National Academy of Sciences of the United States of America* 87:1228–32. doi: 10.1073/PNAS.87.3.1228
- Kramer DM, Johnson G, Kiirats O, Edwards GE (2004a) New fluorescence parameters for the determination of Q A redox state and excitation energy fluxes. *Photosynthesis Research* 79:209–218
- Kramer DM, Johnson G, Kiirats O, Edwards GE (2004b) New Fluorescence Parameters for the Determination of QA Redox State and Excitation Energy Fluxes. *Photosynthesis Research* 79:209–218. doi: 10.1023/B:PRES.0000015391.99477.0d
- Krieger-Liszky A, Feilke K (2015) The Dual Role of the Plastid Terminal Oxidase PTOX: Between a Protective and a Pro-oxidant Function. *Frontiers in plant science* 6:1147. doi: 10.3389/fpls.2015.01147
- Krishnan A, Kumaraswamy GK, Vinyard DJ, et al (2015) Metabolic and photosynthetic consequences of blocking starch biosynthesis in the green alga *Chlamydomonas reinhardtii* sta6 mutant. *Plant Journal* 81:947–960. doi: 10.1111/tpj.12783
- Lambrev PH, Miloslavina Y, Jahns P, Holzwarth AR (2012) On the relationship between non-photochemical quenching and photoprotection of Photosystem II. *Biochimica et Biophysica Acta (BBA) - Bioenergetics* 1817:760–769. doi: 10.1016/J.BBABIO.2012.02.002
- Larkum AWD, Ross IL, Kruse O, Hankamer B (2012a) Selection, breeding and engineering of microalgae for bioenergy and biofuel production. *Trends in Biotechnology* 30:198–205. doi: 10.1016/J.TIBTECH.2011.11.003
- Larkum AWD, Ross IL, Kruse O, Hankamer B (2012b) Selection, breeding and engineering of microalgae for bioenergy and biofuel production. *Trends in Biotechnology* 30:198–205. doi: 10.1016/J.TIBTECH.2011.11.003
- LAUREAU C, DE PAEPE R, LATOUCHE G, et al (2013) Plastid terminal oxidase (PTOX) has the potential to act as a safety valve for excess excitation energy in the alpine plant species *Ranunculus glacialis* L. *Plant, Cell & Environment* 36:1296–1310. doi: 10.1111/pce.12059

- Li Y, Han D, Hu G, et al (2010) Chlamydomonas starchless mutant defective in ADP-glucose pyrophosphorylase hyper-accumulates triacylglycerol. *Metabolic Engineering* 12:387–391. doi: 10.1016/j.ymben.2010.02.002
- Lü J, Sheahan C, Fu P (2011) Metabolic engineering of algae for fourth generation biofuels production. *Energy & Environmental Science* 4:2451. doi: 10.1039/c0ee00593b
- Lysenko V, Guo Y, Chugueva O (2016) Cyclic Electron Transport Around Photosystem II: Mechanisms and Methods of Study. *American Journal of Plant Physiology* 12:1–9. doi: 10.3923/ajpp.2017.1.9
- MacIntyre HL, Kana TM, Anning T, Geider RJ (2002) Photoacclimation of photosynthesis irradiance response curves and photosynthetic pigments in microalgae and cyanobacteria. *Journal of Phycology* 38:17–38. doi: 10.1046/j.1529-8817.2002.00094.x
- Maxwell K, Johnson GN (2000) Chlorophyll fluorescence—a practical guide. *Journal of Experimental Botany* 51:659–668. doi: 10.1093/jexbot/51.345.659
- May P, Wienkoop S, Kempa S, et al (2008) Metabolomics- and proteomics-assisted genome annotation and analysis of the draft metabolic network of *Chlamydomonas reinhardtii*. *Genetics* 179:157–66. doi: 10.1534/genetics.108.088336
- McDonald AE, Ivanov AG, Bode R, et al (2011) Flexibility in photosynthetic electron transport: The physiological role of plastoquinol terminal oxidase (PTOX). *Biochimica et Biophysica Acta (BBA) - Bioenergetics* 1807:954–967. doi: 10.1016/J.BBABIO.2010.10.024
- Mehler A, Brown AH (1952) Studies on reactions of illuminated chloroplasts. III. Simultaneous photoproduction and consumption of oxygen studied with oxygen isotopes. *Archives of biochemistry and biophysics* 38:365–370
- Mehler AH (1951) Studies on reactions of illuminated chloroplasts: I. Mechanism of the reduction of oxygen and other hill reagents. *Archives of Biochemistry and Biophysics* 33:65–77. doi: 10.1016/0003-9861(51)90082-3
- Melis A (2009) Solar energy conversion efficiencies in photosynthesis: Minimizing the chlorophyll antennae to maximize efficiency. *Plant Science* 177:272–280. doi: 10.1016/J.PLANTSCI.2009.06.005
- Melis A, Neidhardt J, Benemann JR (1998) *Dunaliella salina* (Chlorophyta) with small chlorophyll antenna sizes exhibit higher photosynthetic productivities and photon use efficiencies than normally pigmented cells. *Journal of Applied Phycology* 10:515–525. doi: 10.1023/A:1008076231267
- Meuser JE, Boyd ES, Ananyev G, et al (2011) Evolutionary significance of an algal gene encoding an [FeFe]-hydrogenase with F-domain homology and hydrogenase activity in *Chlorella variabilis* NC64A. *Planta* 234:829–843. doi: 10.1007/s00425-011-1431-y

- Michelet L, Zaffagnini M, Morisse S, et al (2013a) Redox regulation of the Calvin-Benson cycle: something old, something new. *Frontiers in plant science* 4:470. doi: 10.3389/fpls.2013.00470
- Michelet L, Zaffagnini M, Morisse S, et al (2013b) Redox regulation of the Calvin–Benson cycle: something old, something new. *Frontiers in Plant Science* 4:. doi: 10.3389/fpls.2013.00470
- Myers J (1980) On the Algae: Thoughts about Physiology and Measurements of Efficiency. In: *Primary Productivity in the Sea*. Springer US, Boston, MA, pp 1–16
- Nawrocki WJ, Tourasse NJ, Taly A, et al (2015) The Plastid Terminal Oxidase: Its Elusive Function Points to Multiple Contributions to Plastid Physiology. *Annual Review of Plant Biology* 66:49–74. doi: 10.1146/annurev-arplant-043014-114744
- Oey M, Ross IL, Stephens E, et al (2013) RNAi Knock-Down of LHCBM1, 2 and 3 Increases Photosynthetic H₂ Production Efficiency of the Green Alga *Chlamydomonas reinhardtii*. *PLoS ONE* 8:e61375. doi: 10.1371/journal.pone.0061375
- Onno Feikema W, Marosvölgyi MA, Lavaud J, van Gorkom HJ (2006) Cyclic electron transfer in photosystem II in the marine diatom *Phaeodactylum tricornutum*. *Biochimica et Biophysica Acta (BBA) - Bioenergetics* 1757:829–834. doi: 10.1016/J.BBABIO.2006.06.003
- Peltier G, Aro E-M, Shikanai T (2016) NDH-1 and NDH-2 Plastoquinone Reductases in Oxygenic Photosynthesis. *Annual Review of Plant Biology* 67:null. doi: 10.1146/annurev-arplant-043014-114752
- Peltier G, Cournac L (2002) Chlororespiration. *Annual Review of Plant Biology* 53:523–550. doi: 10.1146/annurev.arplant.53.100301.135242
- Pereira H, Gangadhar KN, Schulze PSC, et al (2016) Isolation of a euryhaline microalgal strain, *Tetraselmis* sp. CTP4, as a robust feedstock for biodiesel production. *Scientific Reports* 6:35663. doi: 10.1038/srep35663
- Perrine Z, Negi S, Sayre RT (2012) Optimization of photosynthetic light energy utilization by microalgae. *Algal Research* 1:134–142. doi: 10.1016/J.ALGAL.2012.07.002
- Pfister B, Zeeman SC (2016) Formation of starch in plant cells. *Cellular and molecular life sciences : CMLS* 73:2781–807. doi: 10.1007/s00018-016-2250-x
- Poliner E, Takeuchi T, Du Z-Y, et al (2018) Nontransgenic Marker-Free Gene Disruption by an Episomal CRISPR System in the Oleaginous Microalga, *Nannochloropsis oceanica* CCMP1779. *ACS Synthetic Biology* acssynbio.7b00362. doi: 10.1021/acssynbio.7b00362
- Porra RJ, Thompson WA, Kriedemann PE (1989a) Determination of accurate extinction coefficients and simultaneous equations for assaying chlorophylls a and b extracted with

- four different solvents: verification of the concentration of chlorophyll standards by atomic absorption spectroscopy. *Biochimica et Biophysica Acta (BBA) - Bioenergetics* 975:384–394. doi: 10.1016/S0005-2728(89)80347-0
- Porra RJ, Thompson WA, Kriedemann PE (1989b) Determination of accurate extinction coefficients and simultaneous equations for assaying chlorophylls a and b extracted with four different solvents: verification of the concentration of chlorophyll standards by atomic absorption spectroscopy. *The Extinct. Biochimica et Biophysica Acta Modern Methods of Plant Analysis* 975:384–394
- Posewitz MC, Smolinski SL, Kanakagiri S, et al (2004) Hydrogen photoproduction is attenuated by disruption of an isoamylase gene in *Chlamydomonas reinhardtii*. *The Plant Cell* 16:2151–63. doi: 10.1105/tpc.104.021972
- Prasil O, Kolber Z, Berry JA, Falkowski PG (1996) Cyclic electron flow around Photosystem II in vivo. *Photosynthesis Research* 48:395–410. doi: 10.1007/BF00029472
- Quiles MJ (2006) Stimulation of chlororespiration by heat and high light intensity in oat plants. *Plant, Cell & Environment* 29:1463–1470. doi: 10.1111/j.1365-3040.2006.01510.x
- Radakovits R, Jinkerson RE, Darzins A, Posewitz MC (2010) Genetic engineering of algae for enhanced biofuel production. *Eukaryotic cell* 9:486–501. doi: 10.1128/EC.00364-09
- Rahman FA, Aziz MMA, Saidur R, et al (2017) Pollution to solution: Capture and sequestration of carbon dioxide (CO₂) and its utilization as a renewable energy source for a sustainable future. *Renewable and Sustainable Energy Reviews* 71:112–126. doi: 10.1016/J.RSER.2017.01.011
- Ratha SK, Prasanna R (2012) Bioprospecting microalgae as potential sources of “Green Energy”—challenges and perspectives (Review). *Applied Biochemistry and Microbiology* 48:109–125. doi: 10.1134/S000368381202010X
- Ritchie RJ (2008) Universal chlorophyll equations for estimating chlorophylls a, b, c, and d and total chlorophylls in natural assemblages of photosynthetic organisms using acetone, methanol, or ethanol solvents. *Photosynthetica* 46:115–126. doi: 10.1007/s11099-008-0019-7
- Saroussi S, Sanz-Luque E, Kim RG, Grossman AR (2017) Nutrient scavenging and energy management: acclimation responses in nitrogen and sulfur deprived *Chlamydomonas*. *Current Opinion in Plant Biology* 39:114–122. doi: 10.1016/J.PBI.2017.06.002
- Saroussi SI, Wittkopp TM, Grossman AR (2016) The Type II NADPH Dehydrogenase Facilitates Cyclic Electron Flow, Energy-Dependent Quenching, and Chlororespiratory Metabolism during Acclimation of *Chlamydomonas reinhardtii* to Nitrogen Deprivation. *Plant physiology* 170:1975–88. doi: 10.1104/pp.15.02014

- Schmollinger S, Mühlhaus T, Boyle NR, et al (2014) Nitrogen-Sparing Mechanisms in *Chlamydomonas* Affect the Transcriptome, the Proteome, and Photosynthetic Metabolism. *The Plant cell* 26:1410–1435. doi: 10.1105/tpc.113.122523
- Sheehan J, Dunahay T, Benemann J, Roessler P (1998) Look Back at the U.S. Department of Energy's Aquatic Species Program: Biodiesel from Algae; Close-Out Report. Golden, CO
- Shimakawa G, Ishizaki K, Tsukamoto S, et al (2017) The Liverwort, *Marchantia*, Drives Alternative Electron Flow Using a Flavodiiron Protein to Protect PSI. *Plant physiology* 173:1636–1647. doi: 10.1104/pp.16.01038
- Shimogawara K, Fujiwara S, Grossman A, Usuda H (1998) High-Efficiency Transformation of *Chlamydomonas reinhardtii* by Electroporation
- Siaut M, Cuiné S, Cagnon C, et al (2011) Oil accumulation in the model green alga *Chlamydomonas reinhardtii*: characterization, variability between common laboratory strains and relationship with starch reserves. *BMC Biotechnology* 11:7. doi: 10.1186/1472-6750-11-7
- Steinrücken P, Erga SR, Mjøs SA, et al (2017) Bioprospecting North Atlantic microalgae with fast growth and high polyunsaturated fatty acid (PUFA) content for microalgae-based technologies. *Algal Research* 26:392–401. doi: 10.1016/J.ALGAL.2017.07.030
- Stepien P, Johnson GN (2009) Contrasting responses of photosynthesis to salt stress in the glycophyte *Arabidopsis* and the halophyte *thellungiella*: role of the plastid terminal oxidase as an alternative electron sink. *Plant physiology* 149:1154–65. doi: 10.1104/pp.108.132407
- Stern DB, Witman G, Harris EH (2008) *The chlamydomonas sourcebook*. Academic
- Su H, Lin J, Tan F (2017) Progress and perspective of biosynthetic platform for higher-order biofuels. *Renewable and Sustainable Energy Reviews* 80:801–826. doi: 10.1016/j.rser.2017.05.158
- Sun J, Okita TW, Edwards GE (1999) Modification of Carbon Partitioning, Photosynthetic Capacity, and O₂ Sensitivity in *Arabidopsis* Plants with Low ADP-Glucose Pyrophosphorylase Activity. *Plant Physiology* 119:267–276. doi: 10.1104/pp.119.1.267
- Trouillard M, Shahbazi M, Moyet L, et al (2012) Kinetic properties and physiological role of the plastoquinone terminal oxidase (PTOX) in a vascular plant. *Biochimica et Biophysica Acta (BBA) - Bioenergetics* 1817:2140–2148. doi: 10.1016/J.BBABIO.2012.08.006
- Umeno D, Tobias A V, Arnold FH (2005) Diversifying carotenoid biosynthetic pathways by directed evolution. *Microbiology and molecular biology reviews* : *MMBR* 69:51–78. doi: 10.1128/MMBR.69.1.51-78.2005

- Von Wettstein D, Gough S, Kannangara CG (1995) Chlorophyll Biosynthesis. *The Plant cell* 7:1039–1057. doi: 10.1105/tpc.7.7.1039
- Wang S, Shi X, Palenik B (2016) Characterization of *Picochlorum* sp. use of wastewater generated from hydrothermal liquefaction as a nitrogen source. *Algal Research* 13:311–317. doi: 10.1016/J.ALGAL.2015.11.015
- Weissman J, Nielsen R (2016) Algal Growth Kinetics and Productivity. In: *Microalgal Production for Biomass and High-Value Products*. CRC Press, pp 1–19
- Wirtz W, Stitt M, Heldt HW (1982) Light activation of calvin cycle enzymes as measured in pea leaves. *FEBS Letters* 142:223–226. doi: 10.1016/0014-5793(82)80139-7
- Work VH, Bentley FK, Scholz MJ, et al (2013) Biocommodities from photosynthetic microorganisms. *Environmental Progress & Sustainable Energy* 32:989–1001. doi: 10.1002/ep.11849
- Work VH, Radakovits R, Jinkerson RE, et al (2010) Increased lipid accumulation in the *Chlamydomonas reinhardtii* sta7-10 starchless isoamylase mutant and increased carbohydrate synthesis in complemented strains. *Eukaryotic cell* 9:1251–61. doi: 10.1128/EC.00075-10
- Yamamoto H, Takahashi S, Badger MR, Shikanai T (2016) Artificial remodelling of alternative electron flow by flavodiiron proteins in *Arabidopsis*. *Nature Plants* 2:16012. doi: 10.1038/nplants.2016.12
- Yoshida K, Terashima I, Noguchi K (2007) Up-Regulation of Mitochondrial Alternative Oxidase Concomitant with Chloroplast Over-Reduction by Excess Light. *Plant and Cell Physiology* 48:606–614. doi: 10.1093/pcp/pcm033
- Yu X, Chen X, Wang L, et al (2017) Novel insights into the effect of nitrogen on storage protein biosynthesis and protein body development in wheat caryopsis. *Journal of Experimental Botany* 68:2259–2274. doi: 10.1093/jxb/erx108
- Zabawinski C, Koornhuyse N Van Den, D’Hulst C, et al (2001) Starchless Mutants of *Chlamydomonas reinhardtii* Lack the Small Subunit of a Heterotetrameric ADP-Glucose Pyrophosphorylase. *Journal of Bacteriology* 183:1069–1077. doi: 10.1128/JB.183.3.1069-1077.2001
- Zeeman SC, Kossmann J, Smith AM (2010) Starch: Its Metabolism, Evolution, and Biotechnological Modification in Plants. *Annual Review of Plant Biology* 61:209–234. doi: 10.1146/annurev-arplant-042809-112301

APPENDIX A: SUPPLEMENTAL DATA

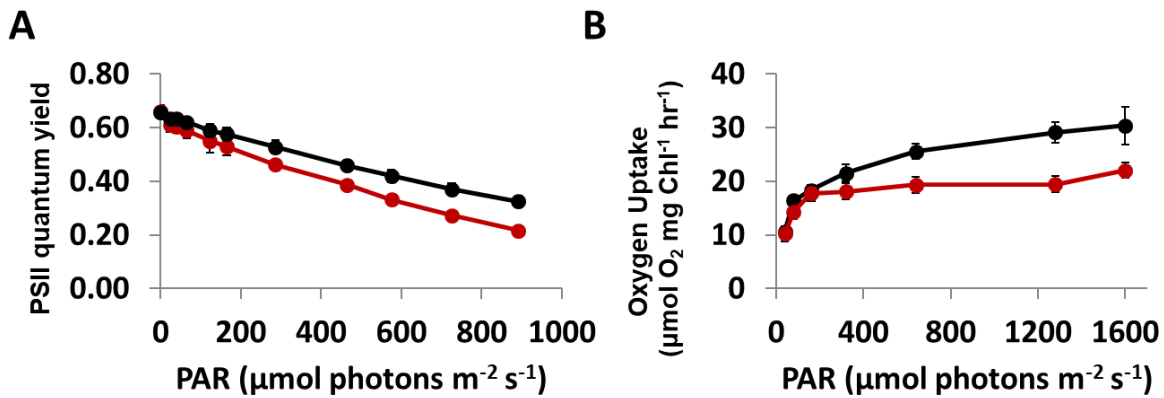


Figure A1. 1 Photosynthetic measurements of photoautotrophically grown *sta6* (red line) and C6 (black line) following dark to light transition. **A.** Apparent efficiency of PSII at different light intensities. The first data point reflects PSII maximal efficiency or Fv/Fm. (N=3 +/- S.D.). **B.** Dark respiration. O₂ uptake was calculated from the slope soon after the cells were transferred from light to dark light (N=3 +/- S.E.). For all measurements 2mM bicarbonate was added during the dark period.

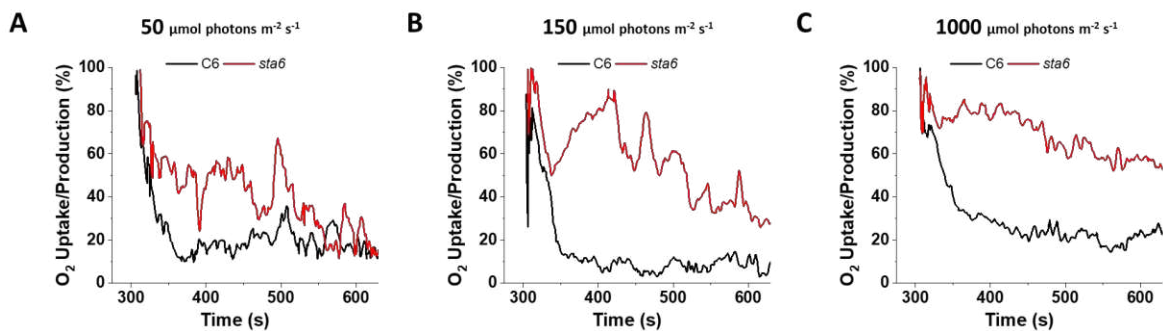


Figure A1. 2 The ratio between gross ¹⁸O₂ uptake and ¹⁶O₂ production (presented as %). Each data line represents an average of 3 biological replicates. Cells were exposed to **A.** 50 **B.** 150 and **C.** 1000 $\mu\text{mol photons m}^{-2} \text{s}^{-1}$.

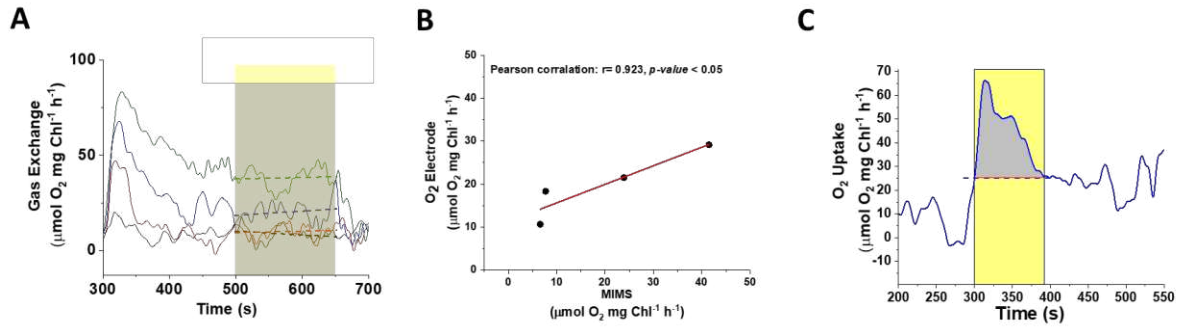


Figure A1.3 Steady state O_2 uptake in the light and overall consumption of O_2 by FLVs. A. $^{18}\text{O}_2$ uptake at steady state were fitted to linear curve and the uptake value at this point was calculated for each light intensity (labeled). The uptake value was estimated as mitochondrial respiration. B. A correlation between the mitochondrial respiration derived from A and the basal rates of O_2 uptake (dominated by mitochondrial respiration) calculated using an O_2 electrode. There is a strong correlation between the values measured by the electrode and by the MIMS and these values are not significantly different. C. Integration of $^{18}\text{O}_2$ uptake to calculate the overall amount of O_2 consumption during by FLVs during the initial O_2 uptake burst. Blue line represents O_2 uptake and dashed blue and red line represent the levels of mitochondrial respiration that act as a baseline for our estimation.

APPENDIX B: PERMISSIONS

Dylan Thomas

From: Shai Saroussi <ssaroussi@carnegiescience.edu>
Sent: Tuesday, October 2, 2018 11:47 AM
To: Dylan Thomas
Subject: Re: Permission to include work from recent PNAS submission in master's thesis materials

Hi Dylan

You have my permission to use any of materials from the mentioned manuscript in your master thesis.

Good luck,

Shai

On Tue, Oct 2, 2018, 8:37 PM Dylan Thomas <dylanthomas@mymail.mines.edu> wrote:

Dear Co-authors,

I am writing to obtain permission from you to include this work in my Master's thesis materials. If you agree, please reply to this email. For record keeping purposes, the article I am referring to is:

Shai Saroussi, Devin A. J. Karns, Dylan C. Thomas, Matthew C. Posewitz, and Arthur R. Grossman.

Alternative Outlets for Sustaining Photosynthetic Electron Transport During Dark to Light Transitions, Proceedings of the National Academy of Sciences of the United States of America. Currently Submitted.

This material will be embargoed until after work is published in a journal.

Thank you in advance, and please let me know if you have any questions.

Sincerely,

Dylan C. Thomas

Dylan Thomas

From: Devin Karns <dkarns@mymail.mines.edu>
Sent: Tuesday, October 2, 2018 2:42 PM
To: Dylan Thomas
Subject: Re: Permission to include work from recent PNAS submission in master's thesis materials

I agree

On Tue, Oct 2, 2018, 11:37 AM Dylan Thomas <dylanthomas@mymail.mines.edu> wrote:

Dear Co-authors,

I am writing to obtain permission from you to include this work in my Master's thesis materials. If you agree, please reply to this email. For record keeping purposes, the article I am referring to is:

Shai Saroussi, Devin A. J. Karns, Dylan C. Thomas, Matthew C. Posewitz, and Arthur R. Grossman.

Alternative Outlets for Sustaining Photosynthetic Electron Transport During Dark to Light Transitions, Proceedings of the National Academy of Sciences of the United States of America. Currently Submitted.

Thesis material will be embargoed until after work is published in a journal.

Thank you in advance, and please let me know if you have any questions.

Sincerely,

Dylan C. Thomas

Dylan Thomas

From: Matthew Posewitz <mposewit@mines.edu>
Sent: Tuesday, October 2, 2018 11:39 AM
To: Dylan Thomas
Subject: RE: Permission to include work from recent PNAS submission in master's thesis materials

Permission granted.

From: Dylan Thomas [dylanthomas@mymail.mines.edu]
Sent: Tuesday, October 02, 2018 11:37 AM
To: Dylan Thomas
Subject: Permission to include work from recent PNAS submission in master's thesis materials

Dear Co-authors,

I am writing to obtain permission from you to include this work in my Master's thesis materials. If you agree, please reply to this email. For record keeping purposes, the article I am referring to is:

Shai Saroussi, Devin A. J. Karns, Dylan C. Thomas, Matthew C. Posewitz, and Arthur R. Grossman.
Alternative Outlets for Sustaining Photosynthetic Electron Transport During Dark to Light Transitions,
Proceedings of the National Academy of Sciences of the United States of America. Currently Submitted.

Thesis material will be embargoed until after work is published in a journal.

Thank you in advance, and please let me know if you have any questions.

Sincerely,

Dylan C. Thomas

Dylan Thomas

From: Arthur Grossman <arthurg@stanford.edu>
Sent: Tuesday, October 2, 2018 11:43 AM
To: Dylan Thomas
Subject: Re: Permission to include work from recent PNAS submission in master's thesis materials

Absolutely fine with me.
Arthur

On Tue, Oct 2, 2018 at 10:37 AM Dylan Thomas <dylanthomas@mymail.mines.edu> wrote:

Dear Co-authors,

I am writing to obtain permission from you to include this work in my Master's thesis materials. If you agree, please reply to this email. For record keeping purposes, the article I am referring to is:

Shai Saroussi, Devin A. J. Karns, Dylan C. Thomas, Matthew C. Posewitz, and Arthur R. Grossman.

Alternative Outlets for Sustaining Photosynthetic Electron Transport During Dark to Light Transitions, Proceedings of the National Academy of Sciences of the United States of America. Currently Submitted.

Thesis material will be embargoed until after work is published in a journal.

Thank you in advance, and please let me know if you have any questions.

Sincerely,

Dylan C. Thomas

--

Arthur Grossman
Department of Plant Biology,
The Carnegie Institution, Stanford,
CA 94305
Ph:650 325 1521 x 212
<http://carnegiedpb.stanford.edu/>

Dylan Thomas

From: Chung, Jeffrey W <JEFFREY.CHUNG@UCDENVER.EDU>
Sent: Thursday, October 25, 2018 10:06 PM
To: Dylan Thomas
Subject: Re: Permission to include our work in my Master's thesis

Hi Dylan,

I agree. Good luck with thesis!

Sincerely,
Jeff

Jeffrey Chung
Doctoral Candidate | Jacobelli lab
Immunology Department
UC Denver | National Jewish Health

From: Dylan Thomas <dylanthomas@mymail.mines.edu>
Sent: Thursday, October 25, 2018 10:03:13 PM
To: Robert.Nielson@exxonmobil.com; Chung, Jeffrey W
Subject: Permission to include our work in my Master's thesis

Dear Co-authors,

I am writing to obtain permission from you to include this work in my Master's thesis materials. If you agree, please reply to this email saying you agree. For record keeping purposes, the article I am referring to is:

Joseph C. Weissman, Maria Likhogrud, Dylan C. Thomas, Wei Fang, Devin A. J. Karns, Jeffrey Chung, Robert Nielsen, and Matthew C. Posewitz. **High-Light Selection Produces a Fast-Growing Picochlorum celeri**, Algal Research. Accepted for publication.

Thank you in advance, and please let me know if you have any questions.

Sincerely,

Dylan C. Thomas

Dylan Thomas

From: 伟方 <ffwww1982@hotmail.com>
Sent: Wednesday, October 24, 2018 3:13 AM
To: Dylan Thomas
Subject: Re: Permission to include our work in my Master's thesis

Of course yes! Congrats for your degree!
Wei

Sent from my iPhone

On Oct 23, 2018, at 7:23 AM, Dylan Thomas <dylanthomas@mymail.mines.edu> wrote:

Dear Co-authors,

I am writing to obtain permission from you to include this work in my Master's thesis materials. If you agree, please reply to this email saying you agree. For record keeping purposes, the article I am referring to is:

Joseph C. Weissman, Maria Likhogrud, Dylan C. Thomas, Wei Fang, Devin A. J. Karns, Jeffrey Chung, Robert Nielsen, and Matthew C. Posewitz. **High-Light Selection Produces a Fast-Growing *Picochlorum celeri***, Algal Research. Accepted for publication.

Thank you in advance, and please let me know if you have any questions.

Sincerely,

Dylan C. Thomas

Dylan Thomas

From: Devin Karns <dkarns@mymail.mines.edu>
Sent: Monday, October 22, 2018 5:39 PM
To: Dylan Thomas
Subject: Re: Permission to include our work in my Master's thesis

Agree

On Mon, Oct 22, 2018, 5:23 PM Dylan Thomas <dylanthomas@mymail.mines.edu> wrote:

Dear Co-authors,

I am writing to obtain permission from you to include this work in my Master's thesis materials. If you agree, please reply to this email saying you agree. For record keeping purposes, the article I am referring to is:

Joseph C. Weissman, Maria Likhogrud, Dylan C. Thomas, Wei Fang, Devin A. J. Karns, Jeffrey Chung, Robert Nielsen, and Matthew C. Posewitz. **High-Light Selection Produces a Fast-Growing Picochlorum celeri**, Algal Research. Accepted for publication.

Thank you in advance, and please let me know if you have any questions.

Sincerely,

Dylan C. Thomas

Dylan Thomas

From: Likhogrud, Maria <maria.likhogrud@exxonmobil.com>
Sent: Wednesday, October 31, 2018 6:04 AM
To: Dylan Thomas
Subject: RE: Permission to include our work in my Master's thesis

Hi Dylan,

Sorry! I haven't realized that, I thought Joe gave the blanket approval.

Your request is approved by me.

Sorry again! Good luck with your thesis!

Maria.

From: Dylan Thomas [mailto:dylanthomas@mymail.mines.edu]
Sent: Tuesday, October 30, 2018 11:43 PM
To: Likhogrud, Maria <maria.likhogrud@exxonmobil.com>
Subject: Fwd: Permission to include our work in my Master's thesis

Hey Maria,

I wanted to reach out to see if you approve of our publication in Algal Research being utilized in my Masters thesis. I need approval from all co-authors before submission.

Hope all is well.

Dylan

----- Forwarded message -----

From: Weissman, Joseph <joseph.weissman@exxonmobil.com>
Date: Tue, Oct 23, 2018 at 4:54 AM
Subject: RE: Permission to include our work in my Master's thesis
To: Dylan Thomas <dylanthomas@mymail.mines.edu>, Matthew Posewitz <mposewit@mines.edu>, Devin Karns <dkarns@mymail.mines.edu>, ? ? <ffwww1982@hotmail.com>, Likhogrud, Maria <maria.likhogrud@exxonmobil.com>

Dear Dylan,

Your request is approved by me.

Joe

Joseph C. Weissman

Distinguished Scientific Associate

(908) 730-3428

Cell: (772) 538-1051

joseph.weissman@exxonmobil.com

From: Dylan Thomas [mailto:dylanthomas@mymail.mines.edu]

Sent: Monday, October 22, 2018 7:24 PM

To: Matthew Posewitz <mposewit@mines.edu>; Devin Karns <dkarns@mymail.mines.edu>; Weissman, Joseph <joseph.weissman@exxonmobil.com>; ? ? <ffwww1982@hotmail.com>; Likhogrud, Maria <maria.likhogrud@exxonmobil.com>

Subject: Permission to include our work in my Master's thesis

Dear Co-authors,

I am writing to obtain permission from you to include this work in my Master's thesis materials. If you agree, please reply to this email saying you agree. For record keeping purposes, the article I am referring to is:

Joseph C. Weissman, Maria Likhogrud, Dylan C. Thomas, Wei Fang, Devin A. J. Karns, Jeffrey Chung, Robert Nielsen, and Matthew C. Posewitz. **High-Light Selection Produces a Fast-Growing Picochlorum celeri**, Algal Research. Accepted for publication.

Thank you in advance, and please let me know if you have any questions.

Sincerely,

Dylan C. Thomas

Dylan Thomas

From: Nielsen, Robert <robert.nielsen@exxonmobil.com>
Sent: Thursday, November 1, 2018 3:52 PM
To: Dylan Thomas
Cc: Weissman, Joseph
Subject: Re: Permission to include our work in my Master's thesis

Dylan,

I agree to your request.

Best,
Robert

Sent from my iPad

On Oct 30, 2018, at 11:47 PM, Dylan Thomas <dylanthomas@mymail.mines.edu> wrote:

Hey Robert,

My name is Dylan. I'm finishing my graduate degree in Chemistry at Colorado School of Mines. I'm including the publication listed below in my masters thesis as is as a chapter. I just need approval from all co-authors. Please let me know if you approve of this and if you have any questions.

Thank you,
Dylan

----- Forwarded message -----

From: **Dylan Thomas** <dylanthomas@mymail.mines.edu>
Date: Thu, Oct 25, 2018 at 10:05 PM
Subject: Permission to include our work in my Master's thesis
To: <Robert.Nielsen@exxonmobil.com>

Dear Co-authors,

I am writing to obtain permission from you to include this work in my Master's thesis materials. If you agree, please reply to this email saying you agree. For record keeping purposes, the article I am referring to is:

Joseph C. Weissman, Maria Likhogrud, Dylan C. Thomas, Wei Fang, Devin A. J. Karns, Jeffrey Chung, Robert Nielsen, and Matthew C. Posewitz. **High-Light Selection Produces a Fast-Growing Picochlorum celeri**, Algal Research. Accepted for publication.

Thank you in advance, and please let me know if you have any questions.

Sincerely,

Dylan C. Thomas

Dylan Thomas

From: Matthew Posewitz <mposewit@mines.edu>
Sent: Monday, October 22, 2018 5:25 PM
To: Dylan Thomas
Subject: RE: Permission to include our work in my Master's thesis

Hi Dylan,

I approve.

Sincerely,
Matt

From: Dylan Thomas [dylanthomas@mymail.mines.edu]
Sent: Monday, October 22, 2018 5:23 PM
To: Matthew Posewitz; Devin Karns; Weissman, Joseph; ? ?; maria.likhogrud@exxonmobil.com
Subject: Permission to include our work in my Master's thesis

Dear Co-authors,

I am writing to obtain permission from you to include this work in my Master's thesis materials. If you agree, please reply to this email saying you agree. For record keeping purposes, the article I am referring to is:

Joseph C. Weissman, Maria Likhogrud, Dylan C. Thomas, Wei Fang, Devin A. J. Karns, Jeffrey Chung, Robert Nielsen, and Matthew C. Posewitz. **High-Light Selection Produces a Fast-Growing Picochlorum celeri**, Algal Research. Accepted for publication.

Thank you in advance, and please let me know if you have any questions.

Sincerely,

Dylan C. Thomas

Dylan Thomas

From: Weissman, Joseph <joseph.weissman@exxonmobil.com>
Sent: Tuesday, October 23, 2018 4:54 AM
To: Dylan Thomas; Matthew Posewitz; Devin Karns; ? ?; Likhogrud, Maria
Subject: RE: Permission to include our work in my Master's thesis

Dear Dylan,

Your request is approved by me.

Joe

Joseph C. Weissman
Distinguished Scientific Associate
(908) 730-3428
Cell: (772) 538-1051
joseph.weissman@exxonmobil.com

From: Dylan Thomas [mailto:dylanthomas@mymail.mines.edu]
Sent: Monday, October 22, 2018 7:24 PM
To: Matthew Posewitz <mposewit@mines.edu>; Devin Karns <dkarns@mymail.mines.edu>; Weissman, Joseph <joseph.weissman@exxonmobil.com>; ? ? <ffwww1982@hotmail.com>; Likhogrud, Maria <maria.likhogrud@exxonmobil.com>
Subject: Permission to include our work in my Master's thesis

Dear Co-authors,

I am writing to obtain permission from you to include this work in my Master's thesis materials. If you agree, please reply to this email saying you agree. For record keeping purposes, the article I am referring to is:

Joseph C. Weissman, Maria Likhogrud, Dylan C. Thomas, Wei Fang, Devin A. J. Karns, Jeffrey Chung, Robert Nielsen, and Matthew C. Posewitz. **High-Light Selection Produces a Fast-Growing Picochlorum celeri**, Algal Research. Accepted for publication.

Thank you in advance, and please let me know if you have any questions.

Sincerely,

Dylan C. Thomas